IMPROVING ENERGY EFFECIENCY OF ELECTRIC AND HYBRID ELECTRIC VEHICLES USING COMPUTER AIDED DESIGN

2021
PhD THESIS
ELECTRICAL AND ELECTRONICS ENGINEERING

KHALED ABUSHAFA AWAILI

Prof. Dr. Mustafa AKTAŞ

IMPROVING ENERGY EFFECIENCY OF ELECTRIC AND HYBRID ELECTRIC VEHICLES USING COMPUTER AIDED DESIGN

Khaled Abushafa AWAILI

T.C.

Karabuk University

Institute of Graduate Programs

Department of Electrical and Electronics Engineering

Prepared as

PhD Thesis

Prof. Dr. Mustafa AKTAŞ

KARABUK

July 2021

I certify that in my opinion the thesis submitted by Khaled Abushafa AWAILI titled "IMPROVING ENERGY EFFECIENCY OF ELECTRIC AND HYBRID ELECTRIC VEHICLES USING COMPUTER AIDED DESIGN" is fully adequate in scope and in quality as a thesis for the degree of PhD.

Prof. Dr. Mustafa AKTAŞ .....
Thesis Advisor, Department of Electrical and Electronics Engineering

This thesis is accepted by the examining committee with a unanimous vote in the Department of Electrical and Electronics Engineering as a PhD thesis. July 14, 2021

Examining Committee Members (Institutions)	Signature
Chairman : Assoc.Prof.Dr. Ömer KARAL (AYBU)	.....
Member : Prof.Dr. Mustafa AKTAŞ (OMU)	.....
Member : Assoc.Prof.Dr. Selim ÖNCÜ (KBU)	.....
Member : Assist.Prof.Dr. Mustafa GÖKDAĞ (KBU)	.....
Member : Assoc.Prof.Dr. Emre ÖZKOP (KTU)	.....

The degree of PhD by the thesis submitted is approved by the Administrative Board of the Institute of Graduate Programs, Karabuk University.

Prof. Dr. Hasan SOLMAZ .....
Director of the Institute of Graduate Programs

“I declare that all the information within this thesis has been gathered and presented in accordance with academic regulations and ethical principles and I have according to the requirements of these regulations and principles cited all those which do not originate in this work as well.”

Khaled Abushafa AWAILI

ABSTRACT

PhD Thesis

IMPROVING ENERGY EFFICIENCY OF ELECTRIC AND HYBRID ELECTRIC VEHICLES USING COMPUTER AIDED DESIGN

Khaled Abushafa AWAILI

Karabük University
Institute of Graduate Programs
The Department of Electrical and Electronics Engineering

Thesis Advisor:
Prof. Dr. Mustafa AKTAS
July 2021, 155 pages

The first aim of this work is to design a simulation platform that can be used to simulate and investigate the behavior of Electric Vehicles and Parallel Hybrid Electric vehicles. This platform is developed from the ground-based using Matlab m-file code, and then the Graphical User Interface is designed using Matlab App designer. To validate the developed software and to observe its suitability to simulate the behavior of EV and Parallel HEV, a different configuration is implemented. However, for the electric traction motor IFOC and DTC control strategies are implemented for IM and PMSM, Also, for Parallel HEV two different energy management strategies were applied, namely are Max-SoC and FRB energy management strategies. The other aim of this work is to improve the energy consumption of the vehicle that will lead to improve the energy efficiency and increase the operating range of the vehicle, thus a simple and effective SMC controller is proposed and utilized as a speed controller for all EVs and

Parallel HEVs configurations. The superior performance of the proposed SMC controller is proved as compared to the performances of PI and FLC controllers. Furthermore, to increase the vehicle operating range and to improve the battery pack range, and increase its lifetime a hybridization of the energy storage system is implemented and investigated for different configurations of the vehicle. To demonstrate this improvement, different drive scenarios were performed and the obtained results were compared. The hybridization of the energy storage sources which are in this thesis the battery pack and the Supercapacitor is performed based on developing rule-based energy management to reduce the complexity of the system. The proposed HESS energy management achieved a good improvement in the energy consumption that increased the vehicle energy efficiency.

Key Words : Electric vehicle, hybrid electric vehicle, induction motor, permanent magnet synchronous motor, sliding mode control, fuzzy logic control, fuzzy rule-based energy management, hybrid energy storage system,

Science Code : 90514

ÖZET

Doktora Tezi

BİLGİSAYAR DESTEKLİ TASARIM İLE ELEKTRİKLİ VE HİBRİT ELEKTRİKLİ TAŞITLARIN ENERJİ VERİMLİLİĞİNİN GELİŞTİRİLMESİ

Khaled Abushafa AWAILI

Karabük Üniversitesi
Lisansüstü Eğitim Enstitüsü
Elektrik Elektronik Mühendisliği Anabilim Dalı

Tez Danışmanı:
Prof. Dr. Mustafa AKTAŞ
Temmuz 2021, 155 sayfa

Bu çalışmanın ilk amacı, Elektrikli Taşıt (ET)'ların ve Paralel Hibrit Elektrikli Taşıt HET)'ların davranışlarını benzetmek ve araştırmak için kullanılabilecek bir simülasyon arayüzü tasarlamaktır. Bu arayüz, Matlab m-file kodu kullanılarak geliştirildi ve ardından Matlab App tasarımcısı kullanılarak Grafik Kullanıcı Arayüzü (GUI) tasarlandı. Geliştirilen yazılımı doğrulamak ve ET ve Paralel HET davranışını benzetime uygunluğunu gözlemlemek için farklı bir konfigürasyon uygulanmaktadır. Ancak elektrikli tahrik motoru için Asenkron Motor ve PMSM için Dolaylı IFOC ve DTC kontrol yöntemleri, Paralel HET için de Max-SoC ve FRB enerji yönetimi olmak üzere iki farklı enerji yönetimi uygulanmıştır. Bu çalışmanın diğer amacı, taşıtın enerji verimliliğini artıracak ve taşıtın çalışma menzilini artıracak şekilde taşıtın enerji tüketimini iyileştirmektir, böylece farklı ET'ler ve Paralel HET'lerin yapıları için yeni bir Sliding Mode Kontrol yöntemi önerilmiş ve hız kontrolörü olarak kullanılmıştır. Önerilen SMC kontrolörünün üstün performansı, PI ve FLC kontrolörlerin performansları ile karşılatırılarak ispatlanmıştır. Ayrıca, taşıt menzilini artırmak ve batarya paketi çalışmasını iyileştirmek ve ömrünü artırmak için, aracın farklı

yapılandırmaları için enerji depolama sisteminin hibridizasyonu uygulanmış ve incelenmiştir. Bu gelişmeyi göstermek için farklı sürüş çevrimleri gerçekleştirilmiş ve elde edilen sonuçlar karşılaştırılmıştır. Bu tezde yer alan enerji depolama kaynaklarının batarya paketi ve Süperkapasitör hibridizasyonu, sistemin karmaşıklığını azaltmak için kural tabanlı enerji yönetimi geliştirilerek gerçekleştirilmiştir. Önerilen HESS enerji yönetimi, taşıt enerji verimliliğini artıran enerji tüketiminde iyi bir gelişme sağlanmıştır.

Anahtar Kelimeler : Elektrikli taşıt, hibrit elektrikli taşıt, asenkron motor, sabit mıknatıslı senkron motor, kayan mod kontrolü, bulanık mantık kontrolü, bulanık kural tabanlı enerji yönetimi, hibrit enerji depolama sistemi.

Bilim Kodu **:** 90514

ACKNOWLEDGMENT

First of all, I would like to give thanks to my advisor, Prof. Dr. Mustafa AKTAS, for his great interest and assistance in preparation of this thesis. And I dedicate this thesis to the memory of my father Abushafa Saleh Awaili, who is no longer with us but his memories continue to inspire us to go on. I am also very grateful to my mother for her prayers and to my dearest wife for her support and encouragement in every step of my life. And finally, I present this work to my flowers (daughters) and my son.

CONTENTS

Page

APPROVAL ii
ABSTRACT iv
ÖZET vi
ACKNOWLEDGMENT viii
CONTENTS ix
LIST OF FIGURES xii
LIST OF TABLES xxi
SYMBOLS AND ABBREVITIONS INDEX xxii

PART 1 1
INTRODUCTION 1

PART 2 6
ELECTRIC AND HYBRID ELECTRIC VEHICLE MODELING 6
2.1. ELECTRIC VEHICLE 6
2.3. HYBRID ELECTRIC VEHICLE 6
2.3.1. Parallel Hybrid Electric Vehicle 7
2.3.2. Series Hybrid Electric Vehicle 9
2.3.3. Series Parallel Hybrid Electric Vehicle 9
2.4. MOTION DYNAMIC MODELLING 10
2.5. TRACTION MOTOR DRIVE 12
2.5.1. Induction Motor Modelling 12
2.5.2. Permanent Magnet Synchronous Motor Modelling 13
2.6. TRACTION MOTOR CONTROL STRATEGIES 14
2.6.1. Field Oriented Control (FOC) 14
2.6.2. Direct Torque Control (DTC) 17
2.7. TRACTION MOTOR SPEED CONTROL 19
2.7.1. Fuzzy Logic Controller (FLC) 19

Page

2.7.2. Sliding Mode Controller (SMC) 21
2.8. INTERNAL COMBUSTION ENGINE (ICE) 25
2.9. ENERGY STORAGE SYSTEM 26
2.9.1. Battery Modelling 26
2.9.2. Supercapacitor Modelling 28
2.9.3. Hybrid Energy Storage System (HESS) 29
2.9.3.1 HESS Rule Based Energy Management Strategy 29
2.10. PARALLEL HEV ENERGY MANAGEMENT STRATEGY 31
2.10.1. Max-SoC Energy management Strategy 33
2.10.2. Fuzzy Rule Based Energy Management Strategy 34

PART 3 37
SOFTWARE DESIGN AND GRAPHICAL USER INTERFACE 37
3.1. GRAPHICAL USER INTERFACE 37

PART 4 42
SIMULATION RESULTS 42
4.1 ELECTRIC VEHICLE SIMULATION RESULTS 42
4.1.1. Electric Vehicle Based IM 42
4.1.1.1. Simulation Based Battery-Only (IFOC for PI, FLC and SMC) 43
4.1.1.2. Simulation Based HESS (IFOC for PI, FLC and SMC) 47
4.1.1.3. Simulation Based Battery-Only (DTC for PI, FLC and SMC) 52
4.1.1.4. Simulation Based HESS (DTC for PI, FLC and SMC) 57
4.1.1.5. Results Comparison 61
4.1.2. Electric Vehicle Based PMSM 64
4.1.2.1. Simulation Based Battery-Only (IFOC for PI, FLC and SMC) 65
4.1.2.2. Simulation Based HESS (IFOC for PI, FLC and SMC) 69
4.1.2.3. Simulation Based Battery-Only (DTC for PI, FLC and SMC) 74
4.1.2.4. Simulation Based HESS (DTC for PI, FLC and SMC) 78
4.1.2.5. Results Comparison 83
4.2. PARALLEL HEV SIMULATION RESULTS 87
4.2.1. Parallel HEV Based IM with Max-SoC EMS 87

Page

4.2.1.1. Simulation Based Battery-Only for SMC controller 87
4.2.1.2. Simulation Based HESS for SMC controller 94
4.2.1.3. Results comparison 100
4.2.2. Parallel HEV Based IM with FRB- EMS 102
4.2.2.1. Simulation Based Battery-Only for SMC controller 102
4.2.2.2. Simulation Based HESS for SMC controller 109
4.2.2.3. Results comparison 114

PART 5 117
SUMMARY 117
REFERENCES 119

APPENDIX A. 126
APPENDIX B. 127
RESUME 129

LIST OF FIGURES

Page

Figure 2.1. Configuration of Electric Vehicle [52]. 6
Figure 2.2. Configuration of Parallel Hybrid Electric Vehicle [52]. 7
Figure 2.3. Configuration of Series Hybrid Electric Vehicle [52]. 9
Figure 2.4. Configuration of Parallel-Seiries Hybrid Electric Vehicle [52]. 10
Figure 2.5. Acting forces on the vehicle. 11
Figure 2.6. Basic scheme of IFOC strategy. 15
Figure 2.7. 3-phase to 2-phase coordinate transformation. 15
Figure 2.8. α-β and d-q coordinates. 16
Figure 2.9. Basic scheme of DTC strategy. 17
Figure 2.10. (a) Voltage space vectors and their appropriate sectors. (b) Stator flux control. 18
Figure 2.11. Fuzzy Logic Controller structure. 20
Figure 2.12. Inputs membership functions of FLC. a) Speed error. b) Change of speed error. 21
Figure 2.13. EV driven by IM-based SMC speed controller. 25
Figure 2.14. Battery electric model. 26
Figure 2.15. Supercapacitor model. 28
Figure 2.16. Hybrid energy storage system in EVs. 29
Figure 2.17. Hybrid energy storage system energy management. 30
Figure 2.18. Classification of HEV energy management strategies. 32
Figure 2.19. Max-SoC energy management strategy flow chart. 34
Figure 2.20. Fuzzy rule-based energy management 35
Figure 2.21. FRB-EMS inputs and output membership functions. 36
Figure 3.1. EV model subfuctions 37
Figure 3.2. GUI sequence flow chart. 38
Figure 3.3. GUI Main window. 39
Figure 3.4. Vehicle type selection window. 39
Figure 3.5. Vehicle type selection & simulator GUI. 40
Figure 3.6. Determining of HEV's parameters, traction motor, EMS and HESS 40

Page

Figure 3.7. Determining traction motor control strategy and speed controller. 41
Figure 4.1. NEDC driving cycle: a) Vehicle speed response. b) Vehicle operating modes. c) Vehicle speed error. d) Motor speed. EV based IM-IFOC-PI. 44
Figure 4.2. NEDC driving cycle: a) Power demand & Power split. b) Battery current. c) State of charge of Battery. EV based IM- IFOC-PI. 44
Figure 4.3. NEDC driving cycle: a) Vehicle speed response. b) Vehicle operating modes. c) Vehicle speed error. d) Motor speed. EV based IM-IFOC-FLC. 45
Figure 4.4. NEDC driving cycle: a) Power demand & Power split. b) Battery current. c) State of charge of Battery. EV based IM- IFOC-FLC. 46
Figure 4.5. NEDC driving cycle: a) Vehicle speed response. b) Vehicle operating modes. c) Vehicle speed error. d) Motor speed. EV based IM-IFOC-SMC. 46
Figure 4.6. NEDC driving cycle: a) Power demand & Power split. b) Battery current. c) State of charge of Battery. EV based IM-IFOC-SMC. 47
Figure 4.7. NEDC driving cycle: a) Vehicle speed response. b) Vehicle operating modes. c) Vehicle speed error. d) Motor speed. EV based IM-IFOC-PI. 48
Figure 4.8. NEDC driving cycle: a) Power demand & Power split. b) Batt/SC currents. c) State of charge of Battery & SC. EV based IM- IFOC-PI. 49
Figure 4.9. NEDC driving cycle: a) Vehicle speed response. b) Vehicle operating modes. c) Vehicle speed error. d) Motor speed. EV based IM-IFOC-FLC. 49
Figure 4.10. NEDC driving cycle: a) Power demand & Power split. b) Batt/SC currents. c) State of charge of Battery & SC. EV based IM- IFOC-FLC. 50
Figure 4.11. NEDC driving cycle: a) Vehicle speed response. b) Vehicle operating modes. c) Vehicle speed error. d) Motor speed. EV based IM-IFOC-SMC. 51
Figure 4.12. NEDC driving cycle: a) Power demand & Power split. b) Batt/SC currents. c) Batt/SC State of charges. EV based IM-IFOC-SMC. 52
Figure 4.13. NEDC driving cycle: a) Vehicle speed response. b) Vehicle operating modes. c) Vehicle speed error. d) Motor speed. EV based IM-DTC-PI. 53
Figure 4.14. NEDC driving cycle: a) Power demand & Power split. b) Battery current. c) State of charge of Battery. Based IM-DTC-PI. 53
Figure 4.15. NEDC driving cycle: a) Vehicle speed response. b) Vehicle operating modes. c) Vehicle speed error. d) Motor speed. EV based IM-DTC-FLC. 54

Page

Figure 4.16. NEDC driving cycle: a) Power demand & Power split. b) Battery current. c) State of charge of Battery. Based IM-DTC-FLC. 55
Figure 4.17. NEDC driving cycle: a) Vehicle speed response. b) Vehicle operating modes. c) Vehicle speed error. d) Motor speed. EV based IM-DTC-SMC. 56
Figure 4.18. NEDC driving cycle: a) Power demand & Power split. b) Battery current. c) State of charge of Battery. Based IM-DTC-SMC. 56
Figure 4.19. NEDC driving cycle: a) Vehicle speed response. b) Vehicle operating modes. c) Vehicle speed error. d) Motor speed. EV based IM-DTC-PI. 57
Figure 4.20. NEDC driving cycle: a) Power demand & Power split. b) Batt/SC currents. c) State of charge of Battery & SC. Based IM-DTC-PI. 58
Figure 4.21. NEDC driving cycle: a) Vehicle speed response. b) Vehicle operating modes. c) Vehicle speed error. d) Motor speed. Based IM-DTC-FLC. 59
Figure 4.22. NEDC driving cycle: a) Power demand & Power split. b) Batt/SC currents. c) State of charge of Battery & SC. Based IM-DTC-FLC. 59
Figure 4.23. NEDC driving cycle: a) Vehicle speed response. b) Vehicle operating modes. c) Vehicle speed error. d) Motor speed. Based IM-DTC-SMC. 60
Figure 4.24. NEDC driving cycle: a) Power demand & Power split. b) Batt/SC currents. c) State of charge of Battery & SC. Based IM-DTC-SMC. 61
Figure 4.25. NEDC driving cycle: a) Battery state of charge comparison. b) Change of energy in battery pack comparison. EV Based IM-IFOC-PI. 61
Figure 4.26. NEDC driving cycle: a) Battery state of charge comparison. b) Change of energy in battery pack comparison. EV Based IM-IFOC-FLC. 62
Figure 4.27. NEDC driving cycle: a) Battery state of charge comparison. b) Change of energy in battery pack comparison. EV Based IM-IFOC-SMC. 62
Figure 4.28. NEDC driving cycle: a) Battery state of charge comparison. b) Change of energy in battery pack comparison. EV Based IM-DTC-PI. 62
Figure 4.29. NEDC driving cycle: a) Battery state of charge comparison. b) Change of energy in battery pack comparison. EV Based IM-DTC-FLC. 63
Figure 4.30. NEDC driving cycle: a) Battery state of charge comparison. b) Change of energy in battery pack comparison. EV Based IM-DTC-SMC. 63
Figure 4.31. NEDC driving cycle: a) Vehicle speed response. b) Vehicle operating modes. c) Vehicle speed error. d) Motor speed. EV based PMSM-IFOC-PI. 65

Page

Figure 4.32. NEDC driving cycle: a) Power demand & Power split. b) Battery current. c) State of charge of Battery. EV based PMSM- IFOC-PI. 66
Figure 4.33. NEDC driving cycle: a) Vehicle speed response. b) Vehicle operating modes. c) Vehicle speed error. d) Motor speed. EV based PMSM-IFOC-FLC. 67
Figure 4.34. NEDC driving cycle: a) Power demand & Power split. b) Battery current. c) State of charge of Battery. EV based PMSM- IFOC-FLC. 68
Figure 4.35. NEDC driving cycle: a) Vehicle speed response. b) Vehicle operating modes. c) Vehicle speed error. d) Motor speed. EV based PMSM-IFOC-SMC. 68
Figure 4.36. NEDC driving cycle: a) Power demand & Power split. b) Battery current. c) State of charge of Battery. EV based PMSM- IFOC-SMC. 69
Figure 4.37. NEDC driving cycle: a) Vehicle speed response. b) Vehicle operating modes. c) Vehicle speed error. d) Motor speed. EV based PMSM-IFOC-PI. 70
Figure 4.38. NEDC driving cycle: a) Power demand & Power split. b) Battery & SC currents. c) State of charge of Battery & SC. EV based PMSM- IFOC-PI. 71
Figure 4.39. NEDC driving cycle: a) Vehicle speed response. b) Vehicle operating modes. c) Vehicle speed error. d) Motor speed. EV based PMSM-IFOC-FLC. 71
Figure 4.40. NEDC driving cycle: a) Power demand & Power split. b) Battery & SC currents. c) State of charge of Battery & SC. EV based PMSM- IFOC-FLC..... 72
Figure 4.41. NEDC driving cycle: a) Vehicle speed response. b) Vehicle operating modes. c) Vehicle speed error. d) Motor speed. EV based PMSM-IFOC-SMC. 73
Figure 4.42. NEDC driving cycle: a) Power demand & Power split. b) Battery & SC currents. c) State of charge of Battery & SC. EV based PMSM- IFOC-SMC. 73
Figure 4.43. NEDC driving cycle: a) Vehicle speed response. b) Vehicle operating modes. c) Vehicle speed error. d) Motor speed. EV based PMSM-DTC-PI. 74
Figure 4.44. NEDC driving cycle: a) Power demand & Power split. b) Battery current. c) State of charge of Battery. EV based PMSM- DTC-PI. 75
Figure 4.45. NEDC driving cycle: a) Vehicle speed response. b) Vehicle operating modes. c) Vehicle speed error. d) Motor speed. EV based PMSM-DTC-FLC. 76
Figure 4.46. NEDC driving cycle: a) Power demand & Power split. b) Battery current. c) State of charge of Battery. EV based PMSM- DTC-FLC..... 76
Figure 4.47. NEDC driving cycle: a) Vehicle speed response. b) Vehicle operating modes. c) Vehicle speed error. d) Motor speed. EV based PMSM-DTC-SMC. 77

Page

Figure 4.48. NEDC driving cycle: a) Power demand & Power split. b) Battery current. c) State of charge of Battery. EV based PMSM- DTC-SMC. 78
Figure 4.49. NEDC driving cycle: a) Vehicle speed response. b) Vehicle operating modes. c) Vehicle speed error. d) Motor speed. EV based PMSM- DTC-PI. 79
Figure 4.50. NEDC driving cycle: a) Power demand & Power split. b) Battery & SC currents. c) State of charge of Battery & SC. EV based PMSM- DTC-PI. 79
Figure 4.51. NEDC driving cycle: a) Vehicle speed response. b) Vehicle operating modes. c) Vehicle speed error. d) Motor speed. EV based PMSM- DTC-FLC. 80
Figure 4.52. NEDC driving cycle: a) Power demand & Power split. b) Battery & SC currents. c) State of charge of Battery & SC. EV based PMSM- DTC-FLC..... 81
Figure 4.53. NEDC driving cycle: a) Vehicle speed response. b) Vehicle operating modes. c) Vehicle speed error. d) Motor speed. EV based PMSM- DTC-SMC. 82
Figure 4.54. NEDC driving cycle: a) Power demand & Power split. b) Battery & SC currents. c) State of charge of Battery & SC. EV based PMSM- DTC-SMC..... 82
Figure 4.55. NEDC driving cycle: a) Battery state of charge comparison. b) Change of energy in battery pack comparison. EV Based PMSM-IFOC-PI. 83
Figure 4.56. NEDC driving cycle: a) Battery state of charge comparison. b) Change of energy in battery pack comparison. EV Based PMSM-IFOC-FLC..... 83
Figure 4.57. NEDC driving cycle: a) Battery state of charge comparison. b) Change of energy in battery pack comparison. EV Based PMSM-IFOC-SMC..... 84
Figure 4.58. NEDC driving cycle: a) Battery state of charge comparison. b) Change of energy in battery pack comparison. EV Based PMSM-DTC-PI..... 84
Figure 4.59. NEDC driving cycle: a) Battery state of charge comparison. b) Change of energy in battery pack comparison. EV Based PMSM-DTC-FLC..... 84
Figure 4.60. NEDC driving cycle: a) Battery state of charge comparison. b) Change of energy in battery pack comparison. EV Based PMSM-DTC-SMC..... 85
Figure 4.61. NEDC driving cycle: a) Vehicle speed. b) Operating modes. c) Vehicle speed error. d) Engine and IM speeds. HEV based IM-SMC-Max-SoC-EMS. 88
Figure 4.62. NEDC driving cycle: a) Power demand & Power split. b) Battery current. c) State of charge of Battery. HEV based IM-SMC-Max-SoC-EMS. 89
Figure 4.63. NEDC driving cycle: a) Engine fuel consumption. b) Engine efficiency. HEV Based IM-SMC-Max-SoC-EMS..... 89

Page

Figure 4.64. FTP75 driving cycle: a) Vehicle speed. b) Operating modes. c) Vehicle speed error. d) Engine and IM speeds. HEV based IM-SMC-Max-SoC-EMS. 90
Figure 4.65. FTP75 driving cycle: a) Power demand & Power split. b) Battery current. c) State of charge of Battery. HEV based IM-SMC-Max-SoC-EMS. 91
Figure 4.66. FTP75 driving cycle: a) Engine fuel consumption. b) Engine efficiency. HEV Based IM-SMC-Max-SoC-EMS..... 91
Figure 4.67. Highway driving cycle: a) Vehicle speed. b) Operating modes. c) Vehicle speed error. d) Engine and IM speeds. HEV based IM-SMC-Max-SoC-EMS. 92
Figure 4.68. Highway driving cycle: a) Power demand & Power split. b) Battery current. c) State of charge of Battery. HEV based IM-SMC-Max-SoC-EMS..... 93
Figure 4.69. Highway driving cycle: a) Engine fuel consumption. b) Engine efficiency. HEV Based IM-SMC-Max-SoC-EMS..... 93
Figure 4.70. NEDC driving cycle: a) Vehicle speed response. b) Vehicle operating modes. c) Vehicle speed error. d) Motor speed. HEV Based IM-SMC-Max-SoC-EMS. 94
Figure 4.71. NEDC driving cycle: a) Power demand & Power split. b) Batt/SC currents. c) State of charge of Battery & SC. HEV Based IM-FLC-Max-SoC-EMS. 95
Figure 4.72. NEDC driving cycle: a) Engine fuel consumption. b) Engine efficiency. HEV Based IM-SMC-Max-SoC-EMS..... 96
Figure 4.73. FTP75 driving cycle: a) Vehicle speed. b) Operating modes. c) Vehicle speed error. d) Engine and IM speeds. HEV based IM-SMC-Max-SoC-EMS. 97
Figure 4.74. FTP75 driving cycle: a) Power demand & Power split. b) Batt/SC currents. c) State of charge of Battery & SC. HEV Based IM-FLC-Max-SoC-EMS. 97
Figure 4.75. FTP75 driving cycle: a) Engine fuel consumption. b) Engine efficiency. HEV Based IM-SMC-Max-SoC-EMS..... 98
Figure 4.76. Highway driving cycle: a) Vehicle speed. b) Operating modes. c) Vehicle speed error. d) Engine and IM speeds. HEV based IM-SMC-Max-SoC-EMS. 99
Figure 4.77. Highway driving cycle: a) Power demand & Power split. b) Batt/SC currents. c) State of charge of Battery & SC. HEV Based IM-FLC-Max-SoC-EMS. 99

Page

Figure 4.78. Highway driving cycle: a) Engine fuel consumption. b) Engine efficiency. HEV Based IM-SMC-Max-SoC-EMS..... 100
Figure 4.79. NEDC driving cycle: a) Battery state of charge of Battery comparison. b) Change of energy in battery pack comparison. HEV Based IM-SMC-Max-SoC-EMS. 100
Figure 4.80. FTP75 driving cycle: a) Battery state of charge of Battery comparison. b) Change of energy in battery pack comparison. HEV Based IM-SMC-Max-SoC-EMS. 101
Figure 4.81. Highway driving cycle: a) Battery state of charge of Battery comparison. b) Change of energy in battery pack comparison. HEV Based IM-SMC-Max-SoC-EMS. 101
Figure 4.82. NEDC driving cycle: a) Vehicle speed response. b) Vehicle operating modes. c) Vehicle speed error. d) Motor speed. HEV Based IM-SMC and FRB-EMS. 103
Figure 4.83. NEDC driving cycle: a) Power demand & Power split. b) Battery current. c) State of charge of Battery. HEV Based IM-SMC and FRB-EMS. 104
Figure 4.84. NEDC driving cycle: a) Engine fuel consumption. b) Engine efficiency. HEV Based IM-SMC and FRB-EMS. 104
Figure 4.85. FTP75 driving cycle: a) Vehicle speed. b) Operating modes. c) Vehicle speed error. d) Engine and IM speeds. HEV Based IM-SMC and FRB-EMS. 105
Figure 4.86. FTP75 driving cycle: a) Power demand & Power split. b) Battery current. c) State of charge of Battery. HEV Based IM-SMC and FRB-EMS. 106
Figure 4.87. FTP75 driving cycle: a) Engine fuel consumption. b) Engine efficiency. HEV Based IM-SMC and FRB-EMS. 106
Figure 4.88. Highway driving cycle: a) Vehicle speed response. b) Vehicle operating modes. c) Vehicle speed error. d) Motor speed. HEV Based IM-SMC and FRB-EMS. 107
Figure 4.89. Highway driving cycle: a) Power demand & Power split. b) Battery current. c) State of charge of Battery. HEV Based IM-SMC and FRB-EMS..... 108
Figure 4.90. Highway driving cycle: a) Engine fuel consumption. b) Engine efficiency. HEV Based IM-SMC and FRB-EMS. 108

Page

Figure 4.91. NEDC driving cycle: a) Vehicle speed response. b) Vehicle operating modes. c) Vehicle speed error. d) Motor speed. HEV Based IM-SMC and FRB-EMS. 109
Figure 4.92. NEDC driving cycle: a) Power demand & Power split. b) Batt/SC currents. c) State of charge of Battery & SC. HEV Based IM-SMC and FRB-EMS. 110
Figure 4.93. NEDC driving cycle: a) Engine fuel consumption. b) Engine efficiency. HEV Based IM-SMC and FRB-EMS. 110
Figure 4.94. FTP75 driving cycle: a) Vehicle speed. b) Operating modes. c) Vehicle speed error. d) Engine and IM speeds. HEV Based IM-SMC and FRB-EMS. 111
Figure 4.95. FTP75 driving cycle: a) Power demand & Power split. b) Battery current. c) State of charge of Battery. HEV Based IM-SMC and FRB-EMS. 112
Figure 4.96. FTP75 driving cycle: a) Engine fuel consumption. b) Engine efficiency. HEV Based IM-SMC and FRB-EMS. 112
Figure 4.97. Highway driving cycle: a) Vehicle speed response. b) Vehicle operating modes. c) Vehicle speed error. d) Motor speed. HEV Based IM-SMC and FRB-EMS. 113
Figure 4.98. Highway driving cycle: a) Power demand & Power split. b) Batt/SC currents. c) State of charge of Battery & SC. HEV Based IM-SMC and FRB-EMS. 114
Figure 4.99. Highway driving cycle: a) Engine fuel consumption. b) Engine efficiency. HEV Based IM-SMC and FRB-EMS. 114
Figure 4.100. NEDC driving cycle: a) Battery state of charge of Battery comparison. b) Change of energy in battery pack comparison. HEV Based IM-SMC- FRB-EMS. 115
Figure 4.101. FTP75 driving cycle: a) Battery state of charge of Battery comparison. b) Change of energy in battery pack comparison. HEV Based IM-SMC- FRB-EMS. 115
Figure 4.102. Highway driving cycle: a) Battery state of charge of Battery comparison. b) Change of energy in battery pack comparison. HEV Based IM-SMC- FRB-EMS. 115
Figure Appendix B.1. GUI executing sequence..... 127

Page

Figure Appendix B.1. (Continuing). 128

LIST OF TABLES

Page

Table 1.1.Brand and EM type of EV/HEV available in industry [2, 11, 12, 45] 4
Table 2.1. Basic switching table of DTC 18
Table 2.2 Membership functions of FLC. 21
Table 2.3. FRB-EMS Rules. 36
Table 4.1. EV based IM numerical comparison. 64
Table 4.2. EV based PMSM numerical comparison. 85
Table 4.3. HEV based IM-SMC-Max-SoC-EMS numerical comparison. 102
Table 4.4. HEV based IM-SMC-FRB-EMS numerical comparison. 116
Table Appendix A.1. Vehicle parameters [26]. 126
Table Appendix A.2. IM parameters [26]. 126
Table Appendix A.3. PMSM parameters [86]. 126

SYMBOLS AND ABBREVITIONS INDEX

SYMBOLS

L_s, L_r : Stator and rotor inductance respectively (*H*).

φ_{rd}, φ_{rq} : Direct and quadrature rotor flux components (*Wb*).

A_v : Exponential voltage.

B_Q : Exponential capacity.

B_m : Motor viscous friction coefficient (*N.ms*).

C_d : Aerodynamic drag force coefficient.

C_{sc} : Supercapacitor capacitance (*F*).

E_0 : The constant voltage (*V*).

E_{sc} : Supercapacitor energy (*J*).

F_{hc} : Hill climbing force (*N*).

F_{ad} : Aerodynamic drag force (*N*).

F_{la} : Acceleration force (*N*).

F_{rr} : Rolling resistance force (*N*).

F_{tr} : Traction force (*N*).

J_m : Motor inertia ($Kg.m^2$).

K_p and K_i : Gains of the PI controller.

L_d, L_q : Direct and quadrature inductance components (*H*).

L_m : Mutual inductance (*H*).

P_E : Engine power (*W*).

P_{batt} : Battery power (*W*).

P_{batt_min} : Minimum battery power (*W*).

P_{dem} : Power demand (*W*).

P_m : Electric motor power (*W*).

P_{sh} : Transmission shaft power (*W*).

P_{sc} : Supercapacitor power (*W*).

P_{tr} : Traction power (*W*).

R_s and R_r : Stator and rotor resistance (Ω).

R_{sc} : Supercapacitor internal resistance (Ω).

SoC_{max} : Battery maximum of state of charge.

SoC_{sc} : Supercapacitor state of charge.

T^* : Torque reference (*N.m*).

T_C : Columbic friction torque (*N.m*).

T_{Cont} : Output of the torque hysteresis controller (*N.m*).

T_E, ω_E : Engine torque (*N.m*) and angular velocity (*rad/s*).

T_L : Load torque (*N.m*).

T_e : Electromagnetic torque (*N.m*).

T_{er} : Torque error (*N.m*).

T_{est} : Estimated torque (*N.m*).

T_m, ω_m : Electric motor torque (*N.m*) and angular velocity (*rad/s*).

T_s : Sampling time (*sec*).

T_{sh}, ω_{sh} : Transmission shaft torque (*N.m*) and angular velocity (*rad/s*).

T_{tr} : Traction torque (*N.m*).

V_{sc} : Supercapacitor terminal voltage (*V*).

$V_{sc1}$and V_{sc2} : Supercapacitor terminal voltages at intervals *t1* and *t2* respectively (*V*).

V_{sc-max} : Supercapacitor maximum of terminal voltage (*V*).

i^* : Dynamics of the low frequency current (*Amp*).

i_a, i_b and i_c : Stator currents in a, b and c coordinates respectively (*Amp*).

i_a^*, i_b^* and i_c^* : Stator currents reference in a, b and c coordinates respectively (*Amp*).

i_{sd}, i_{sq} : Direct and quadrature stator currents (*Amp*).

$i_{s\alpha}$, $i_{s\beta}$: Alpha and beta stator currents (*Amp*).

k_E, k_m : Structural parameters of torque coupler.

v_{min} : Minimum vehicle speed (*Km/h*).

v_{sd}, v_{sq} : Direct and quadrature voltages (*V*).

ΔE_{sc} : Change in energy of Supercapacitor (*J*).

θ_s : Stator flux angle (*Degree*).

λ_{Pm}, phi_pm : The permanent magnet flux linkage (*Wb*).

μ_{rr} : Rolling resistance force coefficient

ρ_{fuel} : Fuel density (*MJ/Kg*).

φ_{Cont} : Output of the stator flux hysteresis controller (*Wb*).

φ_{er} : Stator flux error (*Wb*).

φ_{est} : Estimated stator flux (*Wb*).

φ_s : Stator flux amplitude (*Wb*).

φ_s^* : Stator flux reference (*Wb*).

$\varphi_{sd}, \varphi_{sq}$: Direct and quadrature stator flux components (*Wb*).

ω_e : Electrical angular velocity (*rad/s*).

ω_g : General reference frame speed (*rad/s*).

ω_r : Rotor angular velocity (*rad/s*).

ω_{ref} : Reference angular velocity (*rad/s*).

P : Number of poles.

A : Frontal area (m^2).

C, D : Constants.

G, G_m : Gear ratio and motor gear ratio respectively.

K : Polarization constant.

Q : Maximum of battery capacity (*Ah*).

SoC : Battery state of charge.

V : Lyapunov function.

b : The control surface coefficient.

f : The nonlinear function of the dynamic equation.

fc : Fuel consumption (*Liter/Km*).

g : Gravity constant (*N/kg*).

i : Battery current (*Amp*).

it : Extracted capacity.

m : Vehicle mass (*Kg*).

np : Number of pair poles.

r : Wheel radius (*m*).

s : Sliding mode manifold.

v : Vehicle speed (*Km/h*).

γ : Slope angle (*Degree*).

ρ : Air density (Kg/m^3).

ABBREVITIONS

DRB-EMS	: Deterministic Rule Based Energy Management Strategy.
DTC	: Direct Torque Control.
EMS	: Energy Management Strategy.
ESS	: Energy Storage System.
EV	: Electric Vehicle.
FC	: Fuel cell.
FLC	: Fuzzy Logic Controller.
FOC	: Field Oriented Control.
FRB-EMS	: Fuzzy Rule Based Energy Management Strategy.
GUI	: Graphical User Interface.
HESS	: Hybrid Energy Storage System.
HEV	: Hybrid Electric Vehicle.
ICE	: Internal Combustion Engine.
IFOC	: Indirect Field Oriented Control.
IM	: Induction Motor.
Max-SoC-EMS	: Maximum State of Charge Energy Management Strategy.
PI	: Proportional Integral.
PMSM	: Permanent Magnet Synchronous Motor.
PV	: Photovoltaic panel.
SC	: Super-Capacitor.
SMC	: Sliding Mode Controller.

PART 1

INTRODUCTION

Due to the restriction arises on atmospheric pollution caused by gases emissions from internal combustion engines (ICE) and the need for clean energy sources, developments of electric propulsion drive trains in automotive applications, energy sources, and energy management have become very important research areas. Electric vehicles (EVs) and hybrid electric vehicles (HEVs) provide high efficiency and reduce emissions when compared to conventional automobiles. Adapting another energy storage system such as a battery to conventional vehicles leads to an increase in fuel economy that reduces pollution and green gases. Furthermore; the HEV reduces the usage of fossil fuel that led to enhance the vehicle operating range, and also; increases the efficiency of the vehicle which is one the main key-points behind developing a new generation of the automobile [1-3]. However, both EVs and HEVs utilize more electrical components such as electric motors, batteries, power electronics, and their controls that make these types of vehicles more complex when compared to a conventional vehicle [4, 5]. Also, it is harder to design and investigate new configurations or new control schemes in the case of EVs and HEVs than in conventional vehicles due to its complex system [6]. EVs and HEVs in the last decades have been one of the research areas that attracted the attention of researchers. However, in literature; the research in this type of vehicle involves many subpoints starting from developing new configurations and models [7-9] and then end to developing and implementing new control strategies [10, 11]. The electric traction motor is the heart of EVs. Also, it is utilized as the primary mover in most of HEVs configurations. Hence, improving the control strategies of the electric motors is a crucial point of research to improve energy consumption in EVs and HEVs application. It includes developing robust control strategies to achieve good performance, such as good speed tracking and less energy consumption in both acceleration and deceleration operating modes [12, 13]. However, the Sliding Mode

Control (SMC) is taking attention in the literature as it's proving better performance in controlling ac drives [14, 15]. SMC has several advantages compared to other control methods, such as insensitivity to parameter uncertainty and disturbance [16]. Recently SMC has attracted the researcher's attention in EV application, and its robust control is studied widely in the literature for different configurations. In [17-20] a SMC is presented and its behavior is compared with conventional PI controller. Moreover; a combination of SMC and fuzzy control is proposed to control the IM speed in EV applications in [21, 22]. Also in [23] a combination of SMC-DTC is proposed and tested in MATLAB/Simulink for different road scenarios. However, simplifying the control algorithm and ensuring the ease of implementation and maintaining good performance still a point of research in SMC. In this thesis work, a simple and effective SMC algorithm with superior performance in terms of speed tracking and accuracy compared to previous studies is proposed. Furthermore, improved regenerative braking energy recovery in different EV and HEV configurations achieved utilizing the proposed SMC speed controller is compared to the performances of the conventional PI controller and Fuzzy Logic Controller (FLC). A FLC is developed in this work due to its advantages and widely used in AC motor control applications [24-27]. Also, to validate the performance of the proposed SMC for both EV and HEV and taking into consideration the competition between Induction Motor (IM) and Permanent Magnet Synchronous Motor (PMSM) as the preferred selection for EV and HEV applications [28, 29], both IM and PMSM are modeled and used in this work. In addition, the Indirect Field Oriented Control (IFOC) and Direct Torque Control (DTC) strategies are modeled and implemented to control both IM and PMSM as they are competitive for EV and HEV applications [30]. Another decisive part of the vehicle is the Energy Management Strategy (EMS) that manages the power flow between the energy storage system and the traction mover. The traction mover is represented by the electric motor in EVs and both electric motor and ICE in HEVs. The EMS is the decision-maker in this application. However, due to its significant role in this application, many researchers have focused on this area. And they have proposed different algorithms of EMS for each vehicle configuration which can be classified into different categories [31]. The rule-based EMS [32] has several advantages due to its simple structure, low computation, and ease of modification. Also, the use of fuzzy logic in the Fuzzy Rule-Based (FRB) EMS provide strong robustness and the ability

to implement in real-time give more attention to develop and study these type of EMS [33, 34]. Moreover, additional improvement in the energy consumption of the EVs and HEVs achieved using an alternative energy storage system in parallel with the battery pack. A different proposed combination proposed, but still utilizing the Super Capacitor (SC) with the battery pack as a Hybrid Energy Storage System (HESS) takes more attention in EVs and HEVs applications [35, 36]. However, the implementation of this combination always needs robust energy management to manage the power-sharing between both energy storage systems during acceleration and regenerative braking modes to achieve better usage of energy and reduce charge and discharge cycles of the battery pack. Consequently, develop an EMS is an essential part of implementing HESS for EVs and HEVs applications. Hence, different EMS proposed in the literature for HESS [36-38] to improve energy consumption and battery pack lifetime.

All points mentioned above for the EVs and the HEVs need to develop a detailed model for the overall system to investigate the vehicle performance when applying different designs and control strategies. However, several simulation platforms and models were proposed in the literature [4, 39] to simulate EV and HEV, and each of them has its advantages and drawbacks. Simulation packages provide designers/academics with the appropriate tools to simulate and investigate different designs and various control strategies developed for EVs and HEVs before applying them to real-time vehicles. And also, it can be used in the teaching stage of the university students as a reference model of EV or HEV to understand its working principles [40, 41].

A simulation platform based on Matlab m-file coding is developed to simulate EV and Parallel HEV in this work. Each model of the vehicle's components is arranged in a separate Matlab function. The main program file will call back all needed subfunctions to obtain the results depending on the predetermined configuration. A Graphical User Interface (GUI) is designed via the Matlab app designer [42, 43] for the developed code to make it easier for users to simulate the developed platform and investigate different designs and configurations.

In addition to the above-reviewed literature for the different parts of the vehicle, references[2, 44, 45] provide a comparison review of different types of EVs and HEVs in the market based on brand, configuration, and traction motor. It shows that IM and

PMSM are used for more than 90% of the available vehicles on the market now adays. Also, reference [46] shows that the latest developed technologies in the new energy vehicles are using IM or PMSM and their widely utilized DTC and FOC control strategies.. Also, reference [47, 48] reveal that IM and PMSM are the most competitive in EV applications. Also, they introduce a comparison between FOC and DTC as the most used control strategy for traction motor control in EV/HEV applications. Moreover, they demonstrate that DTC has more advantages and more efficiency against the FOC strategy. The study in [12] also provides a table of EV/HEV brands with their motor type used in automobile markets. Table 1.1 demonstrates that over 90% are using IM and PMSM.

Table 1.1. Brand and EM type of EV/HEV available in industry [2, 11, 12, 45]

Make	Model	Traction Motor
Honda	EV Plus	DC Motor
Holden	Ecommodore	SRM
Nissan	Tino, Leaf, Altra	PMSM
Honda	Insight, Accord, Civic	PMSM
Toyota	Prius C & V, Estima Hybrid	PMSM
Toyota	Highlander, Avalon, Camry	PMSM
Ford	Fusion SE Hybrid	PMSM
Ford	C Max Hybrid SEL	PMSM
Hyundai	Blueon	PMSM
Chevrolet	Volt & Energi	PMSM
Renault	Kangoo	IM
Chevrolet	Silverado	IM
Daimler Chrysler	Durango	IM
Tesla	Roadster	IM
Honda	Fit EV	IM
Toyota	Reva4	IM
REVA	NXR	IM
Ford	Focus Electric, Transit Connect	IM
GM	EV1	IM
BMW	X5	IM

Due to the fast growing in EV/HEV trends, and the needs to further improve and develop their control technologies, and investigate new configurations [49-51], the developed platform provide the tools to perform these tasks in Matlab environment as a simulation package, and then it will be easier to implement new algorithms by convert them from MATLAB code to real time prototyping.

As can be understood from these, the types of Electric Motors used in EVs and HEVs are mainly IM and PMSM. In this thesis, a comprehensive study is made to demonstrate which EM type is more efficient to be used for EV/HEV applications. And a GUI has been created based on the developed software to provide the tools to determine which choice will be made. In addition, the software is expanded, so the decision of which vector control strategy IFOC or DTC for IM or PMSM is made. However, the novelty of this study is the new simulation platform that can help researcher and EV/HEV manufacturers to investigate new technologies and to further improve existing technologies to enhance vehicles' performances and increasing its energy efficiency.

The contributions of the thesis include the superior performance of the proposed SMC in terms of speed tracking and improved energy consumption when utilized for the EV and Parallel HEV as a speed controller as compared to PI and FLC controller performances. Also, the developed simulation platform that consists of detailed models of all parts of the EV and Parallel HEV as Matlab m-file functions has shown good performance and can be used to simulate and investigate different vehicle configuration. Furthermore, the results obtained by applying the HESS to the EV and the Parallel HEV indicate an improvement in energy consumption. The achieved results enhance the battery's lifetime and increases the energy efficiency of the vehicle with advantage to the Max-SoC EMS over the FRB EMS in case of Parallel HEV. And finally, the developed platform provides the needed tools to perform any further comparisons or studies for different configuration, traction motors and their control strategies.

In part one of the thesis, an introduction to the thesis's topic is given, with brief information from the literature. And then, in part two, a detailed explanation of the vehicle configurations, dynamics, and components modeling is given. Also, the proposed SMC and the different EMS utilized in the thesis are explained in detail. In part three, the designed GUI is explained. In part five, the obtained results of the different EV and Parallel HEV configurations are presented, and a detailed data comparison is concluded. And lastly, the conclusion is given in part five.

PART 2

ELECTRIC AND HYBRID ELECTRIC VEHICLE MODELING

2.1. ELECTRIC VEHICLE

EVs mainly use an electric motor to propel the vehicle and chemical battery as energy storage source. They are configured as in Figure 2.1.

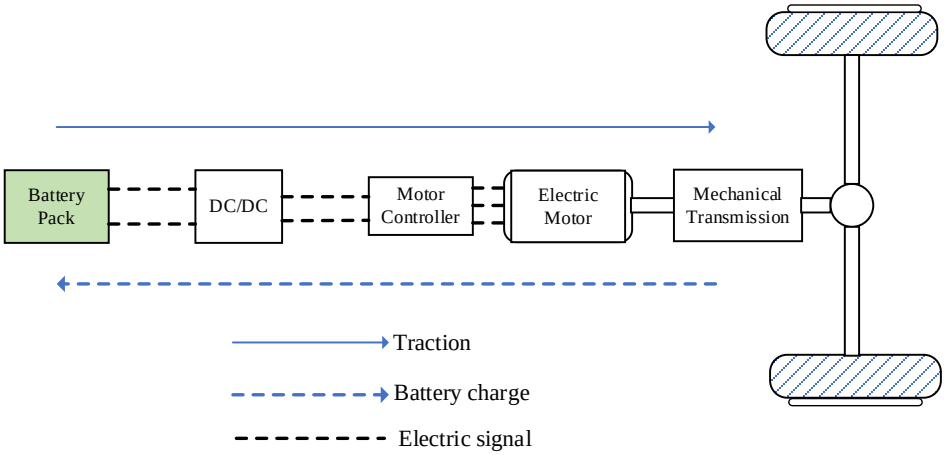

Figure 2.1. Configuration of Electric Vehicle [52].

In EVs, the demand traction power is provided by the electric motor through the mechanical transmission to the vehicle wheels. Also, the demand energy of the traction motor to meet traction power demand is supplied by the battery pack. Furthermore, EVs have three operating modes, which are stop mode, propelling mode and regenerative braking mode, moreover; the power flow in propelling, and regenerative modes are illustrated by traction and charging arrows as in Figure 2.1.

2.3. HYBRID ELECTRIC VEHICLE

The combination of the advantages of EVs such as high energy efficiency and zero environmental pollution with the higher operating range of conventional vehicles due to the higher energy density of the gasoline provides a vehicle with high efficiency and reduced emissions. In HEVs, to reduce complexity usually, two power sources are utilized to develop the traction power needed to propel the vehicle and these two sources should carry sufficient energy onboard to support the sufficient driving range of the vehicle. Generally, in literature, the HEVs are classified into three different configurations, which are Parallel hybrid, Series hybrid, and Series-Parallel Hybrid Electric Vehicles. Each of them has its advantages and drawbacks. The three configurations of the HEVs are shown in Figure 2.2 to Figure 2.4.

2.3.1. Parallel Hybrid Electric Vehicle

The main configuration of Parallel-HEV considered in this study is shown in Figure 2.2.

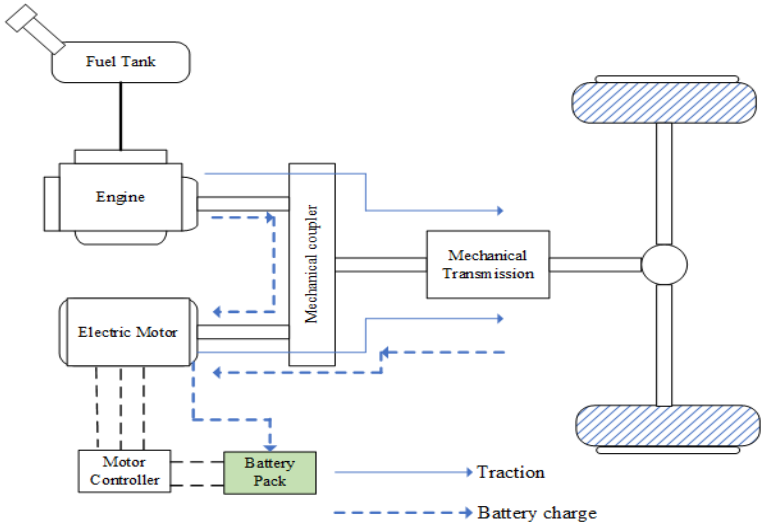

Figure 2.2. Configuration of Parallel Hybrid Electric Vehicle [52].

In parallel HEV configuration both engine and motor are mechanically connected to propel the vehicle, moreover; in this configuration smaller electric motor can be used as both power sources can share the demand power at any instant time. The traction arrows illustrate the direction of the power flow from power sources to transmission to propel the vehicle through the mechanical coupler to the wheels of the vehicle. The battery charge arrow which is represented in the figure as a dashed arrow illustrates

the ways of recharging the battery pack, either by the engine or by regenerative braking energy during deceleration of the vehicle [52]. Additional to modeling of the EV, engine, and torque coupler models are required. However, for reducing the complexity of the system lookup-map tables can be used to model engine characteristics, and they are used to calculate engine variables needed for simulation and to plot engine efficiency and fuel consumption. The ICE data used in look-up tables are obtained from ADVISOR-Simulator and saved as (ICE_data.mat) file in our simulation software. The mechanical coupler in Figure 2.2, has three ports, the first port is connected to the engine side, which can be connected directly or through mechanical transmission depending on the proposed design. The second port is connected to the electric motor side, and the third port is connected to the driven wheels through a mechanical link. In the torque coupler, the input power is always equal to the output power if the losses were ignored [52]. Therefore, the output power can be expressed by:

$$P_{sh} = P_E + P_m \tag{2.1}$$

Where, P_{sh} is the power at the transmission shaft side, P_E is engine power, and P_m is the electric motor power. Equation 2.1 can be rewritten as:

$$T_{sh}\omega_{sh} = T_E\omega_E + T_m\omega_m \tag{2.2}$$

Where, T_{sh}, T_E ,and T_m are transmission shaft torque, engine torque, and motor torque respectively.

ω_{sh}, ω_E, and ω_m are transmission shaft angular velocity, engine angular velocity, and motor angular velocity respectively.

And the torque coupler output can be obtained by:

$$T_{sh} = k_E T_E + k_m T_m \tag{2.3}$$

Where, k_E and k_m are the structural parameters of the torque coupler at ports 1 and 2 respectively.

And the three ports angular speeds are linked as:

$$\omega_{sh} = \frac{\omega_E}{k_E} = \frac{\omega_m}{k_m} \tag{2.4}$$

Where, engine and motor velocity are always relative to shaft angular speed by the values of k_E and k_m.

2.3.2. Series Hybrid Electric Vehicle

The second configuration of HEVs is the series HEV, the most often used configuration of series HEV can be seen in Figure 2.3. In series configuration, the electric motor is only propelling the vehicle and the engine supports the battery pack through the generator, when the battery pack capacity is not sufficient to provide the needed power to the motor to propel the vehicle, furthermore; the engine can be used to charge the battery pack even during standstill mode.

The engine in this configuration is mechanically connected to an electrical generator to produce needed electric energy and the generator is electrically coupled with the battery pack. Moreover; the direction of power flow in this configuration can be observed in Figure 2.3. In propelling mode, the vehicle utilizes energy from the battery pack or both battery and (Engine-generator), also; the battery pack can be recharged using regenerative braking or (Engine-generator). These different operation modes are illustrated by the traction and charging arrows in the figure below.

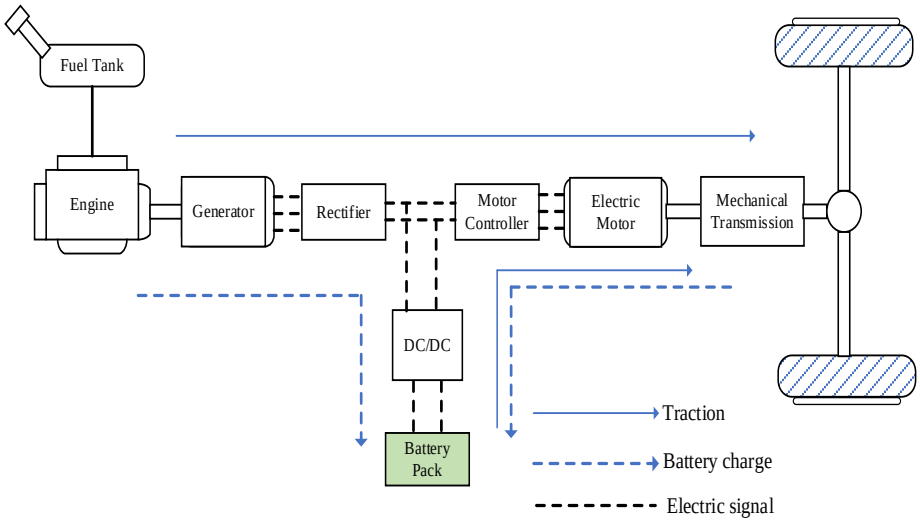

Figure 2.3. Configuration of Series Hybrid Electric Vehicle [52].

2.3.3. Series Parallel Hybrid Electric Vehicle

Another configuration of the HEVs is the series-parallel HEV, which is configured as in Figure 2.4. In the configuration, the engine is mechanically coupled with the generator which is electrically coupled to the battery pack side to configure the series

HEV. Furthermore, the engine is mechanically coupled to the traction electric motor to configure the parallel HEV configuration. The series-parallel HEV configuration is more complicated than the other two configurations and needs a complex control strategy to manage all possible operating modes.

Both advantages of series and parallel are combined, however; a more complex control system is needed in this configuration.

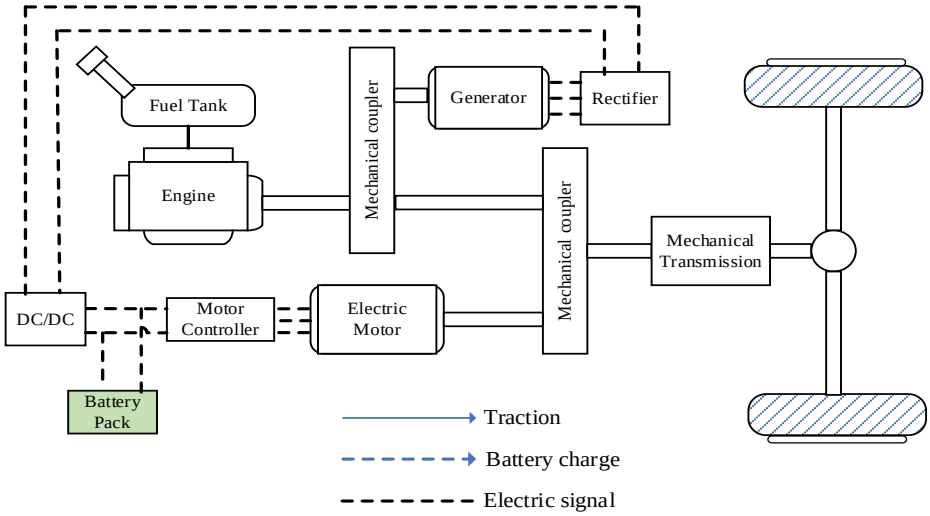

Figure 2.4. Configuration of Parallel-Seiries Hybrid Electric Vehicle [52].

2.4. MOTION DYNAMIC MODELLING

Generally, the vehicle needs to overcome the resistive forces to start moving. It is essential to take these forces into account in the vehicle modeling. The tractive effort represents the total force transmitted to the ground to propel the vehicle [53-55].

It is essential to derive this component when developing a vehicle model. However, this force includes the following four components:

- The rolling resistance force (F_{rr}).
- The hill climbing force (F_{hc}).
- The aerodynamic drag force (F_{ad}).
- The acceleration force (F_{la}).

Consider a vehicle mass m (kg), moving at a speed v (km/h) up an angle γ slope in degree, as shown in Figure 2.5.

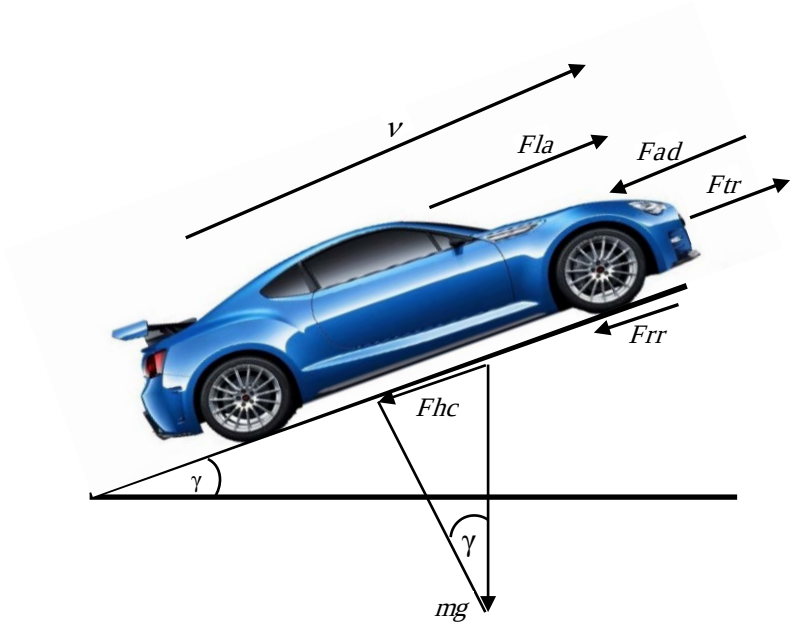

Figure 2.5. Acting forces on the vehicle.

The rolling resistance force (F_{rr}) is arising from the friction of the vehicle tire on the road. Furthermore, it's related to the vehicle weight by the relation:

$$F_{rr} = \mu_{rr} \times m \times g \tag{2.5}$$

The aerodynamic drag force arises from the friction caused by the vehicle body moving through the air and given by:

$$F_{ad} = 0.5 * \rho \times A \times C_d * v \tag{2.6}$$

The hill-climbing force which represents the component of the vehicle weight that acts along the slope is given by:

$$F_{hc} = m \times g \times sin(\gamma) \tag{2.7}$$

If the vehicle speed demand changes When the demand of the vehicle velocity changes, an extra force needs to be added to the total forces. The needed linear acceleration will be provided by this force. This additional force is presented by Newton's law:

$$F_{la} = m \times a \tag{2.8}$$

So, the total tractive force will be given by:

$$F_{tr} = F_{rr} + F_{hc} + F_{ad} + F_{la} \tag{2.9}$$

And the motor torque is related to the total tractive force by the relation:

$$T_{tr} = F_{tr} \times \frac{r}{G} \tag{2.10}$$

The traction power to drive the vehicle at speed v is given by:

$$P_{tr} = F_{tr} \times v \tag{2.11}$$

The transmission of the EV is much simpler than ICE vehicles and Hybrid Vehicles. However, utilizing a clutch is not required because the speed can be increased from zero to maximum speed depending on the electric motor speed range. However, the motor speed is transmitted to the vehicle wheels via the gears.

2.5. TRACTION MOTOR DRIVE

2.5.1. Induction Motor Modelling

Induction motor is preferred in EV and HEVs due to its superior advantages compared with other types of motors. The IM can rapidly reach the desired speed reference with a good energy gain within the limits of safe current both on generator and motor modes [53, 56, 57].

In general, IM can be modeled in a fifth-order model that includes the speed and other variables which are rotor fluxes and stator currents. It is worth noting that both, stator and rotor currents have 2-dimensional components, i.e. direct (d) and quadrature (q) axis components [58].

Therefore, the fifth-order state variable form of an IM can be expressed by:

$$\frac{di_{sd}}{dt} = \frac{L_r R_s + \frac{L_m^2}{\tau_r}}{\sigma\, L_r L_s} i_{sd} + \omega_g i_{sq} + \frac{L_m}{\tau_r \sigma\, L_r L_s} \varphi_{rd} + \frac{L_m}{\sigma\, L_r L_s} \omega_r \varphi_{rq} + \frac{1}{\sigma\, L_s} v_{sd} \tag{2.12}$$

$$\frac{di_{sq}}{dt} = \frac{L_r R_s + \frac{L_m^2}{\tau_r}}{\sigma\, L_r L_s} i_{sq} - \omega_g i_{sd} + \frac{L_m}{\tau_r \sigma\, L_r L_s} \varphi_{rq} - \frac{L_m}{\sigma\, L_r L_s} \omega_r \varphi_{rd} + \frac{1}{\sigma\, L_s} v_{sq} \tag{2.13}$$

$$\frac{d\varphi_{rd}}{dt} = \frac{L_m}{\tau_r} i_{sd} - \frac{L_m}{\tau_r} \varphi_{rd} + (\omega_g - \omega_r)\varphi_{rq} \tag{2.14}$$

$$\frac{d\varphi_{rq}}{dt} = \frac{L_m}{\tau_r} i_{sq} - \frac{L_m}{\tau_r} \varphi_{rq} - (\omega_g - \omega_r)\varphi_{rd} \tag{2.15}$$

$$\frac{d\omega_r}{dt} = -\frac{3npL_m}{2J_m L_r}\left(\varphi_{rd} i_{sq} - \varphi_{rq} i_{sd}\right) - \frac{B_m}{J_m}\omega_r - \frac{1}{J_m} T_C - \frac{1}{J_m} T_L \tag{2.16}$$

Where, τ_r is the rotor time constant, given by: $\tau_r = L_r/R_r$, and σ is the leakage constant given by: $(L_r L_s - L_m^2)/(L_r L_s)$.

v_{sd}, v_{sq} are d and q axis components of stator voltage. i_{sd}, i_{sq} are d and q axis components of stator current. φ_{rd} , φ_{rq} are d and q axis components of rotor flux. L_s, L_r are stator and rotor total inductance respectively. L_m is the mutual inductance between stator and rotor. ω_g is a general reference frame speed in electrical rad/sec. ω_r is the rotor speed in electrical rad/sec. $J_m$and B_m are motor inertia and viscous friction coefficient respectively. np is the number of pole pairs. T_L is the load torque, and T_C is the columbic friction torque.

The electrical dynamics of the IM are represented by Equations (2.12) to (2.15), and Equation (2.16) represents the mechanical dynamics.

2.5.2. Permanent Magnet Synchronous Motor Modelling

PMSMs can offer advantages in terms of higher efficiency, low inertia, and specific power if compared to IMs. However, it's another best-suited traction motor type for HEVs applications. And it is widely investigated in literature and used in the industry of EVs and HEVs applications. The PMSM can be modeled in the d-q frame using the following set of equations [59].

$$\frac{di_{sd}}{dt} = \frac{1}{L_d}(v_{sd} - R_S * i_{sd} + L_q * i_{sq} * \omega_e) \quad (2.17)$$

$$\frac{di_{sq}}{dt} = \frac{1}{L_q}(v_{sq} - R_S * i_{sq} - (L_d * i_{sd} + \lambda_{Pm}) * \omega_e) \quad (2.18)$$

$$T_e = \frac{3}{2} * \frac{P}{2} * (\lambda_{Pm} * i_{sq} + (L_d - L_q) * i_{sd} * i_{sq}) \quad (2.19)$$

$$\frac{d\omega_r}{dt} = \frac{1}{J_m} * (T_e - T_L - B_m * \omega_r) \quad (2.20)$$

Where,

i_{sd} and i_{sq} are the direct and quadrature currents respectively.

v_{sd} and v_{sq} are the direct and quadrature voltages.

L_d and L_d are the direct and quadrature inductances.

R_S is the stator winding resistance.

λ_{Pm} is the permanent magnet flux linkage.

T_e is the electromagnetic torque.

ω_e is the electrical angular velocity.

ω_r is the rotor angular velocity.

J_m is the moment of inertia of the motor, and B_m is the damping coefficient of the motor.

Furthermore; flux components can be calculated using the following expressions:

$$\varphi_{sd} = L_d * i_{sd} + \lambda_{Pm} \quad (2.21)$$

$$\varphi_{sq} = L_q * i_{sq} \quad (2.22)$$

2.6. TRACTION MOTOR CONTROL STRATEGIES

Since the electric motors used in the EVs and HEVs are the main traction drive, thus speed and torque control of these motors is the key point to meet the vehicle speed demand. Utilizing a well-designed and tuned controller that can drive the motor to the reference speed with less effort and time, and reducing torque and current ripples leads to reduce energy consumption. The advantages of vector control methods for AC machines such as high performances and fast response over scalar control method make them a good choice to be used to control AC machines in HEVs applications due to the need for fast and high-performance control strategy [60, 61]. However, FOC and DTC methods are the two well-known vector control methods used to control IM and PMSM.

2.6.1. Field Oriented Control (FOC)

One of the most well-known schemes used to control IM is the FOC. It is a high-performance method used to control IMs by controlling the stator currents. It's based on converting the three-phase currents of the stator into two orthogonal components (i.e. d-q coordinates). The flux is represented by the d component, whereas the q component represents the motor torque. Figure 2.6. illustrates the basic scheme of the

Indirect Field Oriented Control (IFOC), where the angle of space between stator and rotor fields varies with the load in the traction motor drive [58, 62].

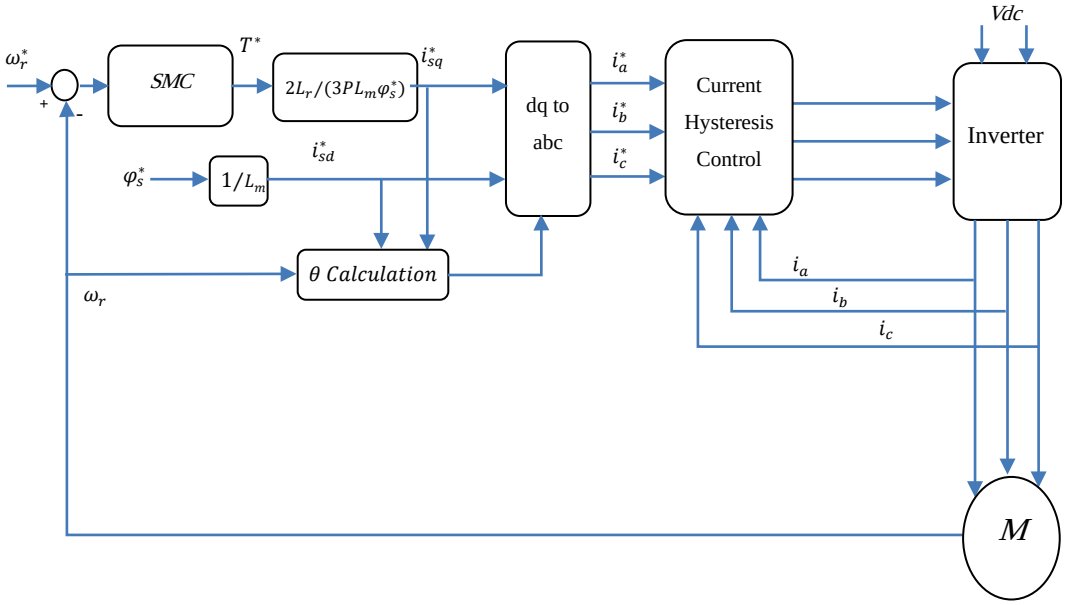

Figure 2.6. Basic scheme of IFOC strategy.

The basic scheme shown in the figure above will be used in the developed system to control the speed of the motor utilized in the EV. Basically, for the 3-phase machine; the 3-phase current (abc) is sensed and then transformed into a stationary reference frame (α-β) when required using Clark transformation as shown in Figure 2.7.

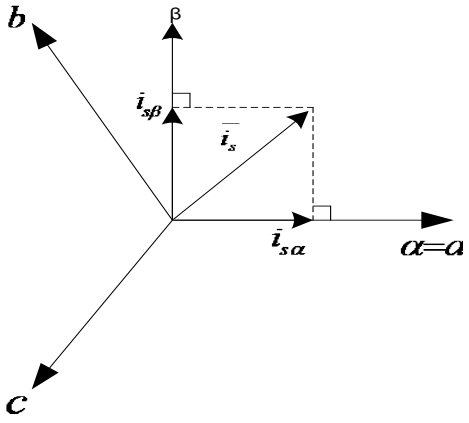

Figure 2.7. 3-phase to 2-phase coordinate transformation.

The transformation illustrated in Figure 2.7 above can be expressed by:

$$i_{s\alpha\beta} = \frac{2}{3} * \begin{bmatrix} 1 & -\frac{1}{2} & -\frac{1}{2} \\ 0 & \frac{\sqrt{3}}{2} & -\frac{\sqrt{3}}{2} \end{bmatrix} \begin{bmatrix} i_a \\ i_b \\ i_c \end{bmatrix} \quad (2.23)$$

Then using Park transformation; the two stationary coordinates are transformed into two rotating coordinates (*d-q*) as shown in Figure 2.8.

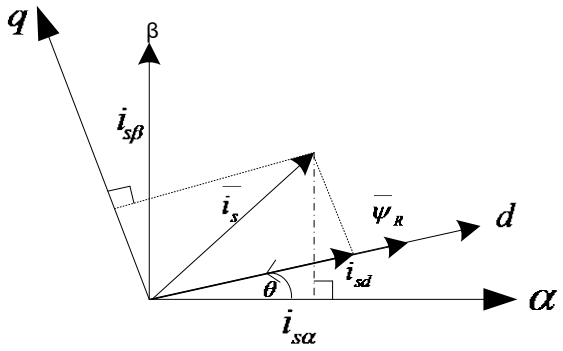

Figure 2.8. α-β and d-q coordinates.

Park transformation can be obtained by:

$$i_{sdq} = \begin{bmatrix} cos(\theta) & sin(\theta) \\ -sin\,(\theta) & cos\,(\theta) \end{bmatrix} \begin{bmatrix} i_{s\alpha} \\ i_{s\beta} \end{bmatrix} \quad (2.24)$$

Where, θ is the rotor flux angle.

However, in the IFOC based hysteresis current control the calculated current reference values i_{sq}^* and i_{sd}^* are transformed from *d-q* coordinate to *abc* coordinate which will be used as inputs to the three hysteresis controllers to produce a switching signal to the inverter to drive the traction motor [63].

In general, the three components i_a, i_b and i_c are compared with their reference values i_a^*, i_b^* and i_c^*. Then the required switching signals for the voltage source inverter are calculated by the three hysteresis controllers to supply the traction motor with the required voltage. The three-phase inverter is supplied by DC voltage, which is the battery pack in this application.

The IFOC strategy-based IM and PMSM control are implemented with conventional PI and FLC and compared with the proposed SMC Controller to investigate the performances of the three controllers.

2.6.2. Direct Torque Control (DTC)

Another well-known control method used to control AC motors is the Direct Torque Control (DTC) method. This method provides robust and fast torque responses. The general scheme of this method is shown in Figure 2.9.

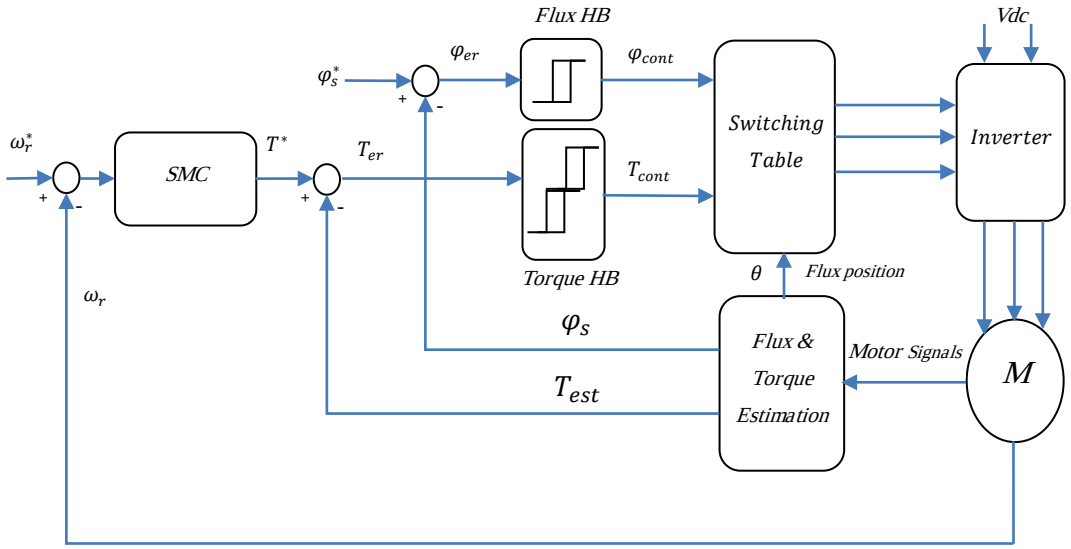

Figure 2.9. Basic scheme of DTC strategy.

The main core of the DTC method is the torque, flux hysteresis controllers, and the logic switching table that is used to select the appropriate voltage space vector. In the DTC method, the measured signal such as stator voltages and currents are used to estimate the stator flux and torque with the following equations:

$$\varphi_{sd} = \int (v_{sd} - R_s i_{sd}) dt \tag{2.25}$$

$$\varphi_{sq} = \int (v_{sq} - R_s i_{sq}) dt \tag{2.26}$$

Where, the amplitude and the angle of the stator flux can be calculated by:

$$\varphi_s = \sqrt{\varphi_{sd}^2 + \varphi_{sq}^2} \tag{2.27}$$

$$\theta_s = tan^{-1}\left(\frac{\varphi_{sq}}{\varphi_{sd}}\right) \tag{2.28}$$

And the torque can be estimated by:

$$T_e = \frac{3}{2} P(\varphi_{sd} * i_{sq} - \varphi_{sq} * i_{sd}) \quad (2.29)$$

Then the estimated flux and torque are compared with their reference values.

The errors of the torque and flux signals are directly used by the hysteresis controllers to generate the required commands that are utilized with the sector number by the appropriate switching table to determine the appropriate voltage vector to drive the inverter in such a way to keep the flux and torque errors within the hysteresis bands as shown in Figure 2.10. The basic switching table used in the DTC method is shown in Table 2.1.

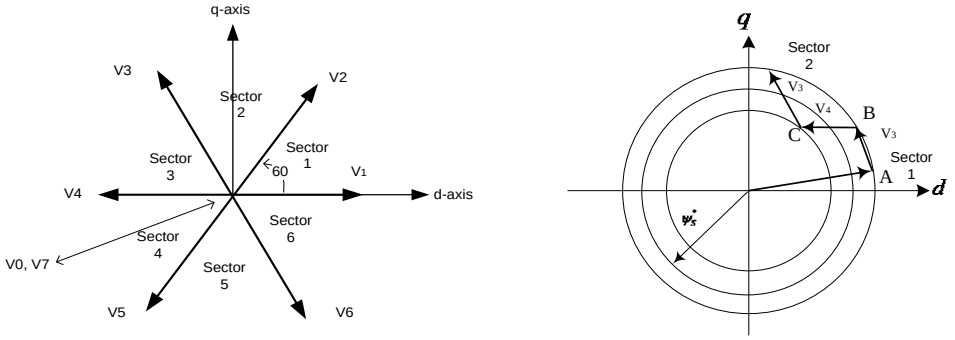

(a) (b)

Figure 2.10. (a) Voltage space vectors and their appropriate sectors. (b) Stator flux control.

Table 2.2. Basic switching table of DTC

Flux	**Torque**	**Sector**					
Δψ	**ΔTe**	**S1**	**S2**	**S3**	**S4**	**S5**	**S6**
1	1	V2	V3	V4	V5	V6	V1
	0	V7	V0	V7	V0	V7	V0
	-1	V6	V1	V2	V3	V4	V5
-1	1	V3	V4	V5	V6	V1	V2
	0	V0	V7	V0	V7	V0	V7
	-1	V5	V6	V1	V2	V3	V4

FOC and DTC methods will be utilized in this work to control the IM and PMSM based on different proposed controllers to improve the energy consumption of the

EV/HEV and to prove the suitability of the developed package to simulate the EV/HEV behavior.

2.7. TRACTION MOTOR SPEED CONTROL

Three different controllers are used in this work to control the traction-motor speed which are conventional Proportional Integral (PI), Fuzzy Logic Controller (FLC), and the proposed Sliding Mode Controller (SMC), however, due to the simple structure of the PI controller which can be implemented easily, it will be used in this study for comparison with the performances of other controllers.

PI controller is one of the simplest and effective types of conventional controller. The control signal of the PI controller in this study is the torque reference signal and it can be obtained with the expression:

$$T^* = K_p * (\omega_{ref} - \omega_r) + K_i \int (\omega_{ref} - \omega_r) * T_s \quad (2.30)$$

Where, T^* is the torque reference signal, ω_{ref} is the speed reference value, ω_r is actual rotor speed, K_p and K_i are the proportional and integral gains respectively and T_s is the time interval.

2.7.1. Fuzzy Logic Controller (FLC)

A Fuzzy Logic Controller (FLC) is designed in this work to control the speed of IM used in the EV application. However, the advantages of the FLC such as simplicity, ease to understand, ease of modification, ease to implementation, and robustness make this controller an appropriate choice in vector control of AC machines, particularly; when high performance is needed due to the operating conditions[26].

In FLC, the membership functions and the rule base are usually modeled with data from the system to be controlled or using human experience. However, using data to model the FLC helps to obtain the suitable fuzzy sets and rules for any specified drive cycle in HEV. Fuzzy logic is an artificial intelligence technique based on linguistic rules that can be defined as: If A is X and B is Y then C is Z.

where,

A and B represent the input to the controller and C is the output of the controller.

X and Y are the input membership functions and Z is the output membership function.

The general structure of the fuzzy controller is shown in Figure 2.11. A fuzzy controller consists of four parts which are: fuzzification, inference engine, rule base, and defuzzification.

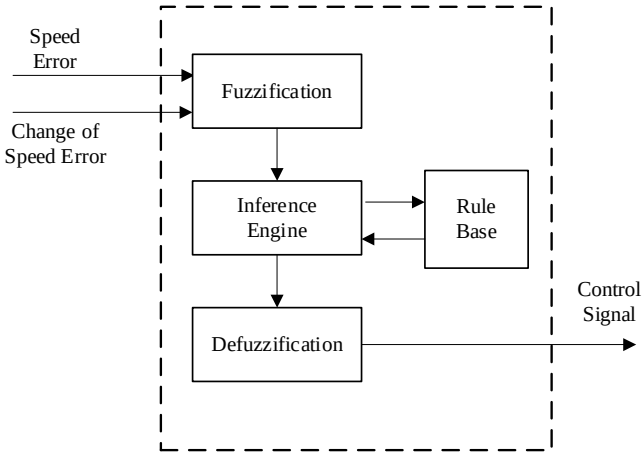

Figure 2.11. Fuzzy Logic Controller structure.

The proposed fuzzy controller consists of two inputs. First is the speed error (e) and the derivative of speed error (de). Both inputs are transformed to fuzzy variables scaled from 0 to 1. The output of the fuzzy controller will be the reference torque. In this work, FLC consists of seven triangular membership function types. Thus, the decision of the fuzzy inference consists of 49 rules for the two inputs (e, de). These rules are expressed in the if-then form to identify the consequence output torque response to the input signals to reach the desired speed. Figure 2.12 shows the arrangement of the two inputs membership functions for the FLC.

The membership functions of the inputs used in the proposed fuzzy controller are named for the speed error signal as NBe (Negative Big error), NMe (Negative Medium error), NSe (Negative Small error), Ze (Zero error), PSe (Positive Small error), PMe (Positive Medium error), and PBe (Positive Big error). And for the change of speed error as NBde (Negative Big change of error), NMde (Negative Medium change of error), NSde (Negative Small change of error), Zde (Zero change of error), PSde (Positive Small change of error), PMde (Positive Medium change of error), and PBde (Positive Big change of error). Table 2.2 shows the 49 rules used in the proposed FLC.

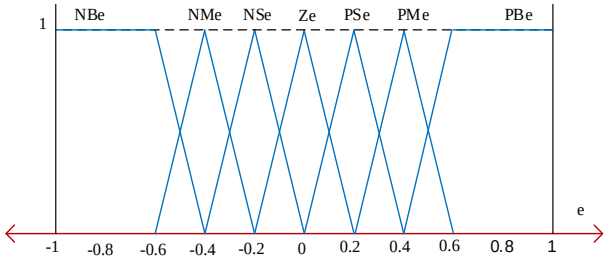

(a)

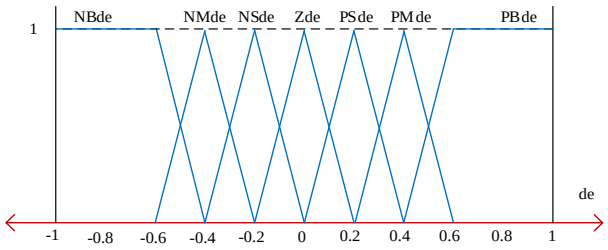

(b)

Figure 2.12. Inputs membership functions of FLC. a) Speed error. b) Change of speed error.

Table 2.3 Membership functions of FLC.

(e) / (de)	NBe	NMe	NSe	Ze	PSe	PMe	Be
NBde	NB	NB	NB	NB	NM	NS	NB
NMde	NB	NB	NB	NM	NS	NM	PS
NSde	NB	NB	NM	NS	NS	PS	PM
Zde	NM	NB	NS	Z	PS	PM	PB
PSde	NS	NM	PS	PS	PM	PB	PB
PMde	PM	NM	PS	PM	PM	PB	PB
PBde	PS	PB	PM	PB	PB	PB	PB

2.7.2. Sliding Mode Controller (SMC)

The sliding mode control (SMC) is a well-established robust control method for the control of uncertain systems. In this thesis, the SMC is employed as a speed controller to the traction motor to track the desired speed trajectory of the EV. The controller is designed using the dynamic equations of the EV system with induction motor in state-space form.

A sliding manifold is selected to define the relationship between state variables and the prescribed dynamics. Then the control law is designed to drive the state trajectories to the manifold and restrict them there. Sliding mode is a working mode of variable structure systems, which can be described by:

$$\begin{cases} \dfrac{dx}{dt} = f(x,t,u), x \in R^n, u \in R^m \\ \quad u = \begin{cases} u^+(x,t), s(x) > 0 \\ u^-(x,t), s(x) < 0 \end{cases} \\ s^T = (s, \dots\dots\dots\dots\dots\dots\dots, s^m) \end{cases} \tag{2.31}$$

For this system, the discontinuous control input forms the sliding surfaces in state space to achieve (s=0). In practice, due to the pulse width modulated signal, the non-ideal switching structure of the signal is an example of the formation of these sliding surfaces. Similarly, in an adaptive control system, the continuous adjustment of the parameters in relation to the output signal also means the generation of a non-continuous control signal, which causes a shift mode in the state space at discontinuous points. The resulting new system motion is defined by an equation of degree of shift mode (n-m). In order to derive this equation of motion in slip mode, the control input must be replaced with the expression “equivalent control”.

The sliding surface expresses the relationship between system state variables and system dynamics. As a result of this discontinuous switching process, it is conceivable that the signal will ideally go to infinity in moments of the gap. However, due to the internal and external disturbance dynamics of the system, the gain is prevented from going to infinity. In order to eliminate the disturbance effect, it is necessary to limit the parameters by defining a boundary layer around the shift mode, given that the time constant is neglected in the non-continuous ideal control signal.

Consequently, a robust control approach is derived by:

$$\frac{dx}{dt} = f(x,t) + b(x,t) \times u \tag{2.32}$$

Where f is the nonlinear function of the dynamic equation and b is the control surface coefficient.

Similarly, the control system in this structure is represented as:

$$x_1 = f_1|x_1, t, s_0(x_1)|, f_1 \in R^{n-m} \tag{2.33}$$

It is possible to decompose the order of the sliding-mode equation and to make it independent regarding the control signal (*u*). For this reason, the function of the appropriate sliding mode surface *s(x)* or $s_0(x1)$, must be determined. Therefore, to ensure stability it is important to have the appropriate discontinuous control signal. On the other hand, in practice, the disadvantage of the SMC method is the chattering problem. This occurs when the sliding controller is switched by non-modeled dynamics of the system during high switching frequency operation. However, when the system state-space representation is considered, a chattering-free SMC algorithm can be developed using derivation in [16].

$$\begin{cases} \dfrac{dx_1}{dt} = x_2 \\ \dfrac{dx_2}{dt} = f + bu \end{cases} \tag{2.34}$$

The sliding mode manifold will be expressed as:

$$s = Ce + \frac{de}{dt}, \qquad (C > 0) \tag{2.35}$$

Where, $e = x_1^r - x_1$ and $^{de}/_{dt} = x_2^r - x_2$ respectively, and *C* is constant.

Moreover, a Lyapunov function (V) is selected to assurance the stability of error dynamics and expressed by:

$$\begin{cases} V = \dfrac{1}{2} s^T s > 0 \\ \dfrac{dV}{dt} = s^T \dfrac{ds}{dt} < 0 \end{cases} \tag{2.36}$$

By selecting the term $^{ds}/_{dt} = -Ds$, for $D > 0$, from (2.30) we obtain:

$$\frac{dV}{dt} = s^T \frac{ds}{dt} = -s^T Ds < 0 \tag{2.37}$$

$$\frac{ds}{dt} + Ds = 0 \tag{2.38}$$

where; *D* is constant,

Similarly, by calculating the derivative of (2.35) and substituting from (2.34), the result obtained is:

$$\frac{ds}{dt} = C\frac{de}{dt} + \frac{d^2e}{dt^2} = C\frac{de}{dt} + \frac{dx_2^r}{dt} - f - bu \tag{2.39}$$

The equivalent control statement that satisfies the relation: $ds/dt = 0 \rightarrow u = u_{eq}$ is attained by:

$$u_{eq} = \frac{1}{b}\left(\frac{dx_2^r}{dt} - f - C\frac{de}{dt}\right) \tag{2.40}$$

In same way, from (2.39) we obtain:

$$\begin{cases} \dfrac{ds}{dt} = b(u_{eq} - u) \\ b(u_{eq} - u) + Ds = 0 \end{cases} \tag{2.41}$$

Discretizing the equations (2.40) and (2.41) gives:

$$\frac{s(k) - s(k-1)}{T_s} = b\left[u_{eq}(k-1) - u(k-1)\right] \tag{2.42}$$

$$b\left[u_{eq}(k) - u(k)\right] + Ds(k) = 0 \tag{2.43}$$

From (2.42) and (2.43), $u_{eq}(k)$ and $u_{eq}(k\text{-}1)$ can be defined as:

$$u_{eq}(k-1) = u(k-1) + \frac{s(k) - s(k-1)}{bT_s} \tag{2.44}$$

$$u_{eq}(k) = u(k) - \frac{D}{b}s(k) \tag{2.45}$$

Assuming that within one period the control signal ueq(k) will remain constant.

$$u_{eq}(k) \cong u_{eq}(k-1) \tag{2.46}$$

Thus,

$$u(k) = u(k-1) + \frac{s(k) - s(k-1)}{bT_s} + \frac{D}{b}s(k) \tag{2.47}$$

Lastly, the control command will be defined by,

$$u(k) = u(k-1) + \frac{1}{bT}[s(k)(1 + DT_s) - s(k-1)] \tag{2.48}$$

Equation (2.48) is used in the proposed study to implement the SMC controller, where *u(k)* represents the control signal, *s(k)* represents the speed error signal, *D* is constant, *b* represents motor inertia and T_s is the sampling time.

However; the error between actual and reference speed is processed through the mathematical model of the proposed SMC to generate the required torque reference to the drive motor to track the desired speed. The proposed SMC is utilized as presented in Figure 2.13.

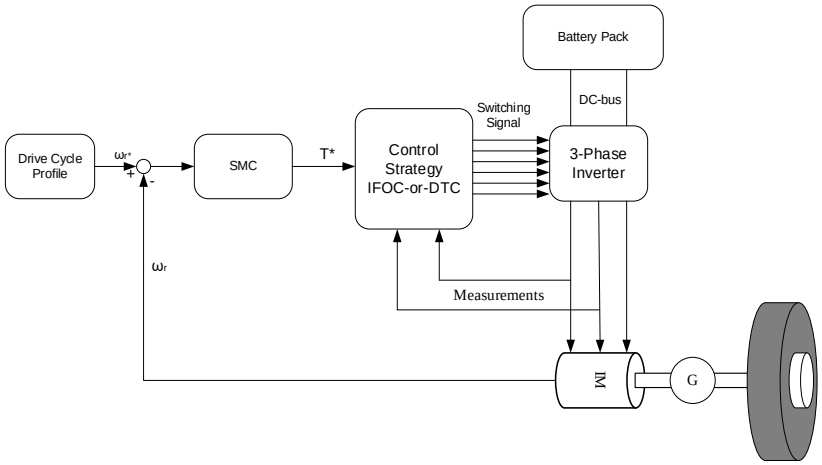

Figure 2.13. EV driven by IM-based SMC speed controller.

Both continuous SMC and discrete SMC methods were applied in this study separately, but the best results were obtained with the discrete SMC method. Therefore, for this reason, in this study, only theoretical information and simulation results of the discrete SMC method are included.

2.8. INTERNAL COMBUSTION ENGINE (ICE)

The Internal Combustion Engine (ICE) is one of the main components of the HEV, it provides the additional necessary energy for the HEV when driving in high way (high speed), either by directly connected to the transmission gears using the mechanical rotating as in parallel configuration or by connecting the mechanical part of the engine to a generator that can be used to supply the motor with the required electric energy to achieve the demand torque and speed, or can be used to recharge the battery when its capacity or the SoC drops to the minimum level. However, in this research due to the complexity of ICE modeling; data lookup tables were downloaded from ADVISOR simulation software used to simulate ICE behavior and to calculate efficiency and fuel consumption of the ICE.

To obtain the fuel consumption for each interval in the simulation period 2-D interpolation method was used based on the lookup tables of the engine data.

Further, to investigate and observe the fuel consumption of the engine for each operating scenario the amount of the fuel used can be calculated by the following expression [64].

$$Liter_{engine} = \int_0^t \frac{fc}{\rho_{fuel}} dt \tag{2.49}$$

Where, *fc* is fuel consumption in grams/sec, ρ_{fuel} is fuel density in (grams/liter).

2.9. ENERGY STORAGE SYSTEM

2.9.1. Battery Modelling

The battery pack is the energy source of the EV. However, developing a battery model is an important issue to investigate the behavior of the whole EV system. Different battery technologies are available such as Lithium-ion, Nickel-metal hydride, Lead-acid, etc. Still, Lithium-ion (Li-ion) battery is the favorite choice for the EV, Due to its distinguishing features as compared to other types. These features include low self-discharge rate, high cell voltage, high energy density, and long cycle life [65, 66]. The battery pack provide the electric motor with the power needed to propel the EV. Therefore, the battery pack has a high effect on the functional performance of the traction motor and the operating range of the EV.

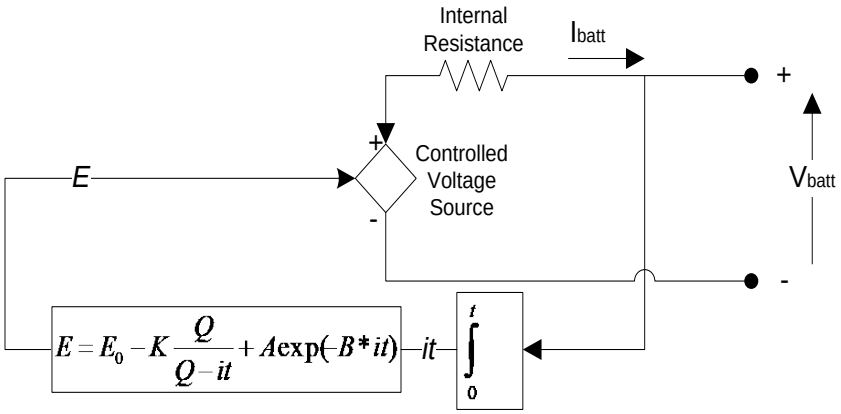

Figure 2.14. Battery electric model.

The battery-electric model shown in Figure 2.14 can represent the battery behavior and can be used to calculate the SoC of the battery pack. The model consists of a voltage source in series with constant resistance.

The mathematical model of the Li-ion battery can be expressed as follows [67].

Discharge model ($i^* > 0$)

$$f_1(it, i^*, i) = E_0 - \frac{K \times Q}{Q - it} \times i^* - \frac{K \times Q}{Q - it} \times it + A_v \times exp\,(-B_Q \times it) \quad (2.50)$$

Charge model ($i^* < 0$)

$$f_2(it, i^*, i) = E_0 - \frac{K \times Q}{it + 0.1 \times Q} \times i^* - \frac{K \times Q}{Q - it} \times it + A_v \times exp\,(-B_Q \times it) \quad (2.51)$$

The capacity of the battery plays a significant role in the performance of the EV. Also, the gathered energy that the battery can deliver to the load is recognized as the State of Charge (SoC).

The change in the SoC value depends upon the discharge and charge cycles of the battery pack. This value can be calculated as the percentage of the current energy of the battery to the nominal energy [68-70].

The available energy in the battery pack can be calculated by:

$$Energy = Energy - Ebatt * i * Ts \quad (2.52)$$

Where; the first part of the right side of equation (2.43) represents the previous value of the battery energy and the second part represents the consumed or recovered energy depends on battery current, and Ebatt represent battery voltage obtained from equations (2.41) or (2.42) above based on charging or discharging mode.

And the state of charge of the battery can be obtained by:

$$SoC = \frac{Energy}{Full\ Energy - Energy} \quad (2.53)$$

During a vehicle driving down a hill or decelerating, the kinetic energy of the EV will be converted into electric energy. This process is called the regenerative braking. The harvested energy returns to the battery to recover part of the consumed energy during propelling of the vehicle. It's very important to control the regenerative braking power so it does not exceed the maximum voltage of the battery [53].

2.9.2. Supercapacitor Modelling

Due to their high-power density, clean energy, short time charging, supercapacitor is widely used as a secondary storage source in the HEVs with the battery as primary energy storage [71]. Both energy storage sources are combined as a hybrid storage source to improve fuel economy consumption. Generally, the ultra-capacitor in HEVs is used to serve short-time power energy demands.

The need for a model that can simulate the supercapacitor behavior is essential especially in applications such as EVs and HEVs, and different models can be found in [72-76]. A simple model of supercapacitor can be represented by resistance and capacitor connected in series as shown in Figure 2.15.

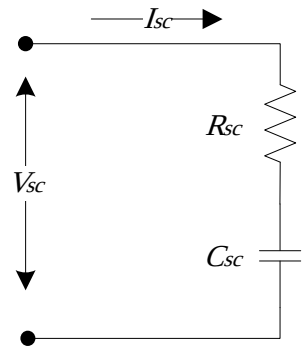

Figure 2.15. Supercapacitor model.

The energy stored in the capacitor E_{SC} can be expressed by:

$$E_{SC} = \frac{1}{2} C_{sc} V_{sc}^2 \tag{2.54}$$

Where, C_{sc} represents the supercapacitor capacitance, $R_{sc}$is the series resistance, $I_{sc}$is the currents, and V_{sc} is the terminal voltage.

The change of the energy drained from the supercapacitor between two intervals *t1* and *t2* can be calculated by:

$$\Delta E_{SC} = \frac{1}{2} C_{sc} * (V_{sc1}^2 - V_{sc2}^2) \tag{2.55}$$

Where $V_{sc1}$and V_{sc2}represent the terminal voltage of the SC at the intervals *t1* and *t2* respectively.

And the SoC of the supercapacitor can be calculated by the expression:

$$SoC_{SC} = \frac{V_{sc}}{V_{sc-max}} * 100\ (\%) \tag{2.56}$$

2.9.3. Hybrid Energy Storage System (HESS)

Energy storage is one of the most important components in electric and hybrid electric vehicles. The peak power and the energy capacity of the storage source must meet the required levels to achieve the demanded operation performance of the vehicle. Presently, almost all EVs and HEVs use chemical batteries as the primary energy storage component. However, the limitation of battery charge and discharge cycles, the limitation of a battery lifetime in service, and the need to replace batteries in EVs and HEVs arise attracting points of research that attracted researchers. As a result, many products come out to be used as second energy storage in this application. One of these products is the supercapacitor.

Different hybrid energy storage system (HESS) topologies are introduced in the literature. The most widely used configurations are Supercapacitor/Battery Configuration, Battery/ Supercapacitor Configuration, Cascaded Configuration, Multiple Converter Configuration, and Multiple Input Converter Configuration. Figure 2.16 illustrates HESS implementation in EVs [77].

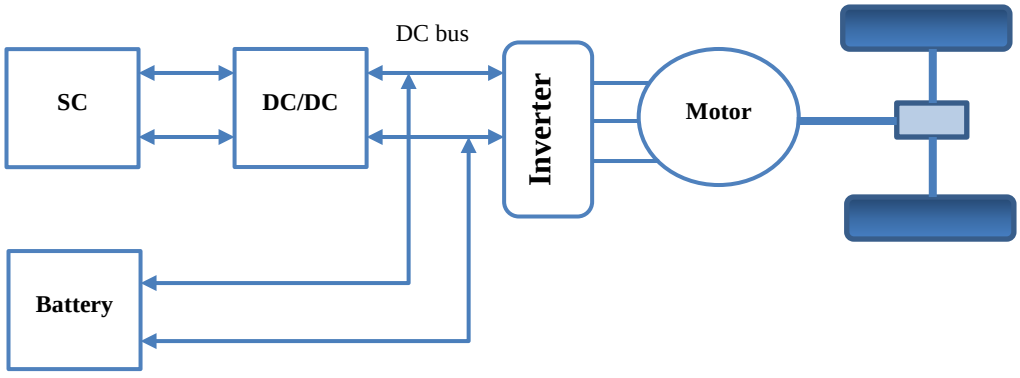

Figure 2.16. Hybrid energy storage system in EVs.

2.9.3.1 HESS Rule Based Energy Management Strategy

The need for an energy management strategy to control power flow between both energy storage systems for this application is very essential. However; controlling

power distribution between battery and supercapacitor is very important to meet power demand during driving the vehicle to ensure operating within the battery operating limits to avoid high discharging and frequently charge and discharge cycles to extend battery lifetime.

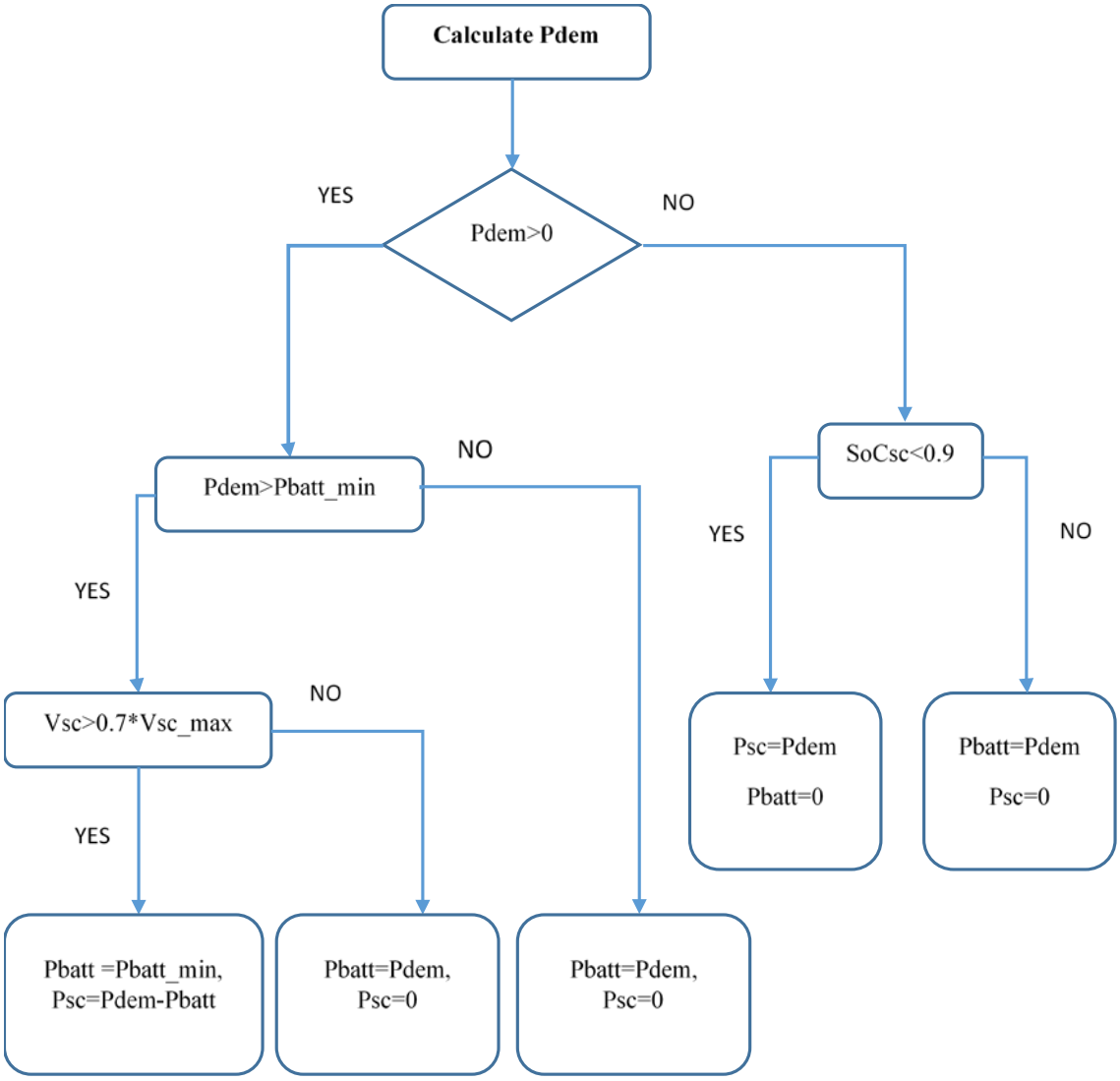

Figure 2.17. Hybrid energy storage system energy management.

All types of HESS configuration need to be controlled with suitable energy management to split the motor power demand between both energy storage systems (battery & SC) and to maintain the energy in both battery and SC within the minimum and maximum limits. In literature, many EMS for HESS has been proposed. One of the energy management methods used in HESS is rule-based energy management, this

type of EMS has some advantages such as ease of implementation and effectiveness and less information is needed [78-81].

The proposed HESS-EMS is based mainly on measuring the power demand (Pdem) and monitoring some other variables of the HESS such as battery state of charge, SC state of charge, and SC voltage. Further, some important limits such as maximum and minimum state of charge of the battery, minimum power that the battery can deliver (Pbatt_min), and SC minimum and maximum state of charge need to be specified. Figure 2.17 represents a flow chart of the proposed EMS for the HESS.

2.10. PARALLEL HEV ENERGY MANAGEMENT STRATEGY

The energy management strategy is used to decide operating mode and to employ the appropriate power split between the energy sources in the HEVs to achieve and improve the fuel economy and reduce gas emissions. However, the EMS usually include inputs such as the vehicle power demands, vehicle speed, battery State of Charge (SoC), and the road load…etc., and the output signal consist of several signal control decision to specify the operating mode of the HEV and to calculate power demanded from each power source of the HEV, which generally will be one of the followings:

- Electric motor-only mode (Electric motor propel alone).
- Assist mode (ICE and electric motor propel).
- Engine-only mode (ICE operates alone).
- Regenerative mode (Electric motor is used for kinetic energy recovery).
- Engine traction + Charge mode (Engine produces power used to propel the vehicle and to charge the battery).

The main objective of the EMS in the HEVs applications is to minimize the fuel consumption and maintain the energy in the energy storage devices (in our study is the battery pack) within a safe and specified range [10, 31].

Generally, the EMS methods can be classified as shown in Figure 2.18. Several power-split strategies have been proposed, evaluated, and employed to different HEV configurations can be found in the literature. One of the interesting energy management strategies is the rule-based energy management strategy, which is classified into two categories; the Deterministic Rule Based (DRB) EMS and the

Fuzzy Rule-Based (FRB) EMS. The main advantages of this strategy are simplicity, reliability, ease to understand and to implement, and it shows satisfactory fuel consumption results [10].

In the DRB-EMS, the rules are determined based on the fuel economy map of the engine and its actual operation, which is predefined in a look-up table. The thermostat control strategy is based on the DRB-EMS that is based on turning on/off the ICE to maintain the SoC of the battery pack within the predefined limits [32, 82].

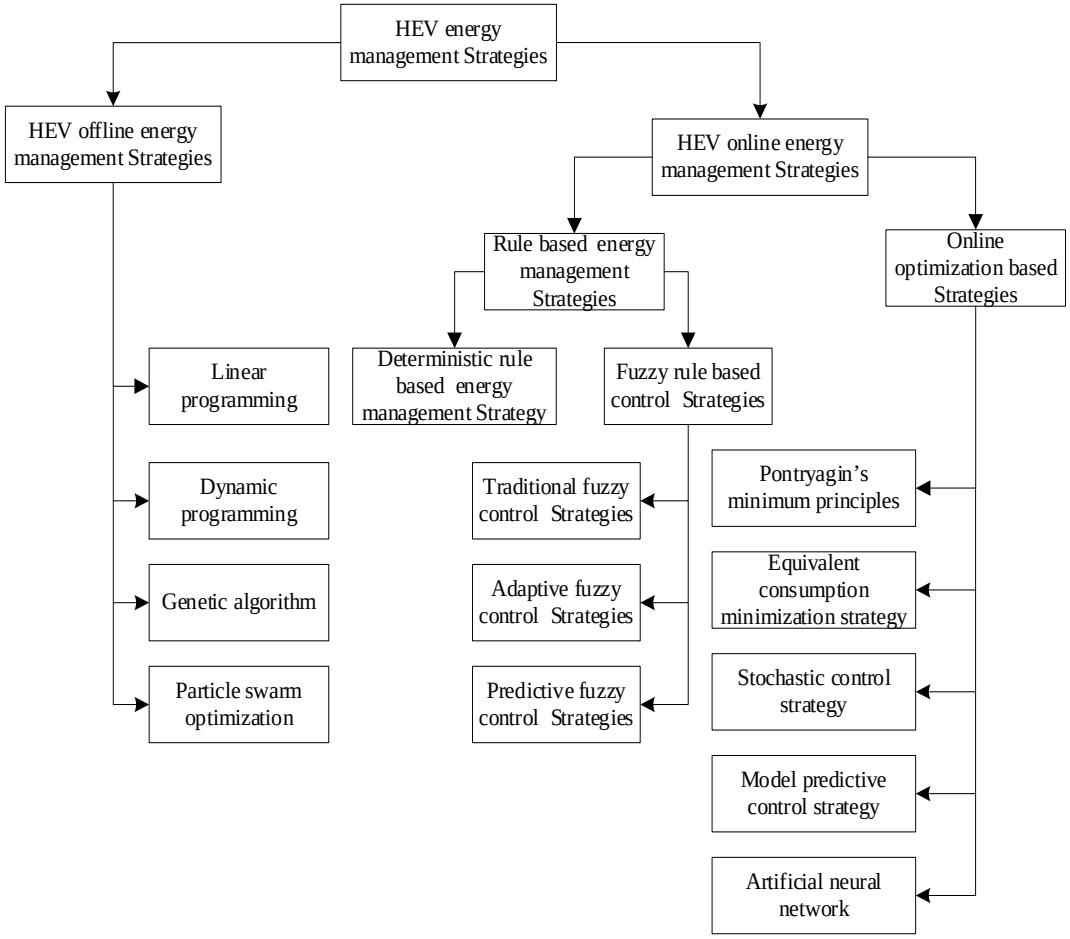

Figure 2.18. Classification of HEV energy management strategies.

Due to the complexity and non-linearity of the HEVs system, where each subsystem has its controller, and simplicity, the robustness of Fuzzy Logic Controller; the FRB-EMS is very suitable to be used in HEVs application, and recently attracts researcher's attention in power energy management of HEVs. Therefore, the FRB-EMS is

considered in this research. This method is implemented to validate and compare the performance of the Maximum State of Charge (Max-SoC) energy management strategy.

2.10.1. Max-SoC Energy management Strategy

In a stop-and-go driving scenario, the battery pack energy source must always have sufficient energy to meet power demand during driving. However, maintain high SoC in the battery pack is essential to be able to deliver sufficient power to the vehicle wheels. In the Max-SoC energy management strategy the engine is utilized as a primary energy source in the vehicle, and the motor is used to support the engine in high power demand or during low-speed driving [52, 83]. The Max-SoC EMS can be implemented as in the flowchart presented in Figure 2.19.

In Figure 2.19, it is obvious that the vehicle under this control strategy has five operating modes depends mainly on the power demand and some other conditions.

These five modes can be presented as follow:

- Motor-alone traction mode: which is performed when the vehicle speed is less than a predetermined value Vmin.
- Hybrid traction mode: which is performed when the power demand is greater than that the engine power can deliver. Therefore, both the engine and motor will deliver their power to the driven wheels.
- Engine-alone traction: this is performed when the power demand is less than the power that the engine can provide while working on its optimum line and the SoC of the battery pack is at the maximum limit.
- Engine traction + charging: this is performed when the power demand is less than the power that can provide while working on its optimum line and the SoC of the battery is less than the maximum limit.
- Regenerative braking: this is performed during deceleration of the vehicle. And is controlled according to the SoC value and the maximum breaking value which can be recovered by the motor when it’s operating in generating mode, and the generative power can be recovered by the motor, otherwise, mechanical breaking or hybrid breaking will be used.

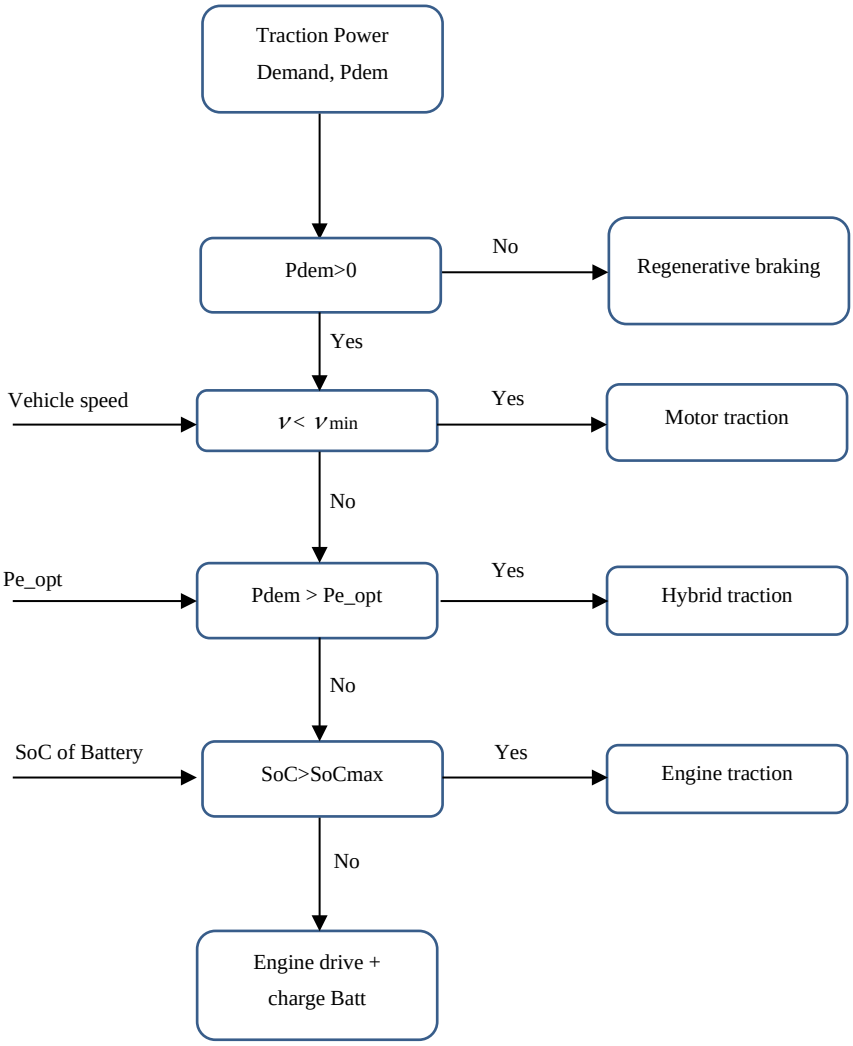

Figure 2.19. Max-SoC energy management strategy flow chart.

2.10.2. Fuzzy Rule Based Energy Management Strategy

Basically, the Fuzzy Logic Rule-Based Energy Management Strategy (FRB-EMS) is based on using a Fuzzy Logic Controller, the controller is designed based on the if-then rule with several inputs such as the power command, the battery SoC, and vehicle speed which depends on the proposed design. The controller will make decisions and perform the calculations based on the determined rules for the operation modes and the power demand from the engine and electric motor to achieve the desired performance.

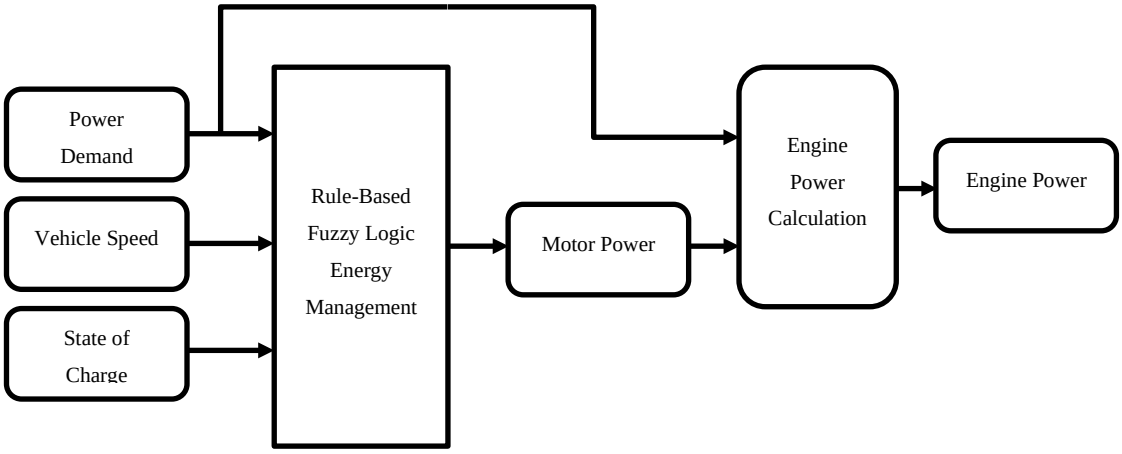

Figure 2.20. Fuzzy rule-based energy management.

Figure 2.20 above illustrates the FRB-EMS applied in our simulation package, which depends on three inputs the power demand for the driving cycle, the SoC of the battery pack, and the current vehicle speed. The output of the FRB-EMS is the motor power demand, then subtracting this value from the total power demand to calculate the engine power demand. This calculation can be performed by:

$$P_{E\_dem} = P_{dem} - P_{m\_dem} \tag{2.57}$$

Where, P_{E_dem} is the engine power demand, P_{dem} is the power demand by the driver, and P_{m_dem} is the motor power demand decided by the FRB-EMS.

For simplicity three triangle membership functions were used in this design to implement the power demand, vehicle speed, and SoC respectively. As shown in Figure 2.21 SoC and vehicle speed represented by three membership functions (Low, Medium, High), and the power demand is presented by five membership functions Negative high (N-High), Negative low (N-Low), Zero (Z), Positive low (P-Low) and Positive high (P-High). And for the output decision (motor power demand) five membership functions were utilized as explained for the power demand.

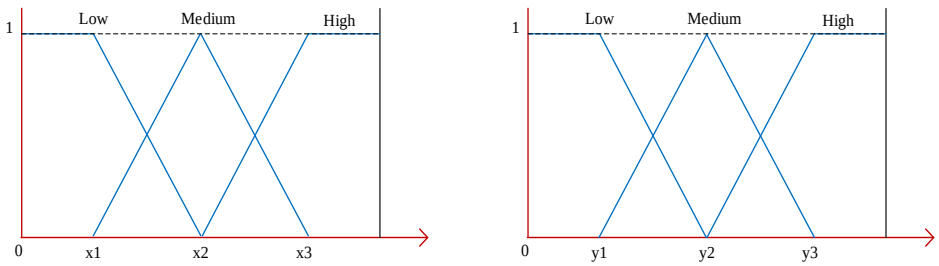

(a) (b)

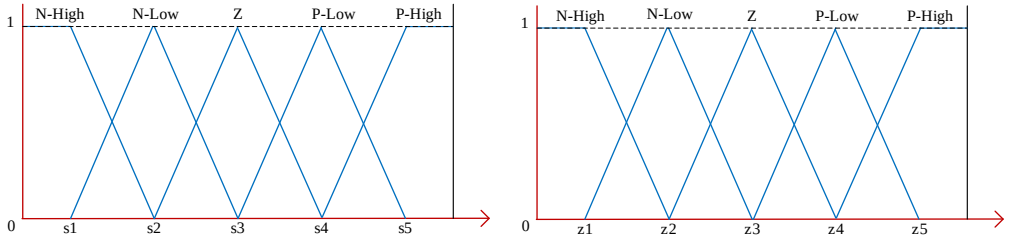

(c) (d)

Figure 2.21. FRB-EMS inputs and output membership functions.

45 rules implemented in this design to decide and calculate demand motor power in each interval of the simulation period [84]. The fuzzy rules utilized are implemented as illustrated in Table 2.3.

Where; SoC is the state of charge of the battery pack and V_{veh} is the vehicle speed.

Table 2.4. FRB-EMS Rules.

Pdem		**N-High**	**N-Low**	**Zero**	**P-Low**	**P-High**
SoC	**V_{veh}**					
Low	**Low**	N-High	N-Low	N-Low	N-Low	Zero
	Medium	N-High	N-Low	N-Low	N-Low	Zero
	High	N-High	N-Low	N-Low	N-Low	Zero
Medium	**Low**	N-High	N-Low	Zero	P-Low	P-High
	Medium	N-High	N-Low	Zero	P-Low	P-Low
	High	N-High	N-Low	Zero	P-Low	P-High
High	**Low**	Zero	Zero	Zero	P-Low	P-High
	Medium	Zero	Zero	Zero	P-Low	P-High
	High	Zero	Zero	Zero	P-Low	P-High

PART 3

SOFTWARE DESIGN AND GRAPHICAL USER INTERFACE

The developed software is arranged in subfunctions as shown in Figure 3.1 to improve its performance and to decrease execution time, however; for each configuration and selected method, only related subfunctions will be executed.

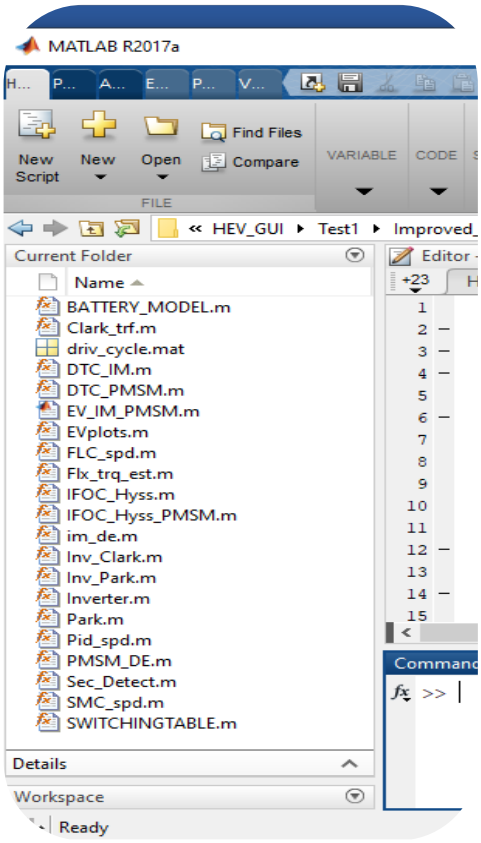

Figure 3.1. EV model subfuctions.

3.1. GRAPHICAL USER INTERFACE

To improve the developed simulation software performance and make it easier for the user to simulate and investigate different structures of the EVs or HEVs; a graphical

user interface (GUI) platform was designed to simulate all different designs modeled in this work. Using the designed GUI, different vehicle configurations, vehicle parameters, different EMS, and different drive cycle scenarios can be simulated. The GUI simulation procedure can be performed by following the sequence shown in the flow chart below.

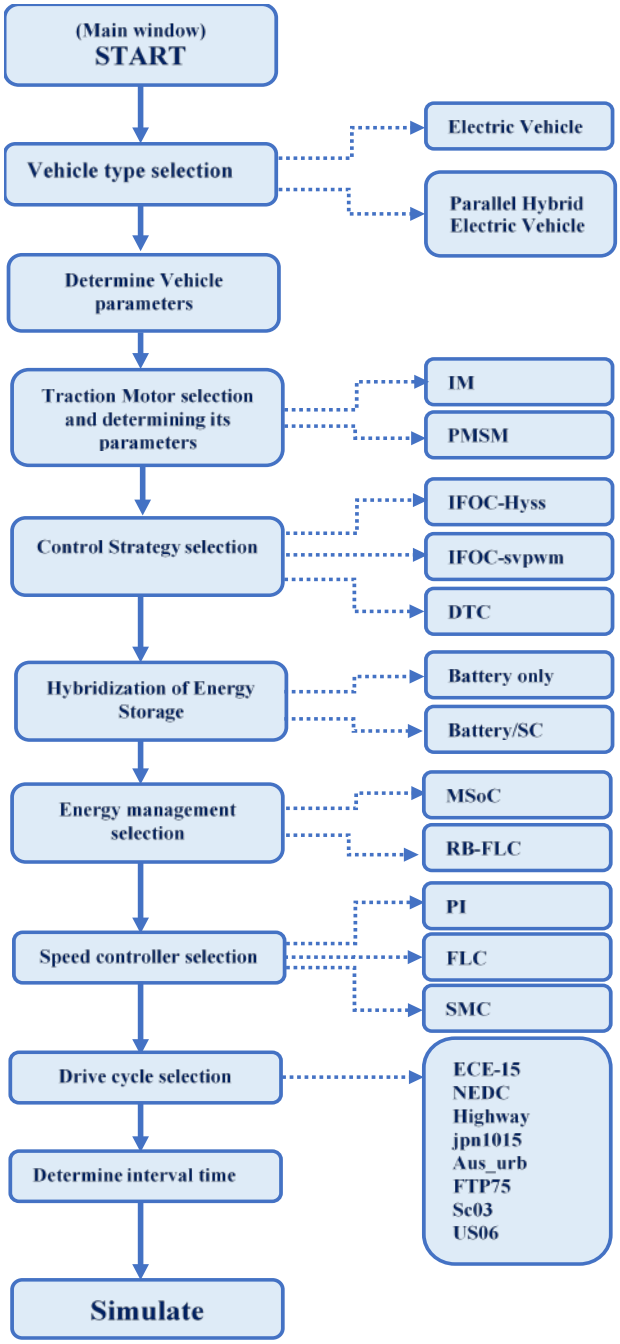

Figure 3.2. GUI sequence flow chart.

When the simulation package is started the main window illustrated in Figure 3.3 will appear.

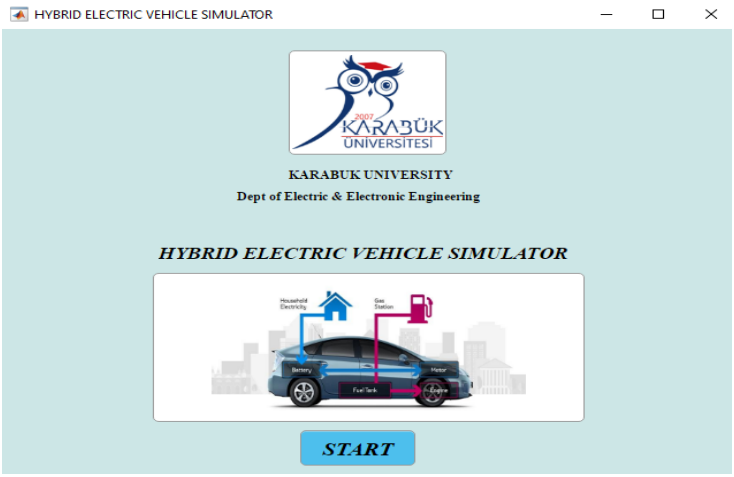

Figure 3.3. GUI Main window.

By pushing the START pushbutton the vehicle type selection window will appear, as shown in Figure 3.4.

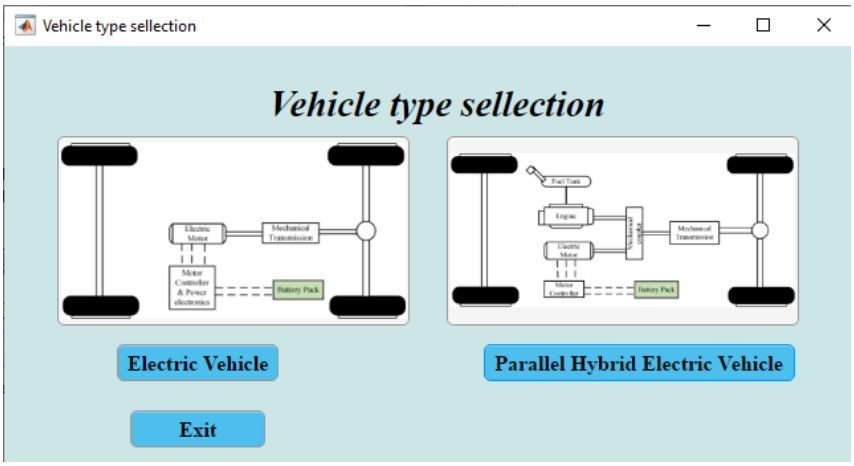

Figure 3.4. Vehicle type selection window.

Here, two different types of vehicles are modeled and can be selected, Electric Vehicle or Parallel Hybrid Electric Vehicle. If the Parallel hybrid electric vehicle is chosen the Parallel HEV simulator will pop up with its initial default selections. In this GUI design, only one simulation window for each type of vehicle was developed. So as illustrated in Figure 3.5 when choosing either vehicle type, the simulator interface for

the specified type will pop up. PMSM parameters were designed to be hidden when IM is selected, on the other hand when PMSM is selected the IM parameters will be hidden.

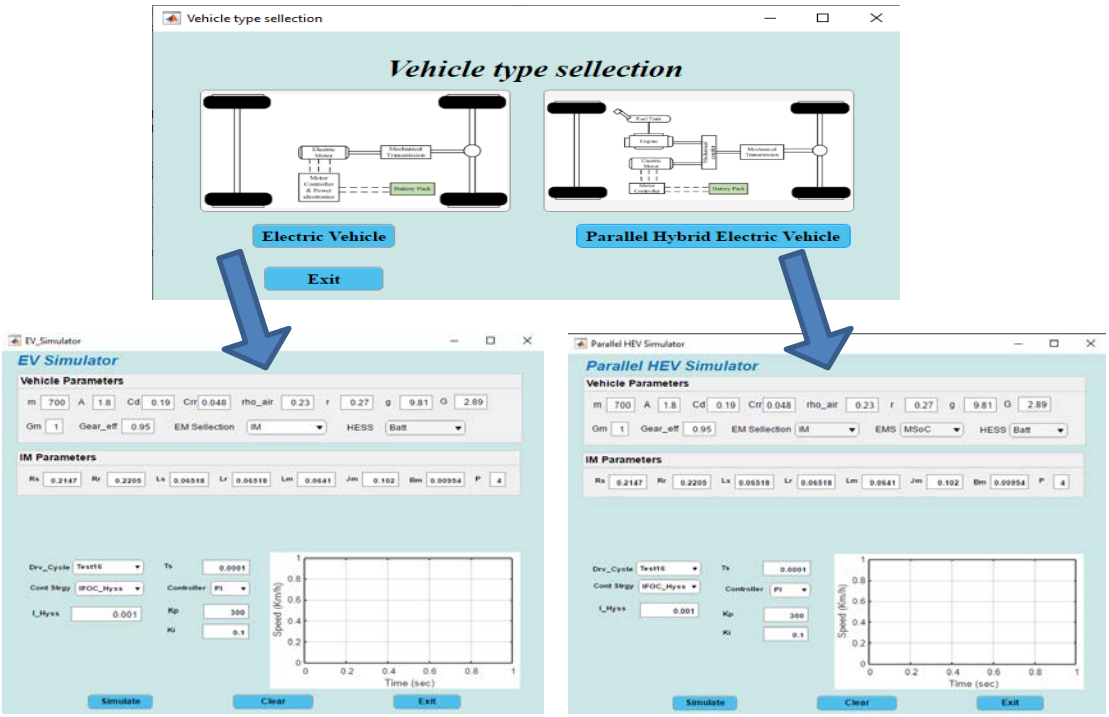

Figure 3.5. Vehicle type selection & simulator GUI.

In Parallel HEV Simulator the vehicle parameters, traction motor type, EMS and HESS can be determined as shown in the following figure.

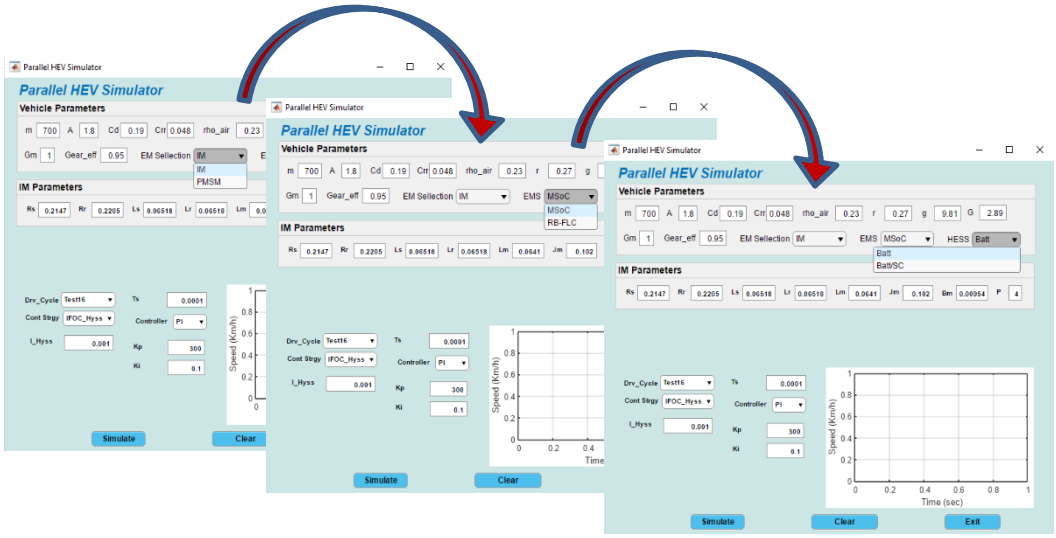

Figure 3.6. Determining of HEV's parameters, traction motor, EMS and HESS.

Further, traction motor control strategy and the speed controller type can be selected from the dropdown menus as shown in Figure 3.7 below.

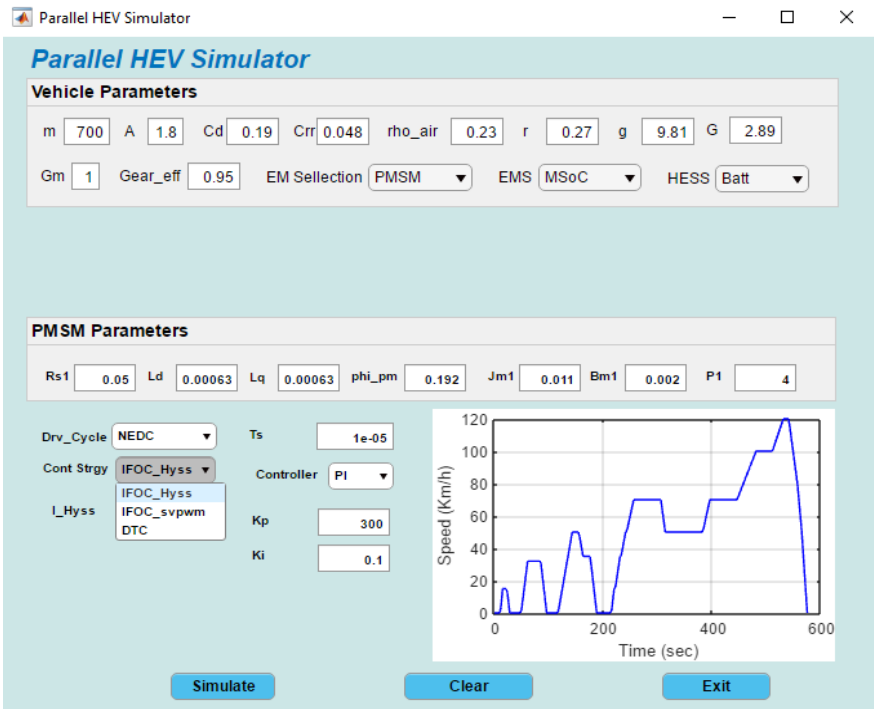

Figure 3.7. Determining traction motor control strategy and speed controller.

Also, the drive cycle that to be used for simulation can be determined from the Drv_Cycle dropdown menu, as shown in the figure above.

And finally, after determining sampling time from the Ts dropdown menu, it's ready to start the simulation by pressing Simulate push-button. At the end of the simulation time which is different for each driving cycle performed a number of some predetermined important plots will be pop up automatically to investigate the performance achieved for the design selected.

A flow chart that explaining the executing sequence of the developed platform is illustrated in Appendix B.

PART 4

SIMULATION RESULTS

The developed code is used to simulate EV and Parallel HEV behavior via the designed GUI. The simulation results are divided into two main sections based on the type of vehicle, the first section is the simulation results of EV, and the section is the simulation results of Parallel HEV.

4.1 ELECTRIC VEHICLE SIMULATION RESULTS

In this section; to validate the simulation code and to compare the performance of the different speed controllers used in simulation, the NEDC driving cycle was utilized to simulate the behavior of the EV under these different designs. The NEDC driving cycle has been used because it is widely used in literature. The NEDC drive cycle is consists of two driving cycles (ECE15+EUDC). In this driving cycle, regenerative power can be obtained and it is noticed very clear during deceleration of the vehicle speed, while the power delivered from the battery to the electric motor can be observed during acceleration of the vehicle. Moreover; the simulation of the NEDC driving cycle was performed for 575 seconds with a maximum speed of 120 km/h as shown in Figure 4.1a. Furthermore; the behavior of the vehicle is simulated based on two different traction motors, thus simulation results of each type of EV are illustrated in the following subsections based on the type of the traction motor.

4.1.1. Electric Vehicle Based IM

In this section, the simulation of the vehicle is performed based on using IM as the traction motor of the EV. To compare the effect of using the developed code of IFOC

and DTC control strategies for the IM, and further to investigate the effect of the developed HESS as a hybrid energy storage system and the energy management strategy of this system; the simulation of each different configuration is presented in following subsections. Then all simulation results are compared and discussed in the comparison section.

4.1.1.1. Simulation Based Battery-Only (IFOC for PI, FLC and SMC)

As mentioned earlier; each configuration of EV is simulated based on three different speed controller PI, FLC, and SMC. Figure 4.1a and Figure 4.1c show the good performance of the EV using the PI controller in speed tracking with an average speed error of 0.1040 (km/h). Also, Figure 4.1b presents the EV operating modes, where mode=1 represents vehicle propelling mode, mode=2 represents regenerative braking mode, and mode=0 represents stop mode. Further, Figure 4.1d illustrates electric motor speed in rad/s.

Moreover, Figure 4.2a represents the vehicle power demand and the power delivered by the electric traction motor for the simulated drive cycle. The battery current and the battery state of charge are shown in 4.2b and 4.2c respectively, where the end value of the battery state of charge is reduced to 0.7673.

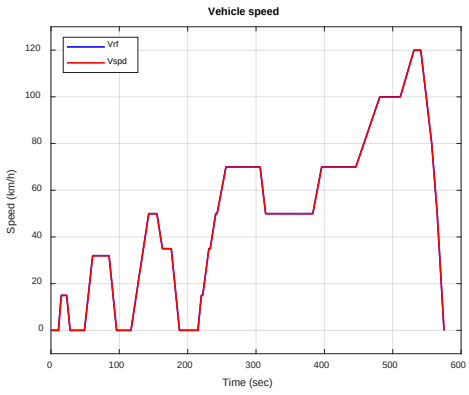

(a)

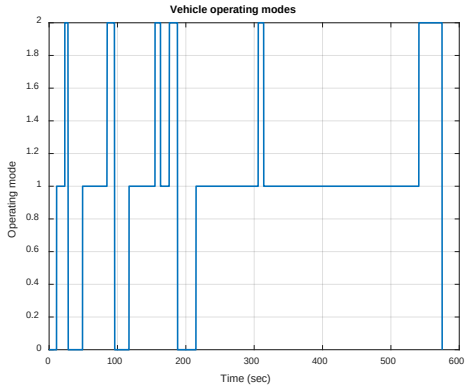

(b)

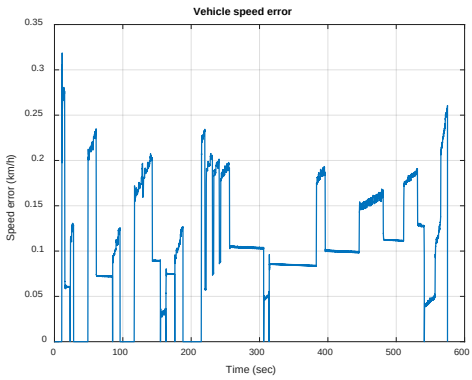

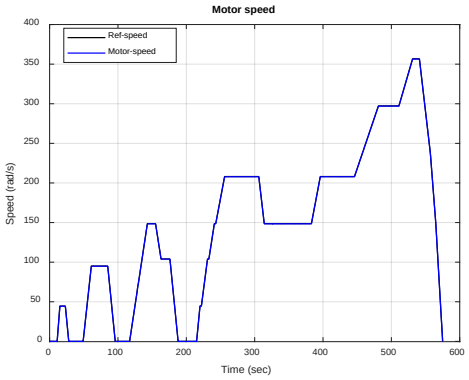

(c) (d)

Figure 4.1. NEDC driving cycle: a) Vehicle speed response. b) Vehicle operating modes. c) Vehicle speed error. d) Motor speed. EV based IM-IFOC-PI.

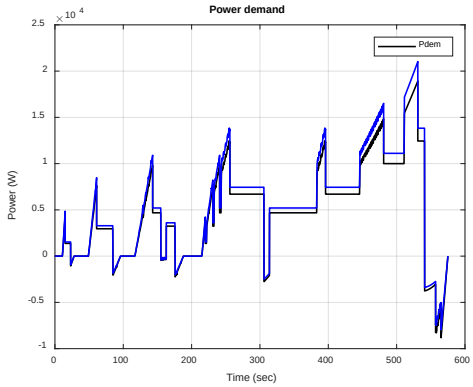

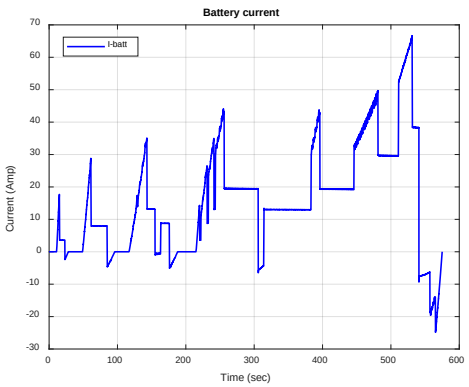

(a) (b)

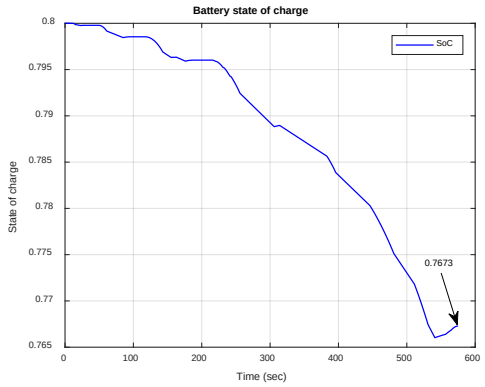

(c)

Figure 4.2. NEDC driving cycle: a) Power demand & Power split. b) Battery current. c) State of charge of Battery. EV based IM- IFOC-PI.

Furthermore, Figure 4.3a to Figure 4.3d illustrate good speed tracking of the vehicle using the FLC controller, with an average speed error equal to 0.0779 (km/h). Also, the end value of the battery state of charge is 0.7679 as shown in Figure 4.4c.

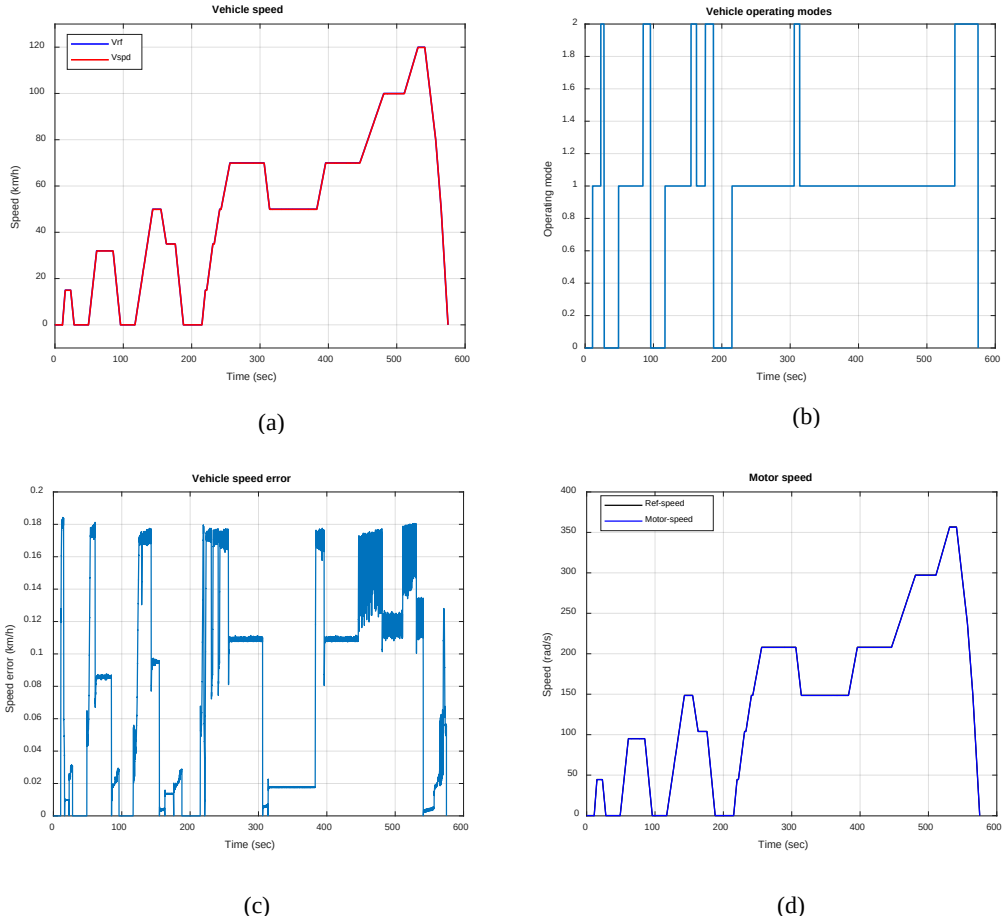

(a) (b)

(c) (d)

Figure 4.3. NEDC driving cycle: a) Vehicle speed response. b) Vehicle operating modes. c) Vehicle speed error. d) Motor speed. EV based IM-IFOC-FLC.

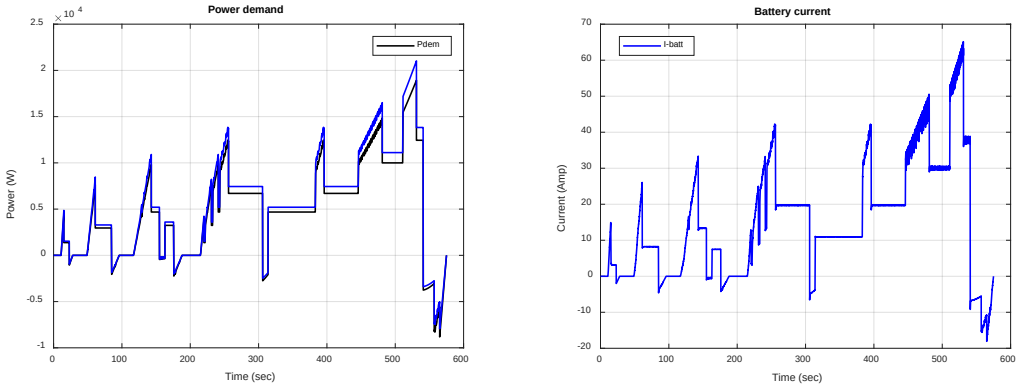

(a) (b)

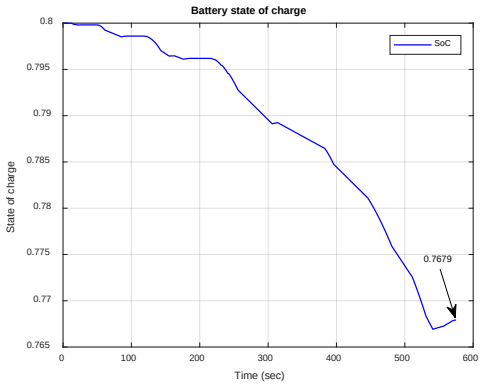

(c)

Figure 4.4. NEDC driving cycle: a) Power demand & Power split. b) Battery current. c) State of charge of Battery. EV based IM- IFOC-FLC.

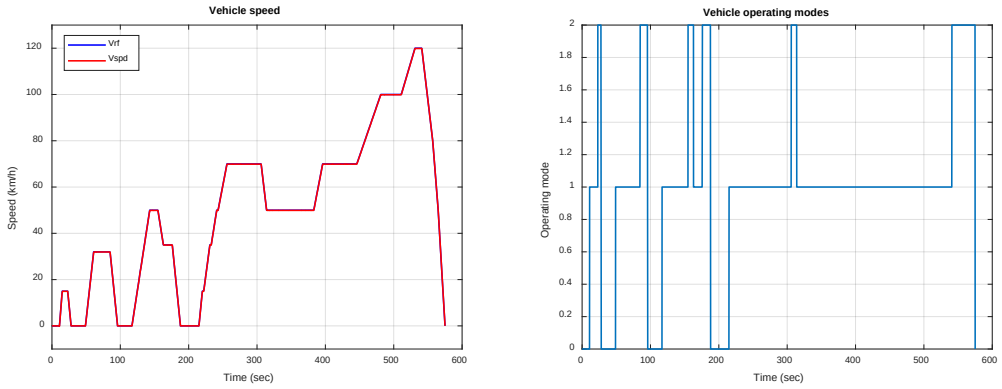

(a)

(b)

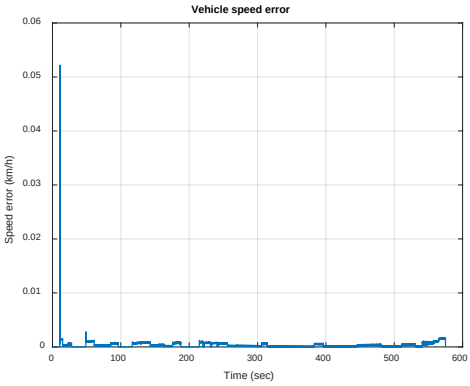

(c)

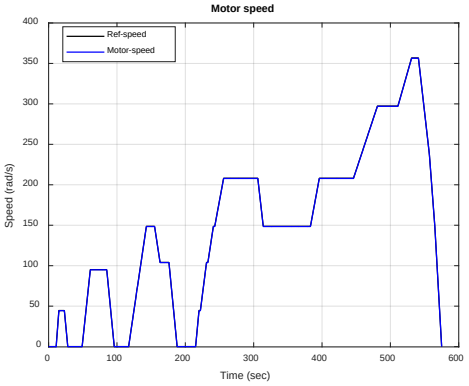

(d)

Figure 4.5. NEDC driving cycle: a) Vehicle speed response. b) Vehicle operating modes. c) Vehicle speed error. d) Motor speed. EV based IM-IFOC-SMC.

Moreover, Figure 4.5a to Figure 4.5d show superior speed tracking of the vehicle using the SMC controller, with an average speed error equal to 3.2700e-4 (km/h). Also, in Figure 4.6c, the end value of the battery state of charge is 0.7690.

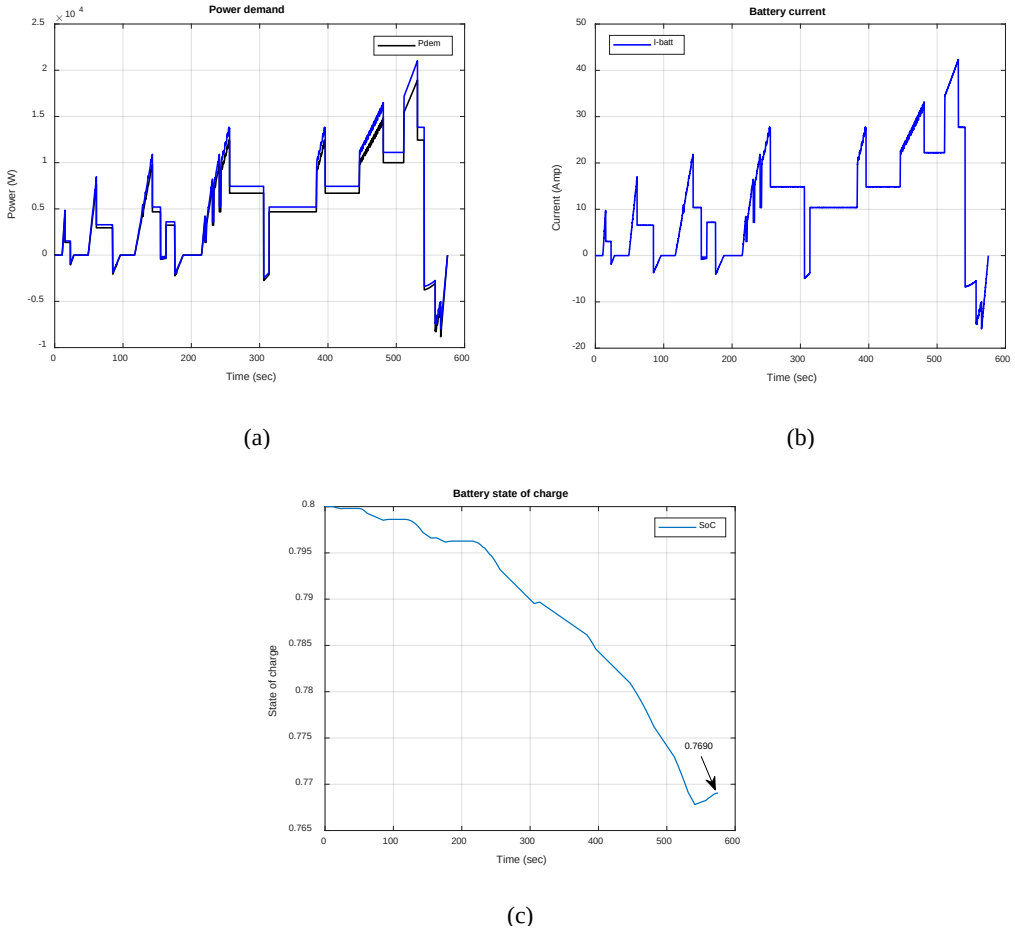

Figure 4.6. NEDC driving cycle: a) Power demand & Power split. b) Battery current. c) State of charge of Battery. EV based IM-IFOC-SMC.

4.1.1.2. Simulation Based HESS (IFOC for PI, FLC and SMC)

In this section of the simulation, the EV is simulated under IFOC for PI, FLC, and SMC based on utilizing HESS to provide all demand energy to the electric traction motor.

Figure 4.7 and Figure 4.8 presents the results obtained when using the PI controller. It shows good behavior in terms of speed tracking with an average speed error equal to

0.1039 (km/h). And the state of charge end values is 0.7719 and 0.7751 for the battery and the SC respectively as shown in Figure 4.8c.

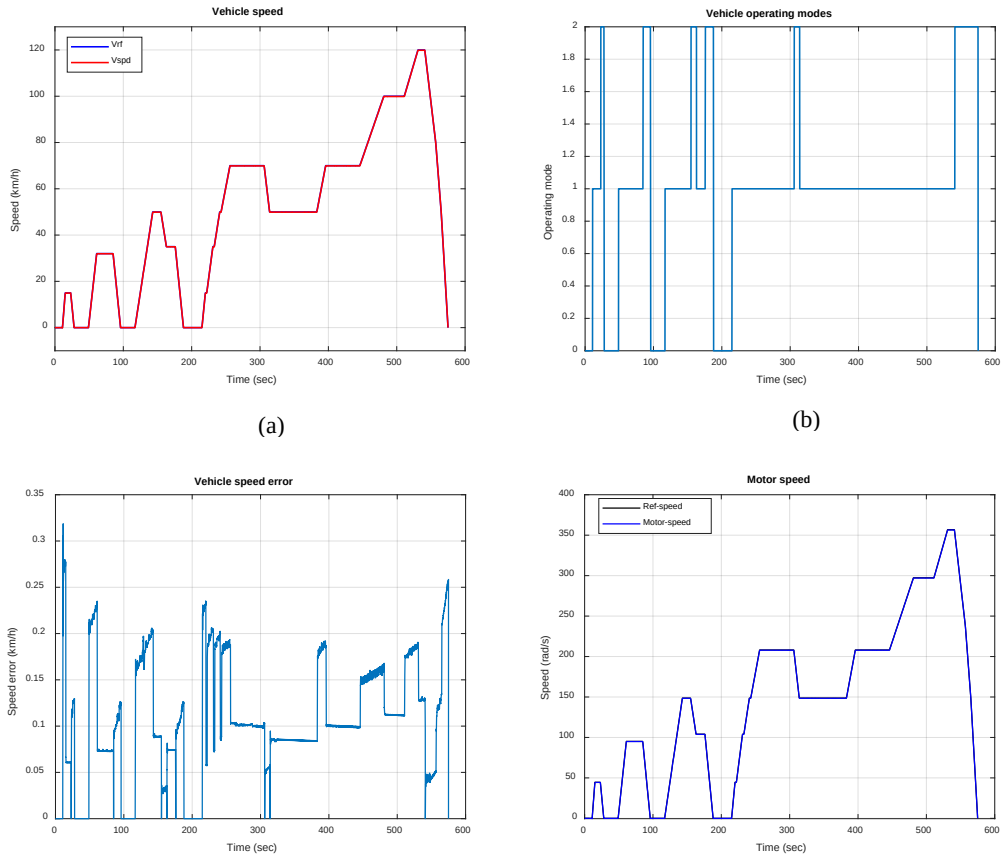

Figure 4.7. NEDC driving cycle: a) Vehicle speed response. b) Vehicle operating modes. c) Vehicle speed error. d) Motor speed. EV based IM-IFOC-PI.

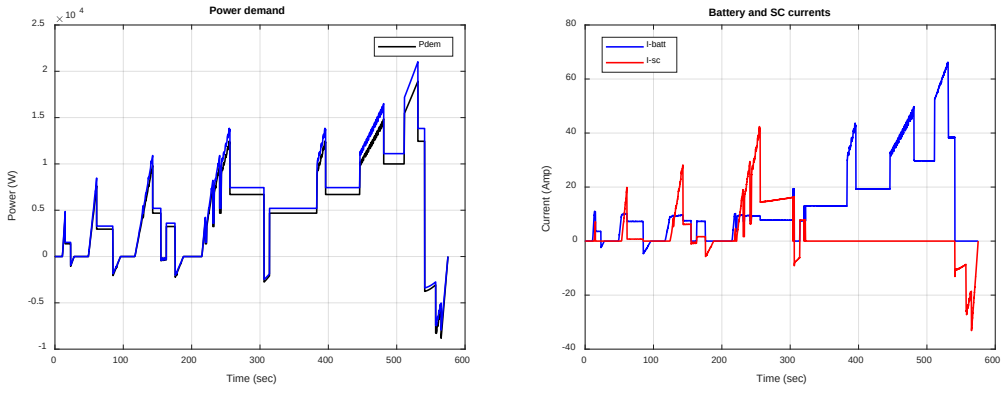

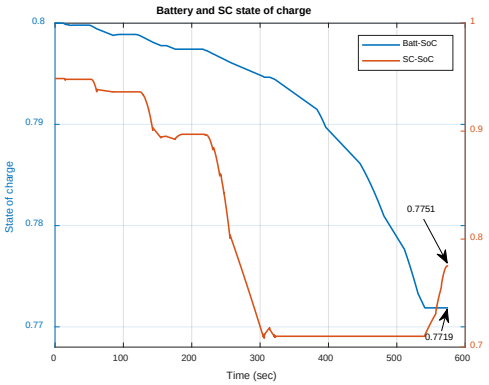

(c)

Figure 4.8. NEDC driving cycle: a) Power demand & Power split. b) Batt/SC currents. c) State of charge of Battery & SC. EV based IM- IFOC-PI.

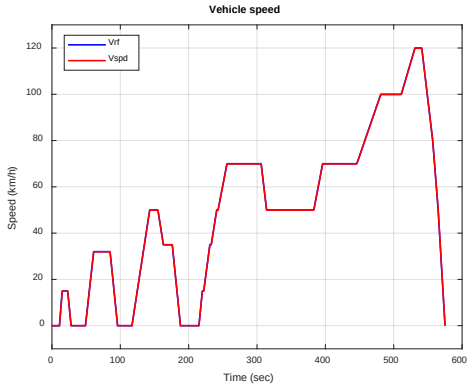

(a)

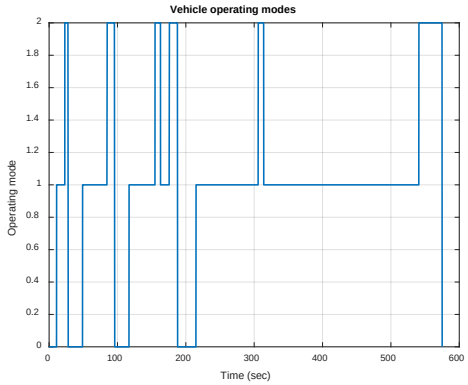

(b)

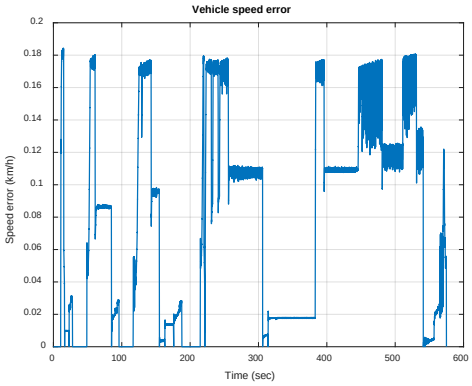

(c)

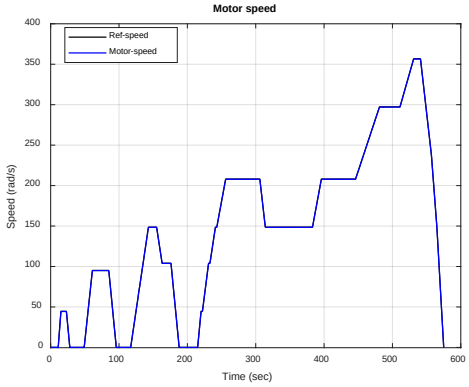

(d)

Figure 4.9. NEDC driving cycle: a) Vehicle speed response. b) Vehicle operating modes. c) Vehicle speed error. d) Motor speed. EV based IM-IFOC-FLC.

On the other hand, for the case of the FLC controller in Figure 4.9 and Figure 4.10; the performance was better in the case of speed tracking with an average speed error equal to 0.0778 (km/h), and the end value of the state of charge for the battery pack is 0.7727 and for SC is 0.7617.

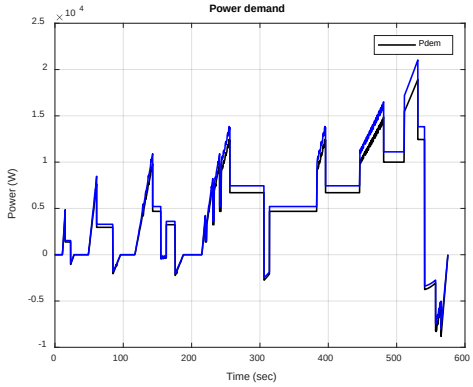

(a)

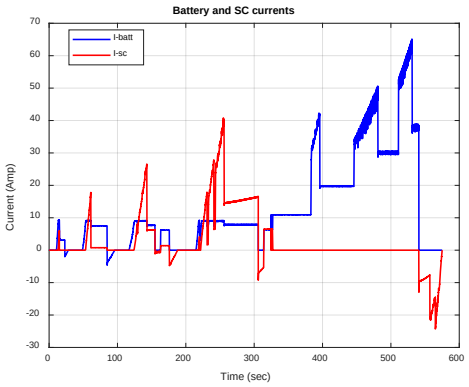

(b)

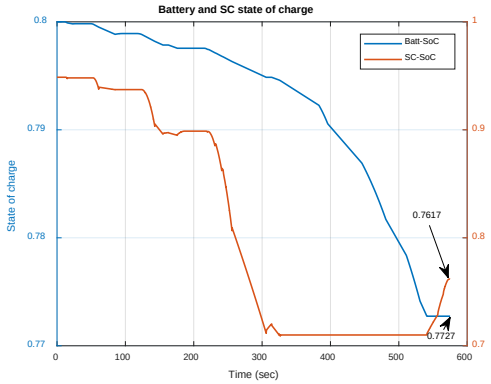

(c)

Figure 4.10. NEDC driving cycle: a) Power demand & Power split. b) Batt/SC currents. c) State of charge of Battery & SC. EV based IM- IFOC-FLC.

Additionally, for the case of the SMC controller in Figure 4.11 and Figure 4.12; the performance was superior in the case of speed tracking with an average speed error equal to 3.2692e-4 (km/h), and the end value of the state of charge for the battery pack is 0.7816 and for SC is 0.7584.

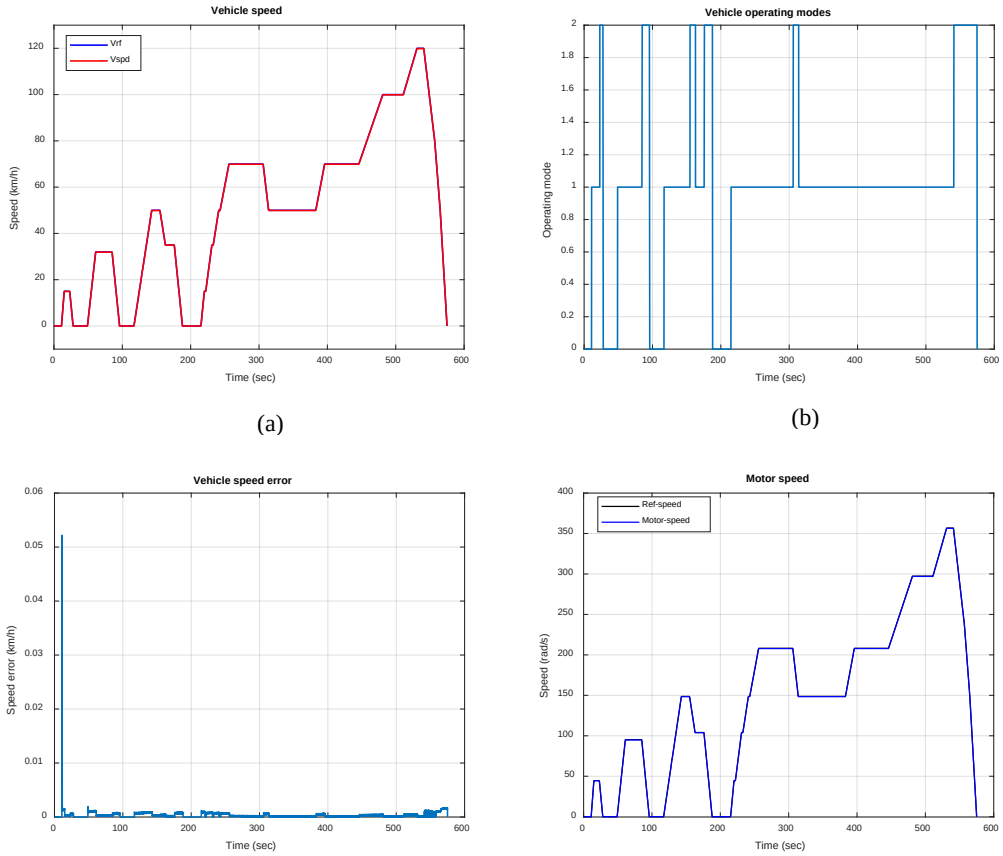

Figure 4.11. NEDC driving cycle: a) Vehicle speed response. b) Vehicle operating modes. c) Vehicle speed error. d) Motor speed. EV based IM-IFOC-SMC.

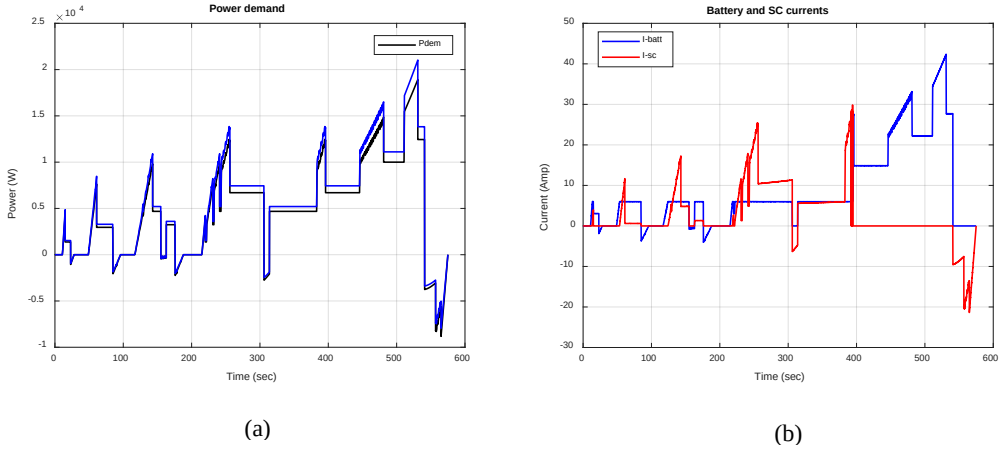

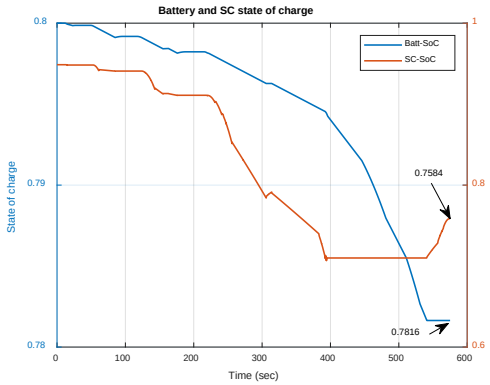

(c)

Figure 4.12. NEDC driving cycle: a) Power demand & Power split. b) Batt/SC currents. c) Batt/SC State of charges. EV based IM-IFOC-SMC.

4.1.1.3. Simulation Based Battery-Only (DTC for PI, FLC and SMC)

Similarly, in the case of using the DTC strategy; the results are presented in the same order to investigate the EV behavior under PI, FLC, and SMC controllers. However, in the case of the PI controller as presented in Figure 4.13 and Figure 4.14; the performance is accepted in terms of speed tracking with an average speed error equal to 0.0750 (km/h), and the SoC of the battery pack is 0.7699.

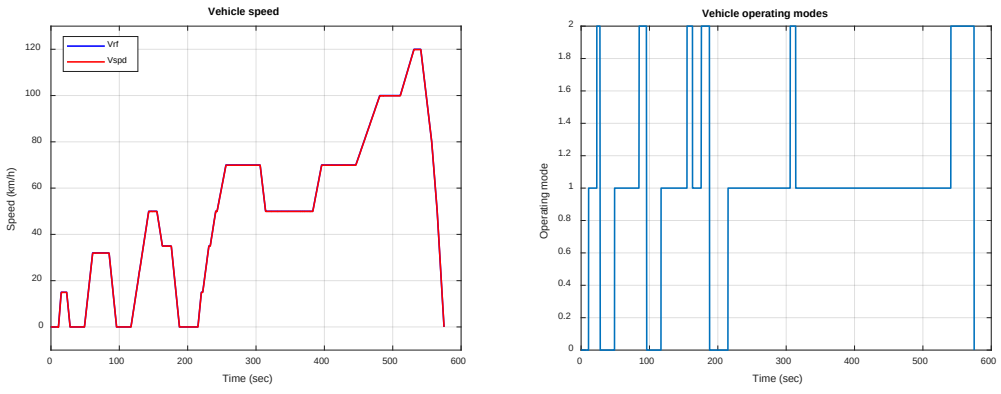

(a) (b)

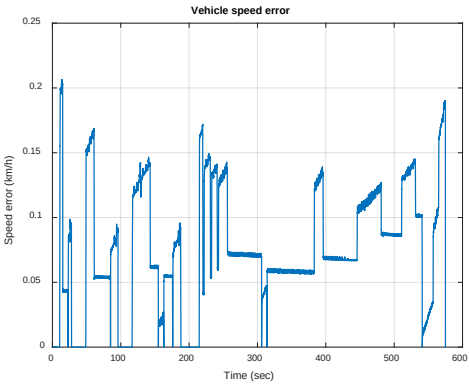

(c)

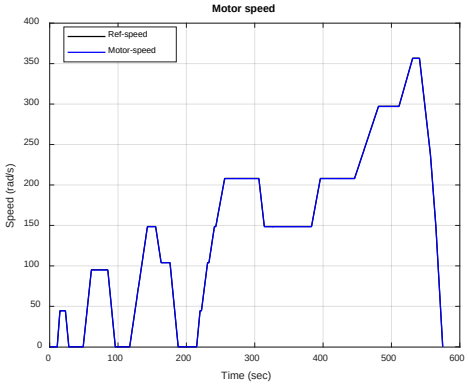

(d)

Figure 4.13. NEDC driving cycle: a) Vehicle speed response. b) Vehicle operating modes. c) Vehicle speed error. d) Motor speed. EV based IM-DTC-PI.

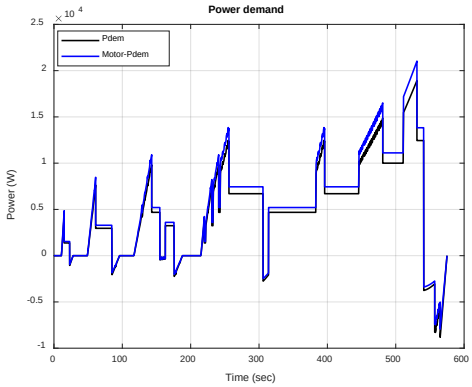

(a)

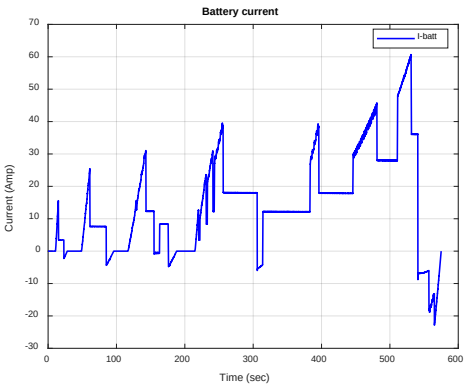

(b)

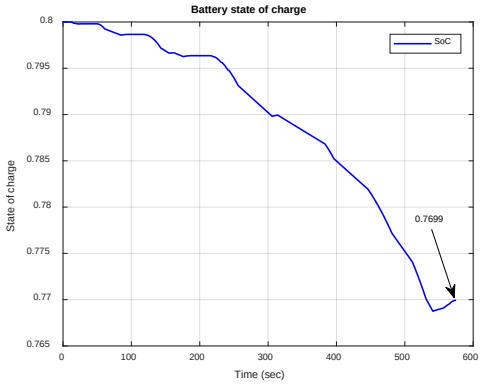

(c)

Figure 4.14. NEDC driving cycle: a) Power demand & Power split. b) Battery current. c) State of charge of Battery. Based IM-DTC-PI.

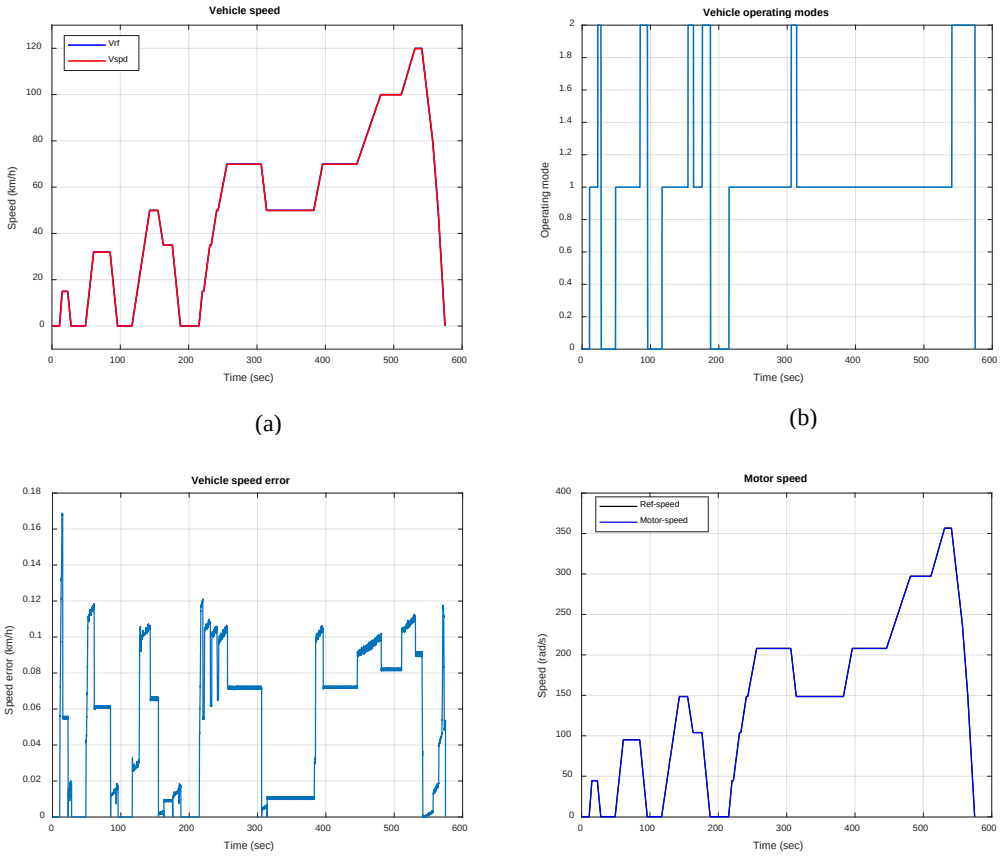

Figure 4.15. NEDC driving cycle: a) Vehicle speed response. b) Vehicle operating modes. c) Vehicle speed error. d) Motor speed. EV based IM-DTC-FLC.

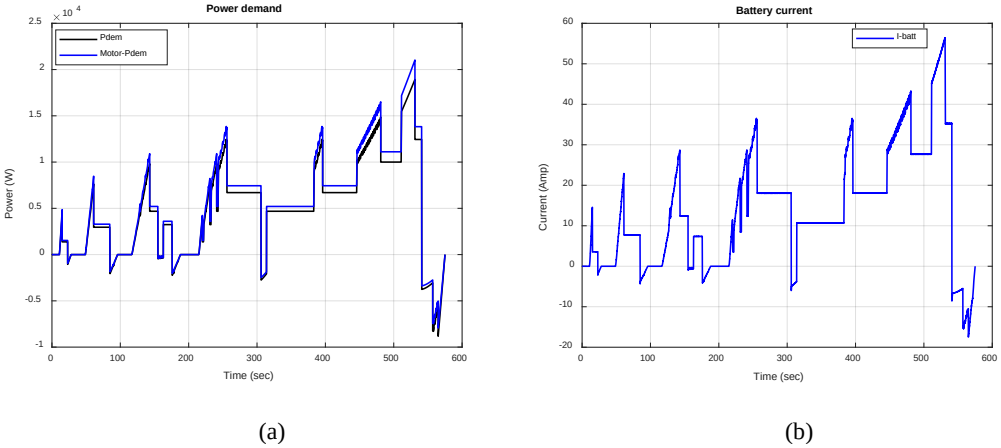

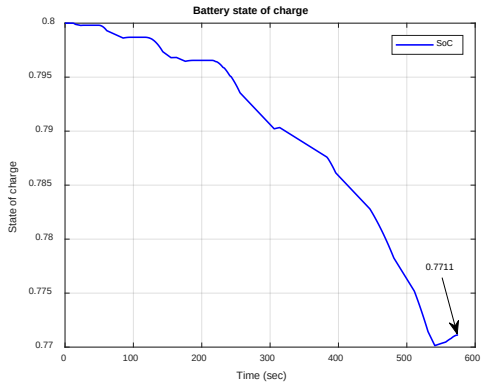

(c)

Figure 4.16. NEDC driving cycle: a) Power demand & Power split. b) Battery current. c) State of charge of Battery. Based IM-DTC-FLC.

Moreover, when utilizing the FLC controller; the average speed error is 0.0515 (km/h), and the SoC end value is 0.7711. as shown in Figure 4.15 and Figure 4.16. Furthermore, for the SMC controller in Figure 4.17 and Figure 4.18; the performance was better than PI and FLC cases with an average speed error 0.0065 (km/h), and SoC end value equal to 0.7762.

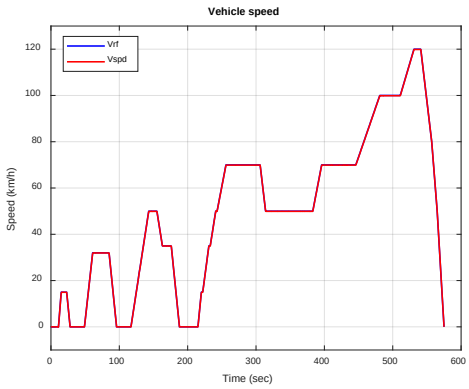

(a)

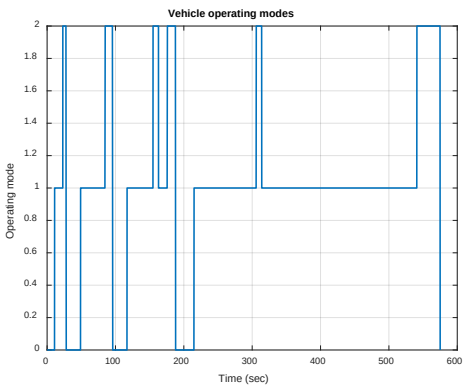

(b)

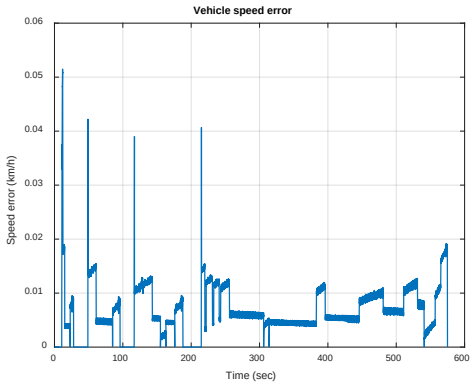

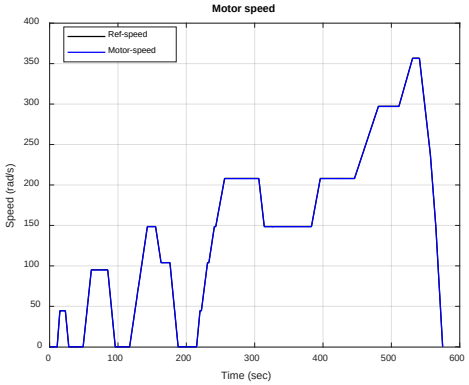

(c) (d)

Figure 4.17. NEDC driving cycle: a) Vehicle speed response. b) Vehicle operating modes. c) Vehicle speed error. d) Motor speed. EV based IM-DTC-SMC.

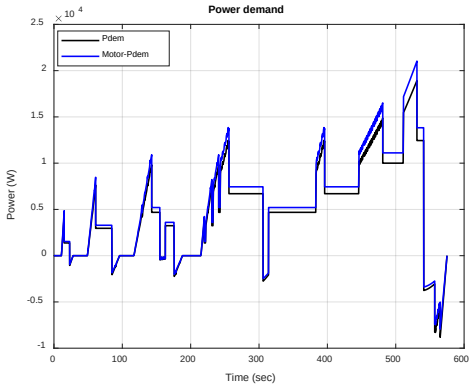

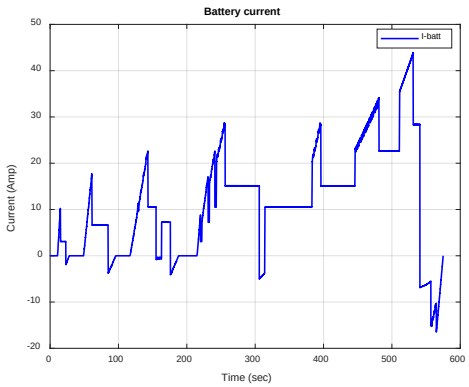

(a) (b)

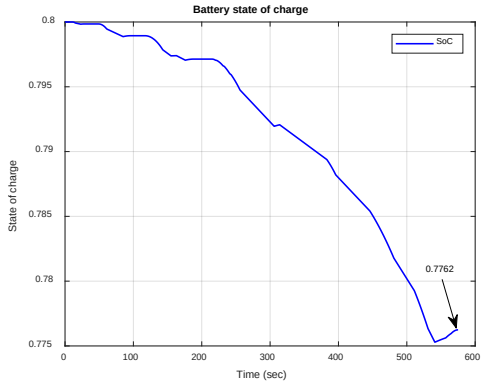

(c)

Figure 4.18. NEDC driving cycle: a) Power demand & Power split. b) Battery current. c) State of charge of Battery. Based IM-DTC-SMC.

4.1.1.4. Simulation Based HESS (DTC for PI, FLC and SMC)

Also, to investigate the performance of the EV under DTC strategy utilizing HESS and compare it with its performance when using only battery pack as an energy storage source; the EV simulated for PI, FLC, and SMC controller and the results presented in the following figures.

In the case of the PI controller, the EV tracked the desired reference speed with an average speed error equal to 0.0755 (km/h), and the end value of the SoC of the battery pack reduced to 0.7746, on the other hand; the end value of the SoC of the SC was equal to 0.7717 at end of simulation time.

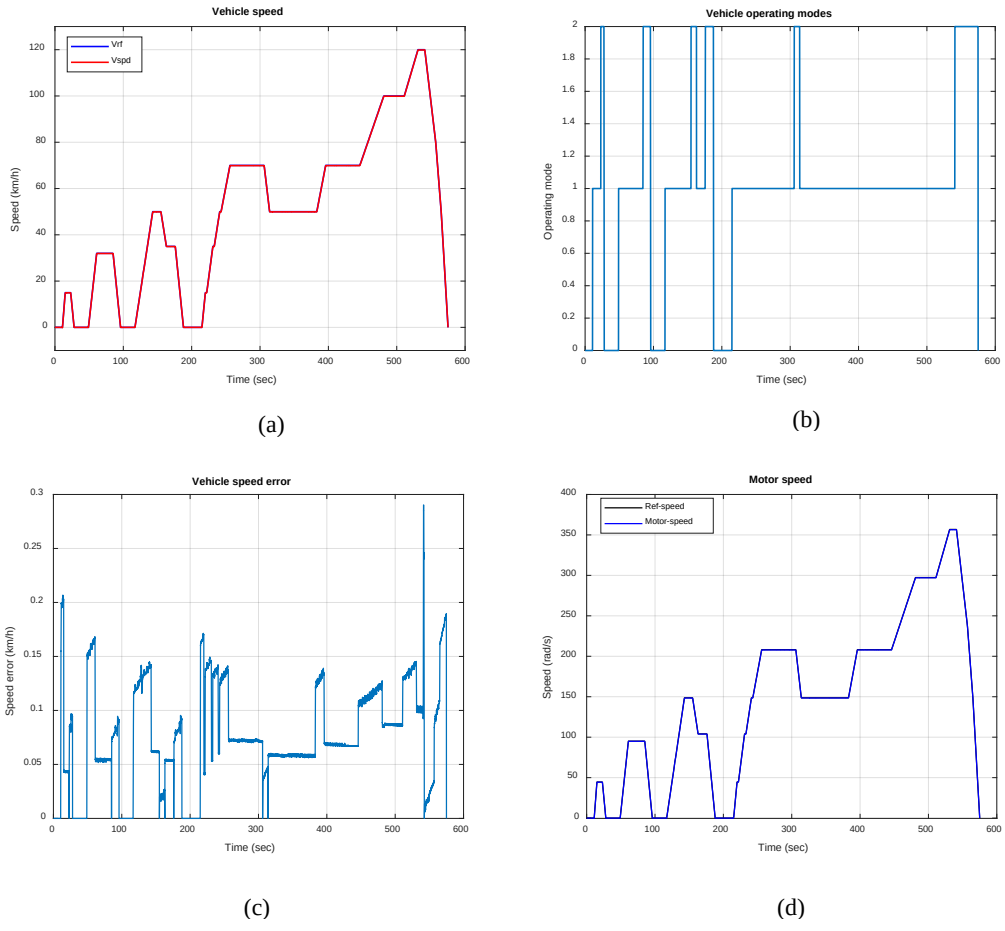

Figure 4.19. NEDC driving cycle: a) Vehicle speed response. b) Vehicle operating modes. c) Vehicle speed error. d) Motor speed. EV based IM-DTC-PI.

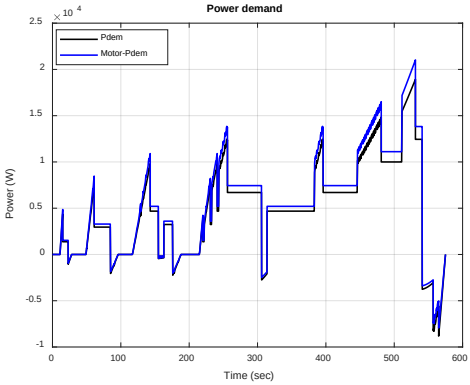

(a)

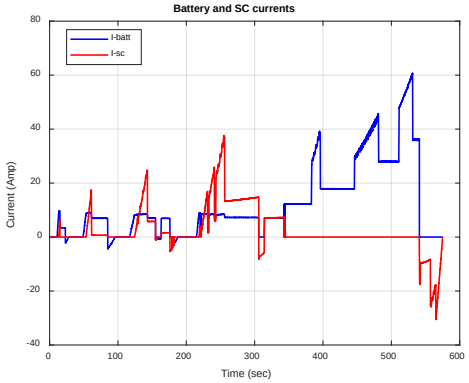

(b)

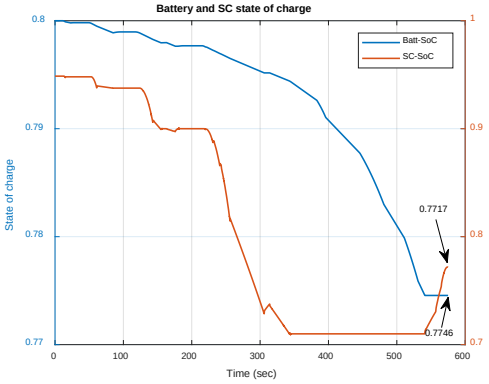

(c)

Figure 4.20. NEDC driving cycle: a) Power demand & Power split. b) Batt/SC currents. c) State of charge of Battery & SC. Based IM-DTC-PI.

In Figure 4.21 and Figure 4.22 for the FLC controller, the EV tracked the reference desired speed with better performance with an average speed error equal to 0.0518 (km/h), and for the SoC of both battery pack and SC, the end values were 0.7759 and 0.7622 respectively.

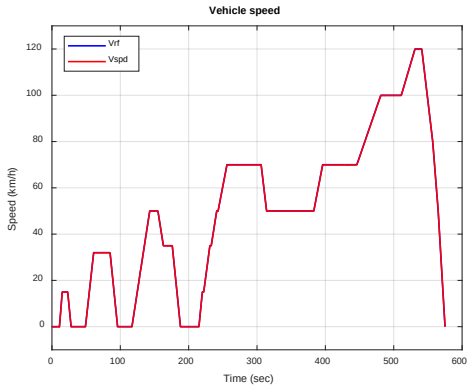

(a)

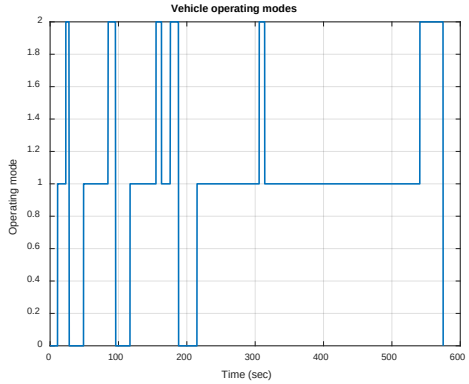

(b)

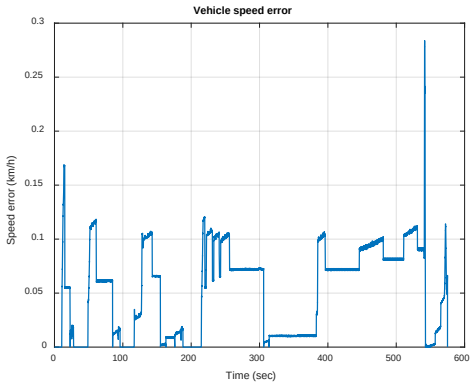

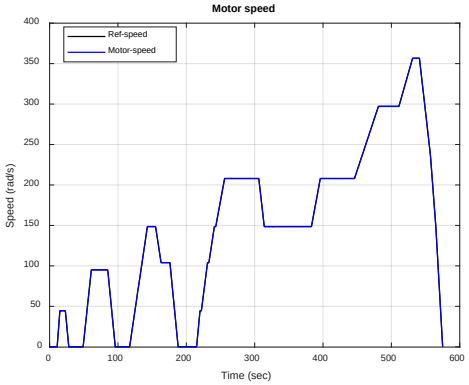

(c) (d)

Figure 4.21. NEDC driving cycle: a) Vehicle speed response. b) Vehicle operating modes. c) Vehicle speed error. d) Motor speed. Based IM-DTC-FLC.

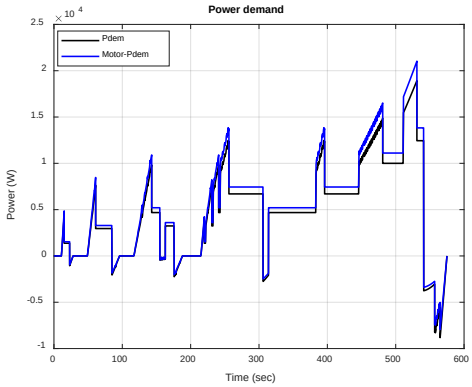

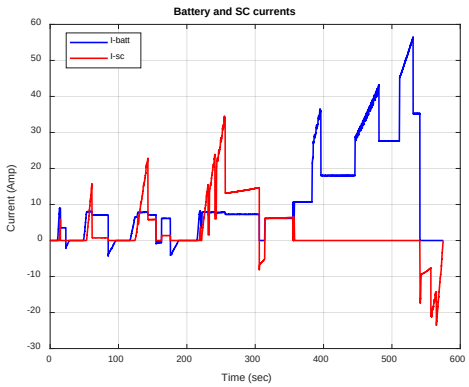

(a) (b)

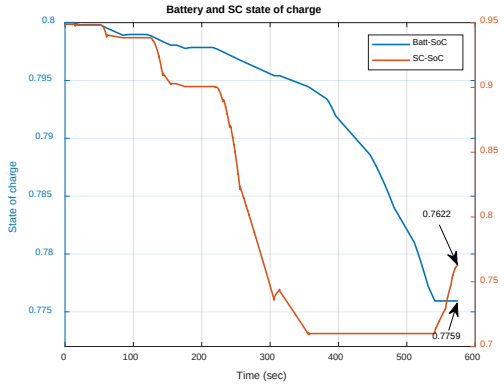

(c)

Figure 4.22. NEDC driving cycle: a) Power demand & Power split. b) Batt/SC currents. c) State of charge of Battery & SC. Based IM-DTC-FLC.

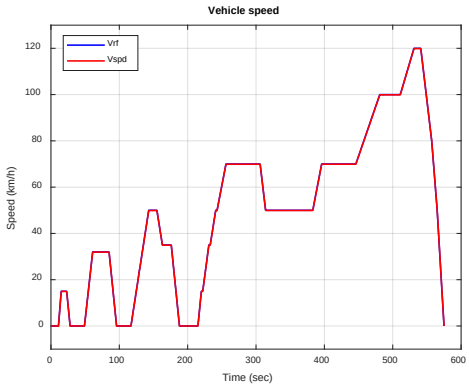

(a)

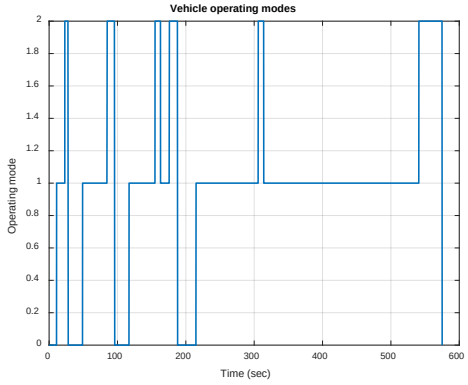

(b)

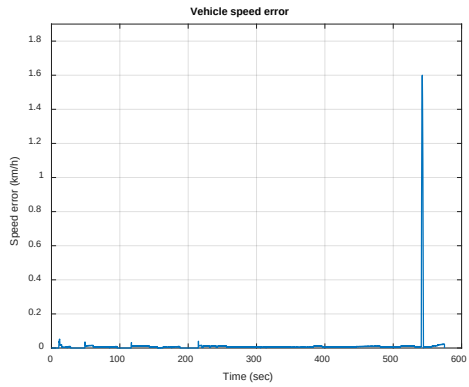

(c)

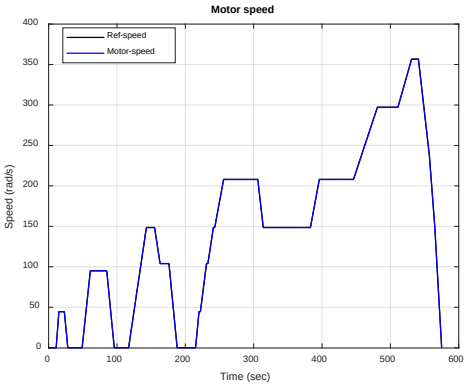

(d)

Figure 4.23. NEDC driving cycle: a) Vehicle speed response. b) Vehicle operating modes. c) Vehicle speed error. d) Motor speed. Based IM-DTC-SMC.

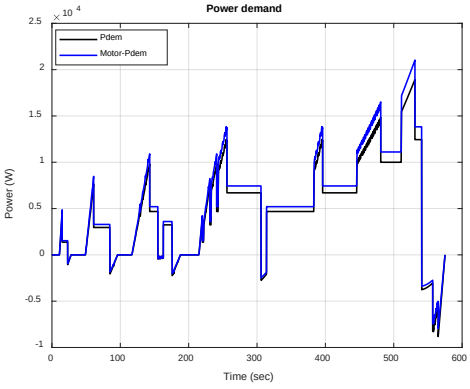

(a)

(b)

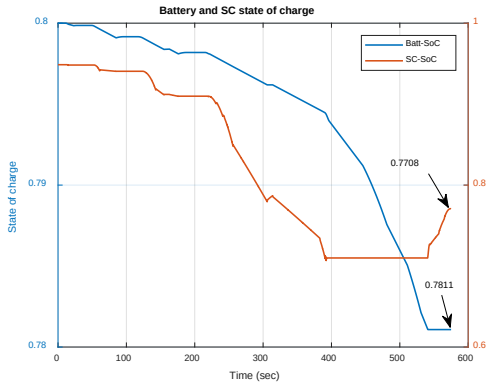

(c)

Figure 4.24. NEDC driving cycle: a) Power demand & Power split. b) Batt/SC currents. c) State of charge of Battery & SC. Based IM-DTC-SMC.

Finally, in the case of the SMC controller as presented in Figure 4.23 and Figure 4.24; the performance was as expected with much less average speed error at 0.0123 (km/h) if compared to the case of PI and FLC controllers. Also, the end value of SoC for both energy storage sources was 0.7811 for the battery pack and 0.7708 for SC.

4.1.1.5. Results Comparison

Figure 4.25 to Figure 4.30 illustrate comparison plots of the state of charge and the change of energy in the battery pack of both HESS and battery-only cases for all simulated situations. Moreover, a detailed comparison table was created from these plots.

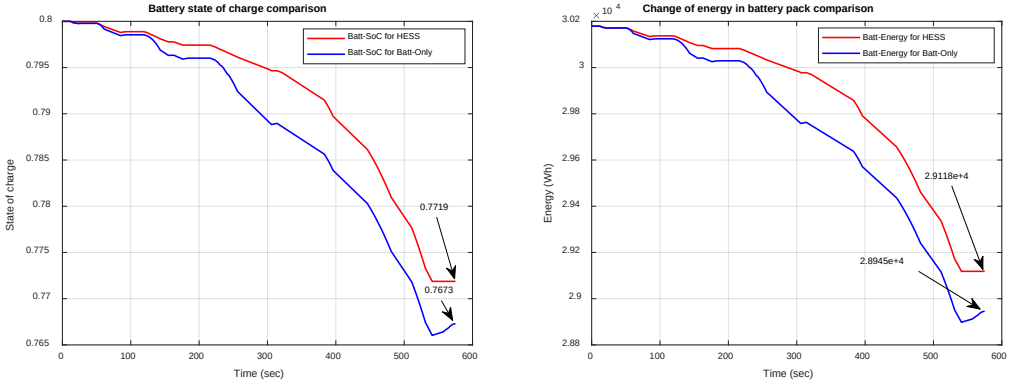

(a) (b)

Figure 4.25. NEDC driving cycle: a) Battery state of charge comparison. b) Change of energy in battery pack comparison. EV Based IM-IFOC-PI.

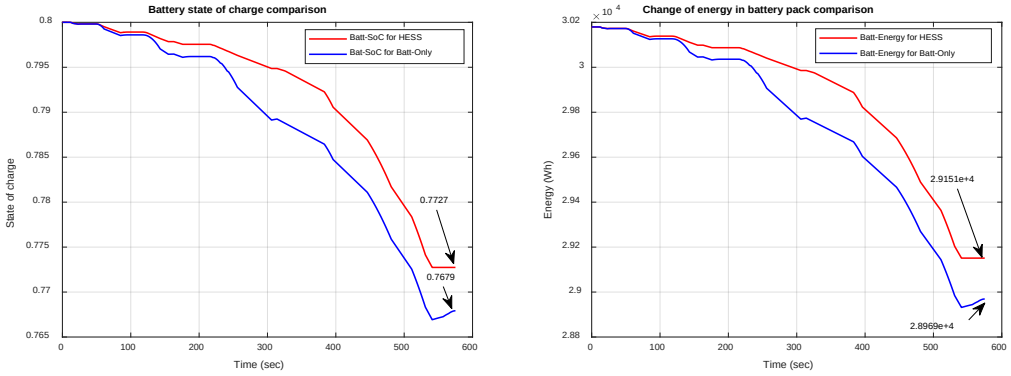

(a) (b)

Figure 4.26. NEDC driving cycle: a) Battery state of charge comparison. b) Change of energy in battery pack comparison. EV Based IM-IFOC-FLC.

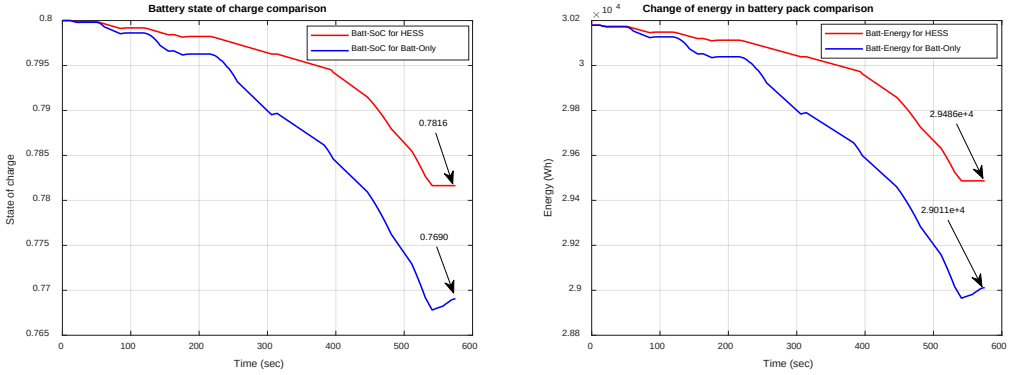

(a) (b)

Figure 4.27. NEDC driving cycle: a) Battery state of charge comparison. b) Change of energy in battery pack comparison. EV Based IM-IFOC-SMC.

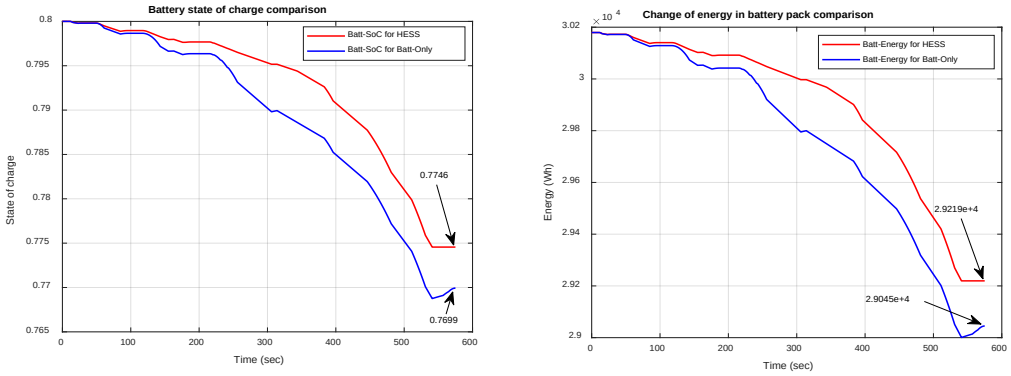

(a) (b)

Figure 4.28. NEDC driving cycle: a) Battery state of charge comparison. b) Change of energy in battery pack comparison. EV Based IM-DTC-PI.

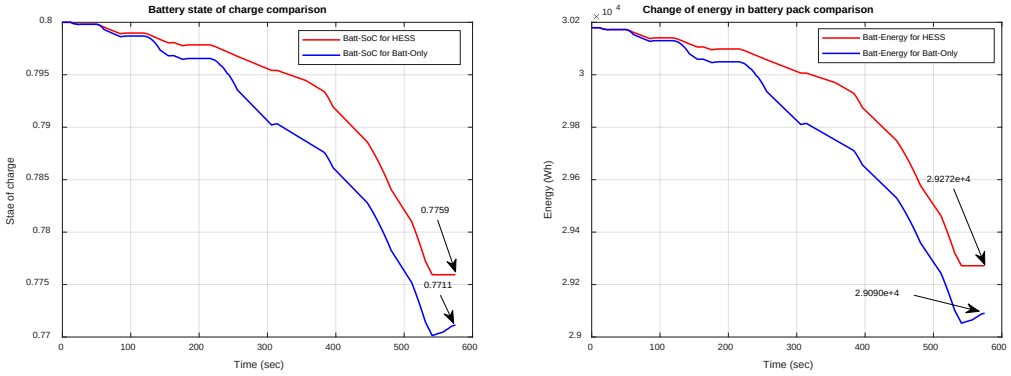

(a) (b)

Figure 4.29. NEDC driving cycle: a) Battery state of charge comparison. b) Change of energy in battery pack comparison. EV Based IM-DTC-FLC.

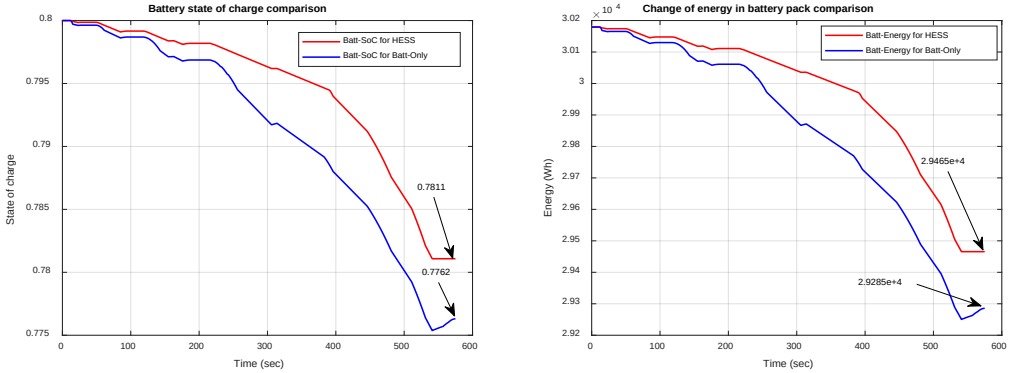

(a) (b)

Figure 4.30. NEDC driving cycle: a) Battery state of charge comparison. b) Change of energy in battery pack comparison. EV Based IM-DTC-SMC.

Table 4.1 presents detailed values of the SoC and the remained energy at the end of the simulation in the battery pack in both HESS and battery-only cases for IFOC and DTC control strategies and also for PI, FLC, and SMC controllers used to obtain these results. Also, a percentage of the energy reduction in the battery pack is introduced in Table 4.1 for further comparison.

However, from the table below in the case of EV-IM-IFOC, it can be seen that more energy consumed in case of using a PI controller if compared to FLC and SMC cases, also SMC shows better performance if compared to PI and FLC, where it reached the end of the simulation time with 3.87% reduction of the start value of the energy in the battery pack, while it was 4.088% and 4.009% for PI and FLC respectively. Moreover,

the effectiveness of utilizing the HESS is noticed as it reduces the reduction in the energy of the battery pack from 4.088% to 3.515% in the case of PI controller, and from 4.009% to 3.406% in the case of the FLC controller, and from 3.87% to 2.29% for the SMC controller.

Table 4.1. EV based IM numerical comparison.

	Controller Type	Energy Storage Configuration	SoC end value	Energy end value	Energy reduction (%)
EV-IM-IFOC	PI	Batt-only	0.7673	2.8945e+4	4.088%
		Batt/SC	0.7719	2.9118e+4	3.515%
	FLC	Batt-only	0.7679	2.8969e+4	4.009%
		Batt/SC	0.7727	2.9151e+4	3.406%
	SMC	Batt-only	0.7690	2.9011e+4	3.87%
		Batt/SC	0.7816	2.9486e+4	2.29%
EV-IM-DTC	PI	Batt-only	0.7699	2.9045e+4	3.757%
		Batt/SC	0.7746	2.9219e+4	3.181%
	FLC	Batt-only	0.7711	2.9090e+4	3.608%
		Batt/SC	0.7759	2.9272e+4	3.005%
	SMC	Batt-only	0.7762	2.9285e+4	2.962%
		Batt/SC	0.7811	2.9465e+4	2.365%

Likewise, in the case of EV-IM-DTC, the superior performance of the SMC is achieved if compared to the detailed results obtained when utilizing PI and FLC controllers. Also, reduction of the battery pack energy consumption is attained when applying hybridization of the energy storage system that led to improving the EV range and battery life.

In detail, consumed energy is improved from 3.757% to 3.181% for PI controller, and from 3.608% to 3.005% in case of FLC controller while for SMC was saved from 2.962% to 2.365%.

4.1.2. Electric Vehicle Based PMSM

Further investigation of the developed platform is carried out by simulating the EV driven by PMSM based on both IFOC and DTC control strategies utilizing the three different speed controllers used previously for IM which are PI, FLC, and SMC. Also, in this section, both cases of using HESS and battery-only are simulated and good

results are obtained. All possible configurations are presented in the following subsections, then the obtained results are discussed in the comparison section.

4.1.2.1. Simulation Based Battery-Only (IFOC for PI, FLC and SMC)

Similar to the EV-IM section; the results are grouped in two groups for each possible configuration, the first group contains the plots of vehicle speed tracking, vehicle speed error, motor speed, and vehicle operating mode, then the second group contains vehicle power demand, motor power demand, battery pack current and state of charge.

Figure 4.31a and Figure 4.31c show the acceptable performance of the EV using the PI controller in speed tracking with an average speed error of 0.1096 (km/h). Also, Figure 4.31b and Figure 4.31d present the EV operating modes and relative traction motor speed in rad/s.

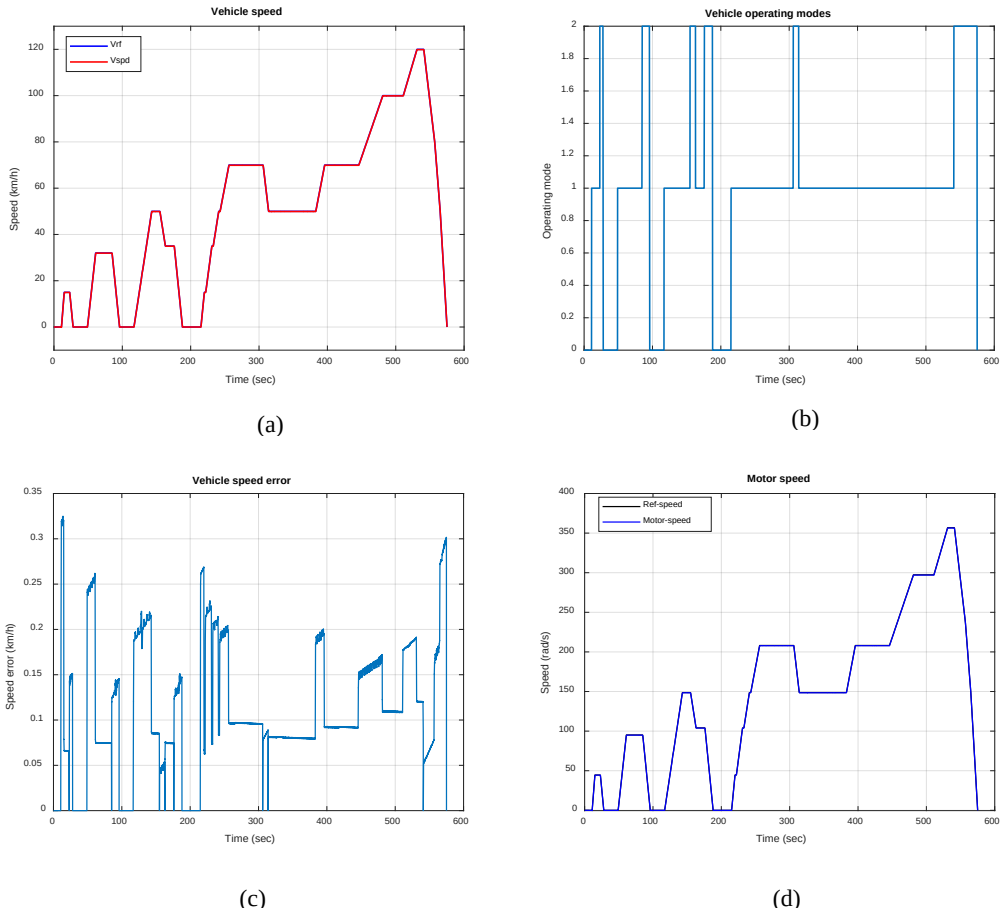

Figure 4.31. NEDC driving cycle: a) Vehicle speed response. b) Vehicle operating modes. c) Vehicle speed error. d) Motor speed. EV based PMSM-IFOC-PI.

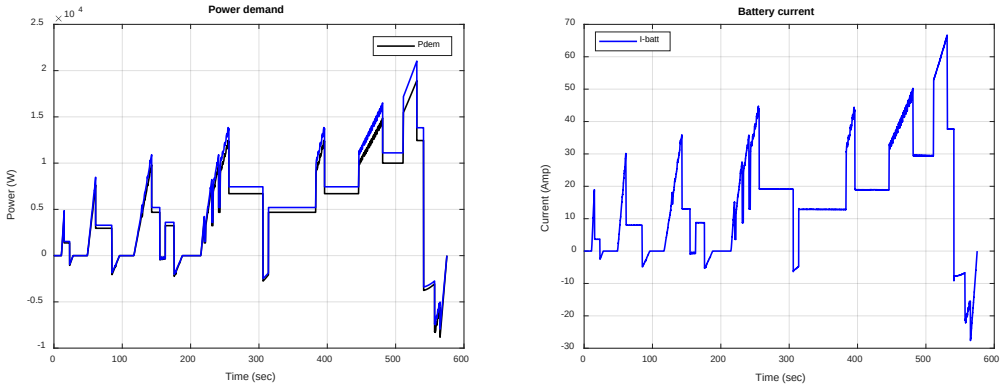

(a) (b)

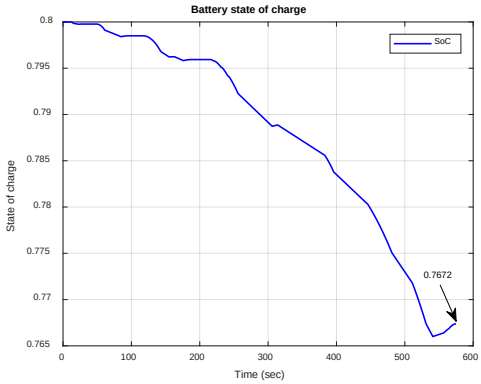

(c)

Figure 4.32. NEDC driving cycle: a) Power demand & Power split. b) Battery current. c) State of charge of Battery. EV based PMSM- IFOC-PI.

Moreover, the vehicle power demand and the power delivered by the electric traction motor are plotted in Figure 4.32a, while the battery current and the SoC of the battery are shown in Figure 4.32b and Figure 4.32c respectively, where the SoC end value of the battery pack is 0.7672.

On the other hand, the FLC achieved better performance than the PI controller with an average speed error of 0.0550 (km/h) as illustrated in Figure 4.33a and Figure 4.33d. Then in Figure 4.34c, the reduction in the SoC of the battery pack during the vehicle propelling and recharging process during regenerative braking can be noticed with an end value equal to 0.7709. Also, the relative battery pack current is presented in Figure 4.34b.

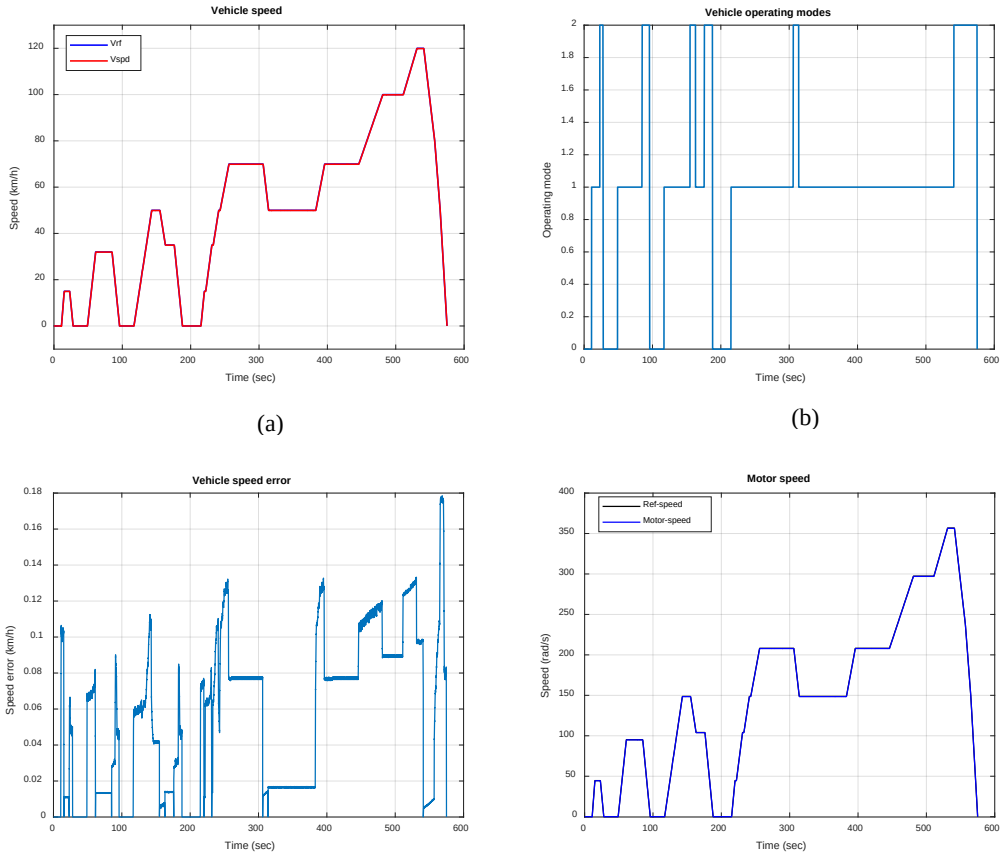

Figure 4.33. NEDC driving cycle: a) Vehicle speed response. b) Vehicle operating modes. c) Vehicle speed error. d) Motor speed. EV based PMSM-IFOC-FLC.

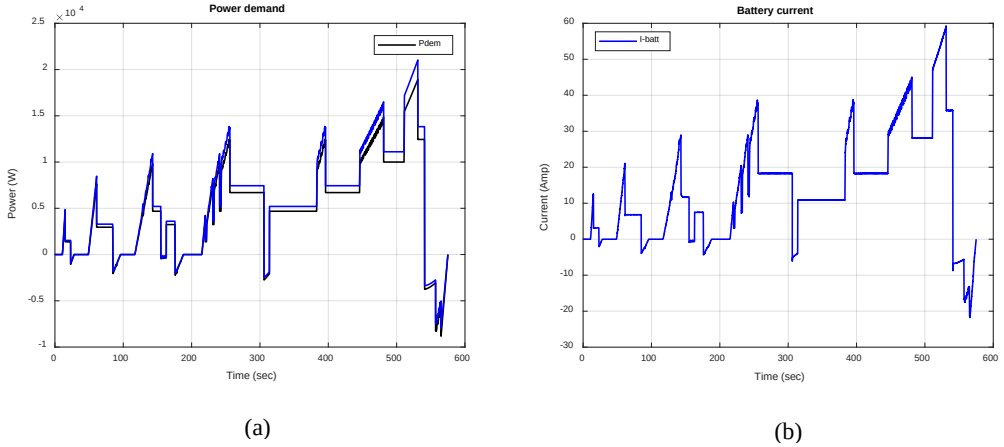

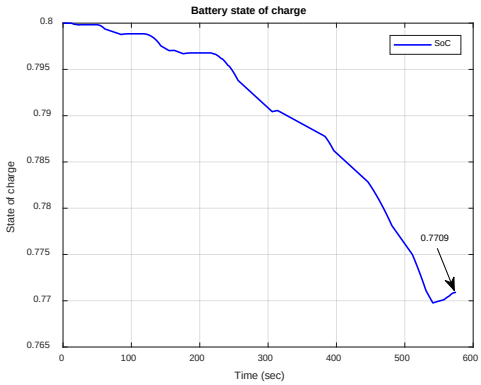

(c)

Figure 4.34. NEDC driving cycle: a) Power demand & Power split. b) Battery current. c) State of charge of Battery. EV based PMSM- IFOC-FLC.

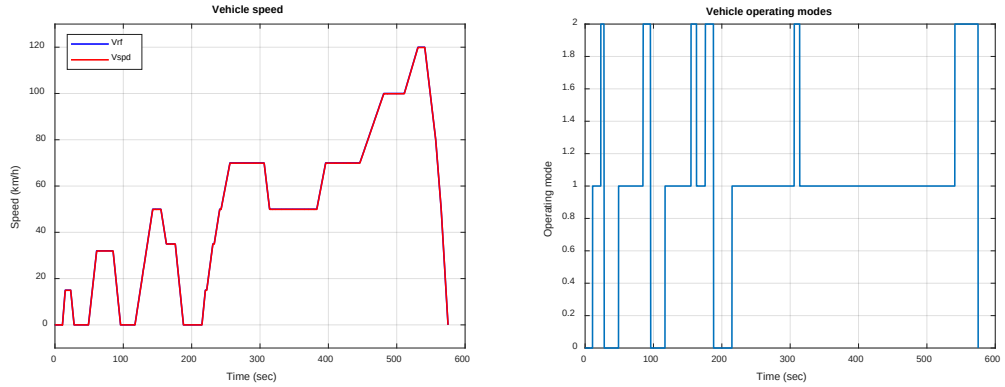

(a)

(b)

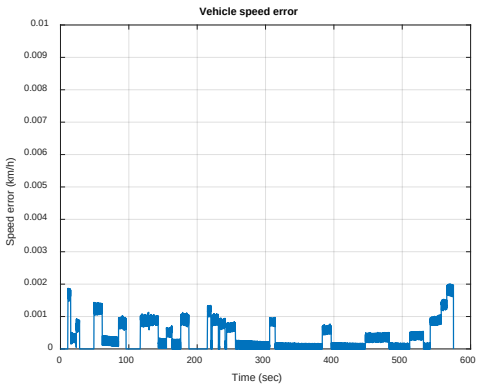

(c)

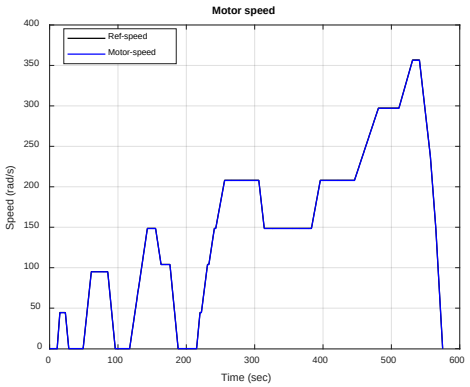

(d)

Figure 4.35. NEDC driving cycle: a) Vehicle speed response. b) Vehicle operating modes. c) Vehicle speed error. d) Motor speed. EV based PMSM-IFOC-SMC.

Furthermore, the SMC in Figure 4.35a and Figure 4.35d show superior speed tracking of the vehicle with an average speed error equal to 3.5957e-4 (km/h), while the end value of the battery pack state of charge was equal to 0.7768 as shown in Figure 4.36c.

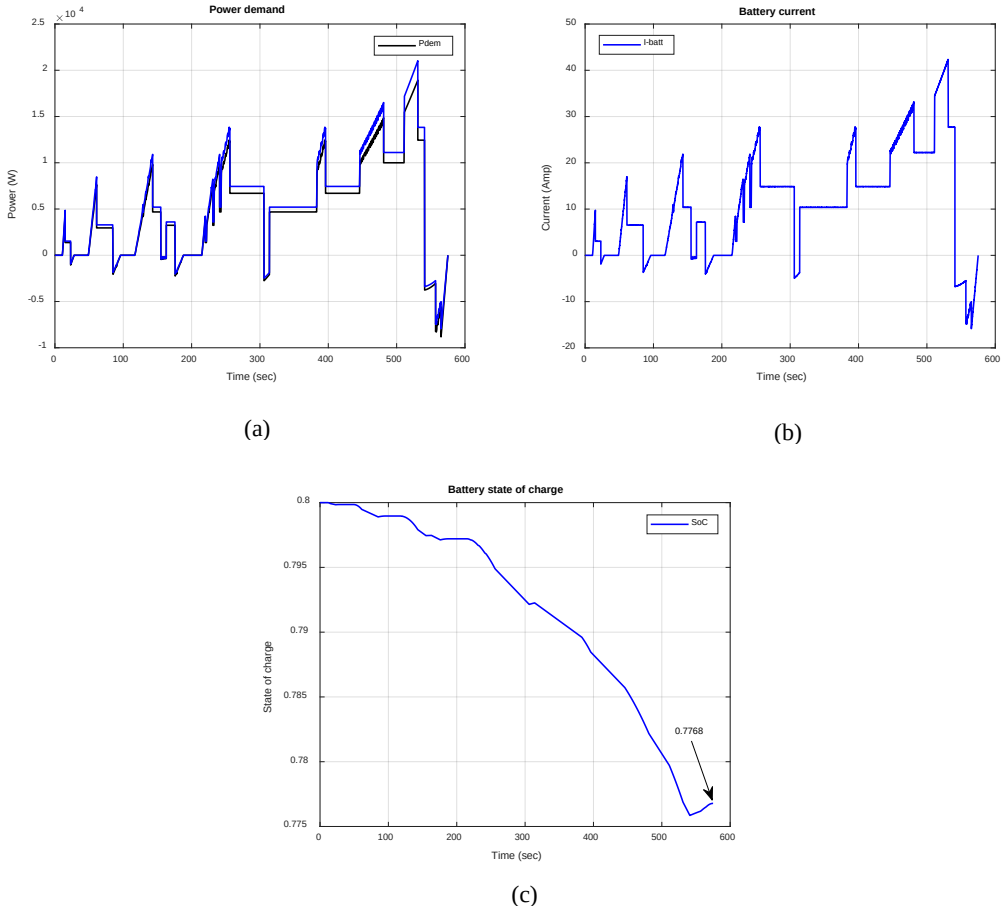

(a) (b)

(c)

Figure 4.36. NEDC driving cycle: a) Power demand & Power split. b) Battery current. c) State of charge of Battery. EV based PMSM- IFOC-SMC.

4.1.2.2. Simulation Based HESS (IFOC for PI, FLC and SMC)

EV driven by PMSM is simulated in this subsection under IFOC for PI, FLC and SMC, moreover; HESS is used to provide all demand energy to the electric traction motor. Figure 4.37 and Figure 4.38 reveal that the PI controller shows good behavior in terms of speed tracking with an average speed error equal to 0.1098 (km/h), and the SoC end values are 0.7718 and 0.7808 for the battery and the SC respectively as shown in Figure 4.38c. Whereas the performance in the case of the FLC controller was better than in the case of the PI controller with an average speed error equal to 0.0551 (km/h), and

the end value of the state of charge for the battery pack is 0.7755 and for SC is 0.7674 as illustrated in Figure 4.39 and Figure 4.40.

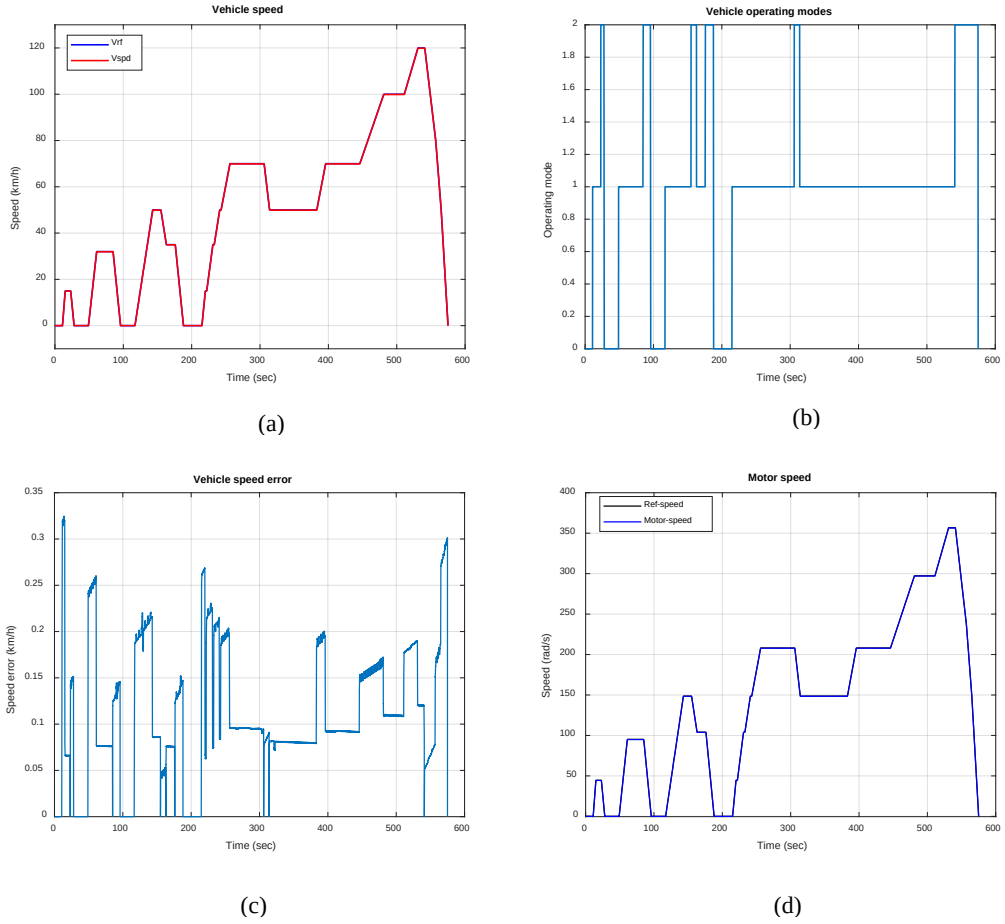

Figure 4.37. NEDC driving cycle: a) Vehicle speed response. b) Vehicle operating modes. c) Vehicle speed error. d) Motor speed. EV based PMSM-IFOC-PI.

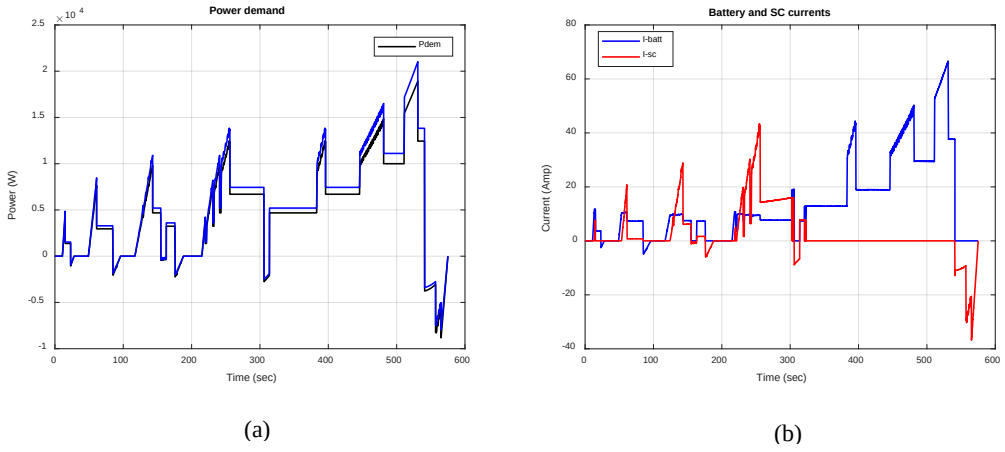

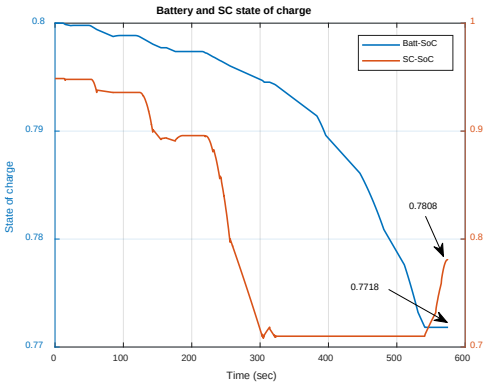

(c)

Figure 4.38. NEDC driving cycle: a) Power demand & Power split. b) Battery & SC currents. c) State of charge of Battery & SC. EV based PMSM- IFOC-PI.

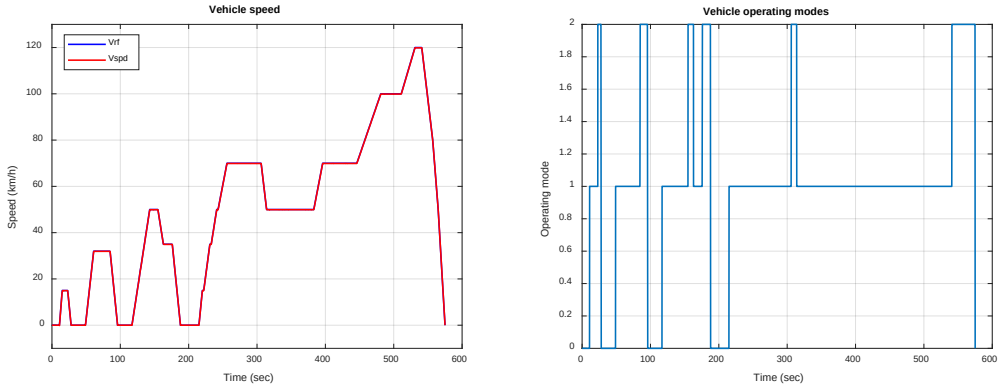

(a)

(b)

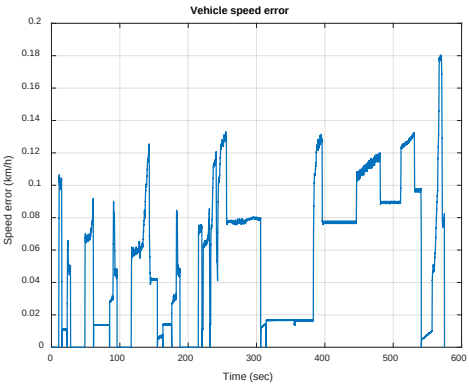

(c)

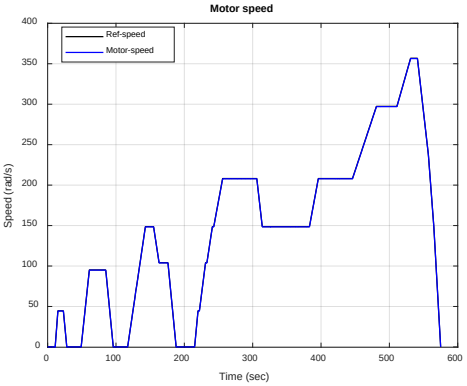

(d)

Figure 4.39. NEDC driving cycle: a) Vehicle speed response. b) Vehicle operating modes. c) Vehicle speed error. d) Motor speed. EV based PMSM-IFOC-FLC.

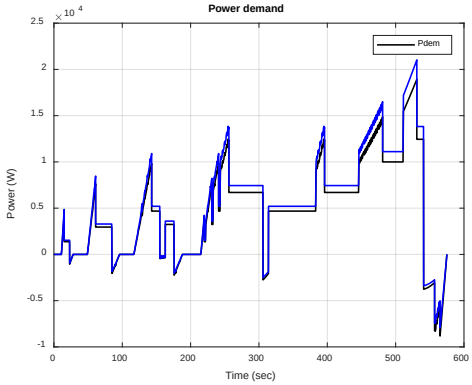

(a)

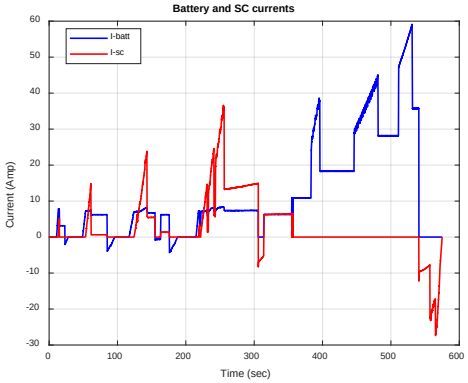

(b)

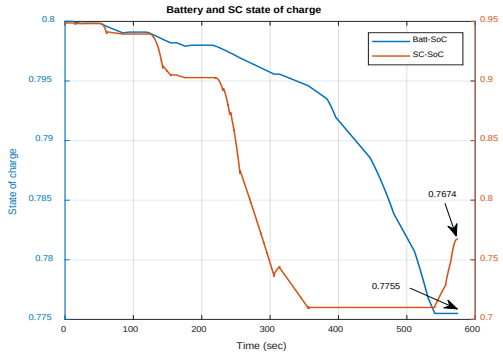

(c)

Figure 4.40. NEDC driving cycle: a) Power demand & Power split. b) Battery & SC currents. c) State of charge of Battery & SC. EV based PMSM- IFOC-FLC.

The results obtained in Figure 4.41 and Figure 4.42; reveal the superior performance of the SMC controller in the case of speed tracking with an average speed error equal to 3.5866e-4 (km/h), with an end value of the SoC for the battery pack, is 0.7816 and for SC is 0.7585.

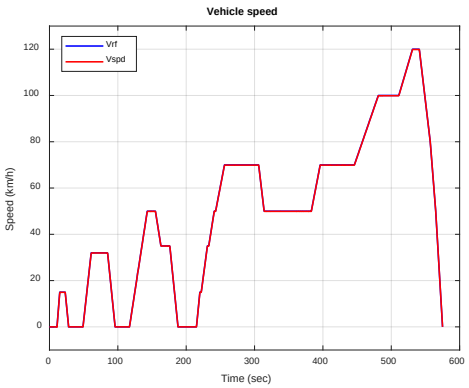

(a)

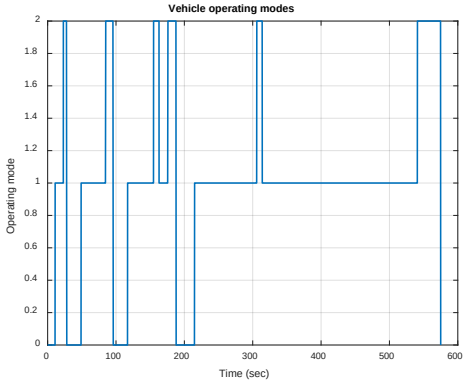

(b)

.

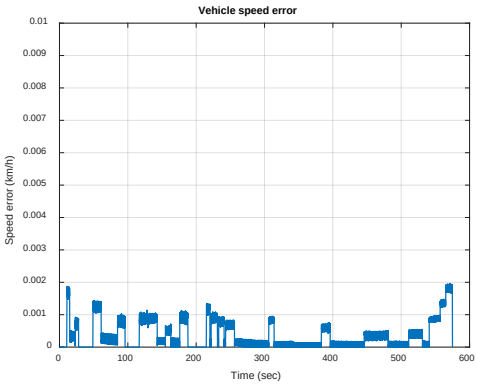

(c)

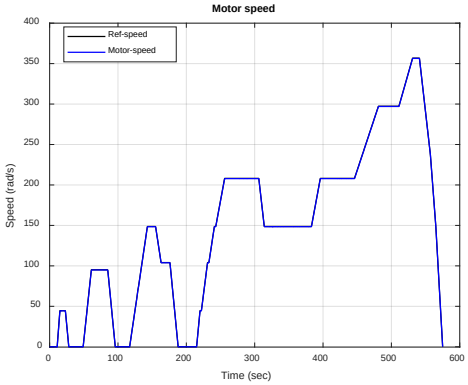

(d)

Figure 4.41. NEDC driving cycle: a) Vehicle speed response. b) Vehicle operating modes. c) Vehicle speed error. d) Motor speed. EV based PMSM-IFOC-SMC.

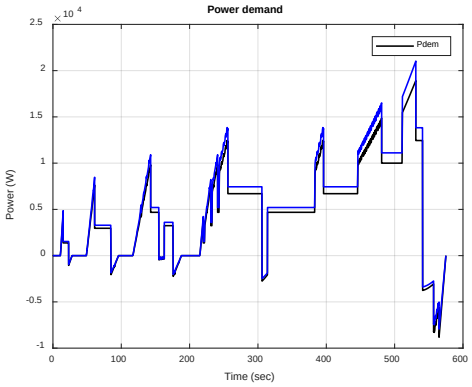

(a)

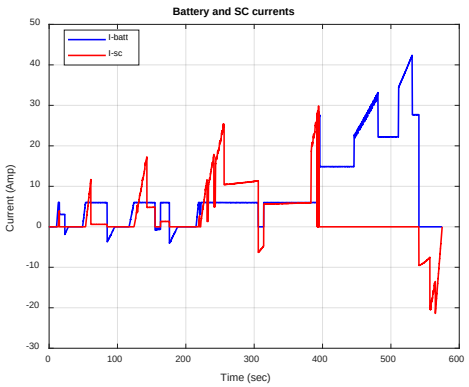

(b)

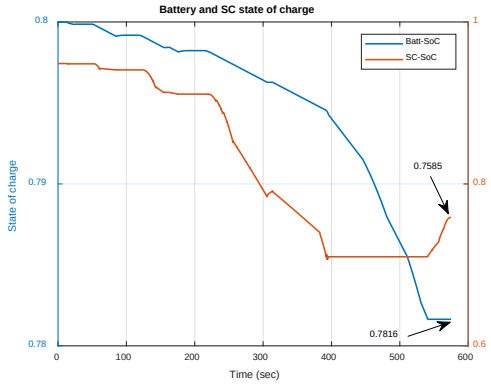

(c)

Figure 4.42. NEDC driving cycle: a) Power demand & Power split. b) Battery & SC currents. c) State of charge of Battery & SC. EV based PMSM- IFOC-SMC.

4.1.2.3. Simulation Based Battery-Only (DTC for PI, FLC and SMC)

In the same way, in this subsection, the EV driven by PMSM under the DTC control strategy is simulated for the NEDC drive cycle. the simulation carried out for PI, FLC, and SMC controllers. PI controller achieved acceptable performance with an average speed error equal to 0.1291 (km/h) as seen in Figure 4.43, also battery pack current and its corresponding SoC behavior are plotted in Figure 4.44, where the SoC end value is equal to 0.7659.

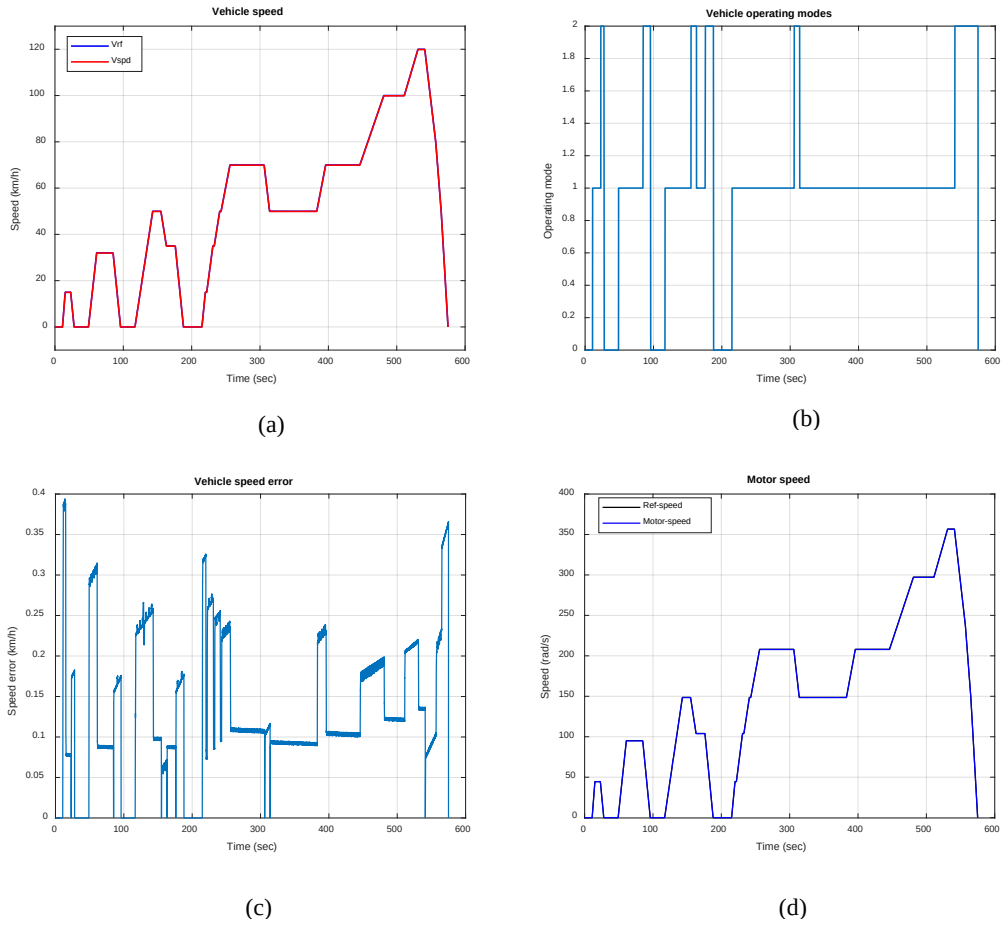

Figure 4.43. NEDC driving cycle: a) Vehicle speed response. b) Vehicle operating modes. c) Vehicle speed error. d) Motor speed. EV based PMSM-DTC-PI.

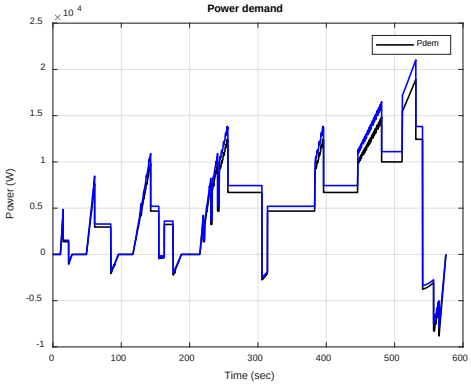

(a)

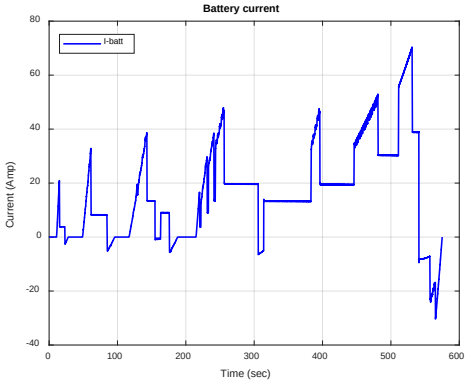

(b)

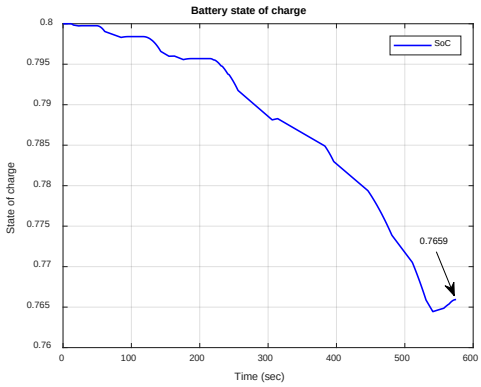

(c)

Figure 4.44. NEDC driving cycle: a) Power demand & Power split. b) Battery current. c) State of charge of Battery. EV based PMSM- DTC-PI.

Moreover, the FLC controller tracked the desired reference speed with an average speed error equivalent to 0.0538 (km/h), and the SoC end value is 0.7718. as shown in Figure 4.45 and Figure 4.46.

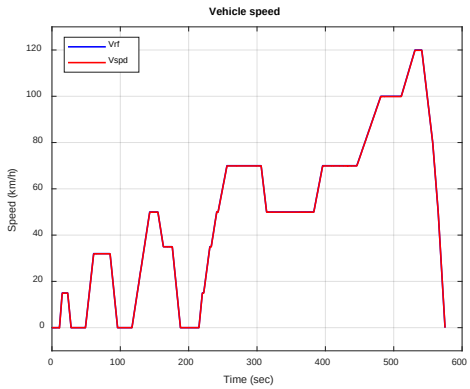

(a)

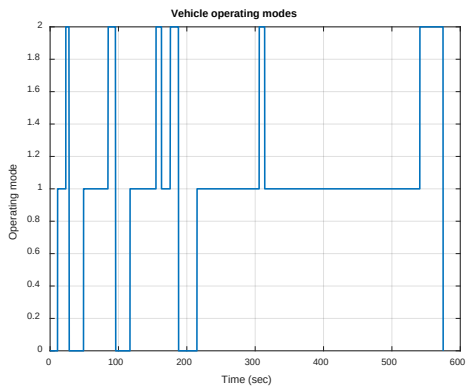

(b)

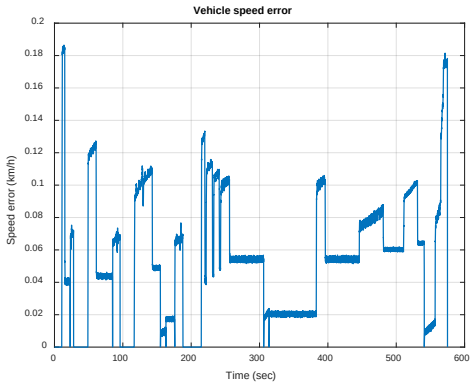

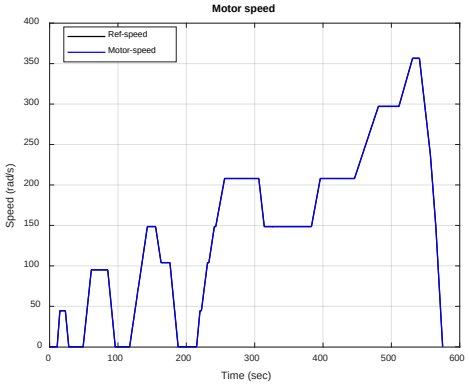

(c) (d)

Figure 4.45. NEDC driving cycle: a) Vehicle speed response. b) Vehicle operating modes. c) Vehicle speed error. d) Motor speed. EV based PMSM-DTC-FLC.

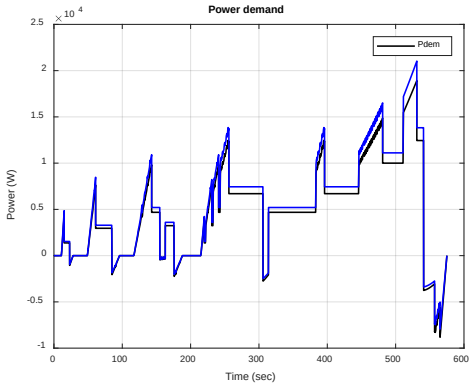

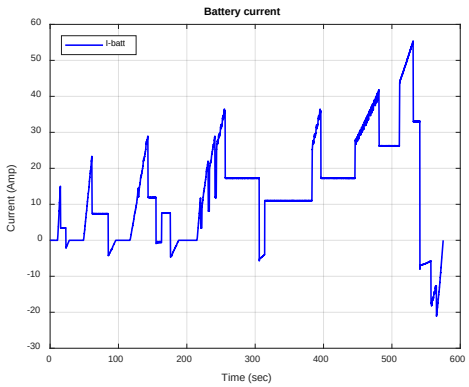

(a) (b)

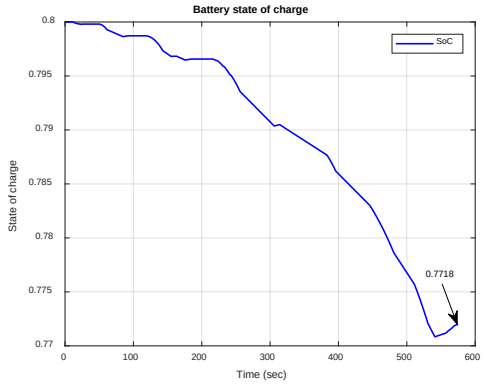

(c)

Figure 4.46. NEDC driving cycle: a) Power demand & Power split. b) Battery current. c) State of charge of Battery. EV based PMSM- DTC-FLC.

Furthermore, in Figure 4.47 and Figure 4.48; the performance of the SMC controller was better than PI and FLC cases with an average speed error 0.0111 (km/h). and SoC ends value equal to 0.7759.

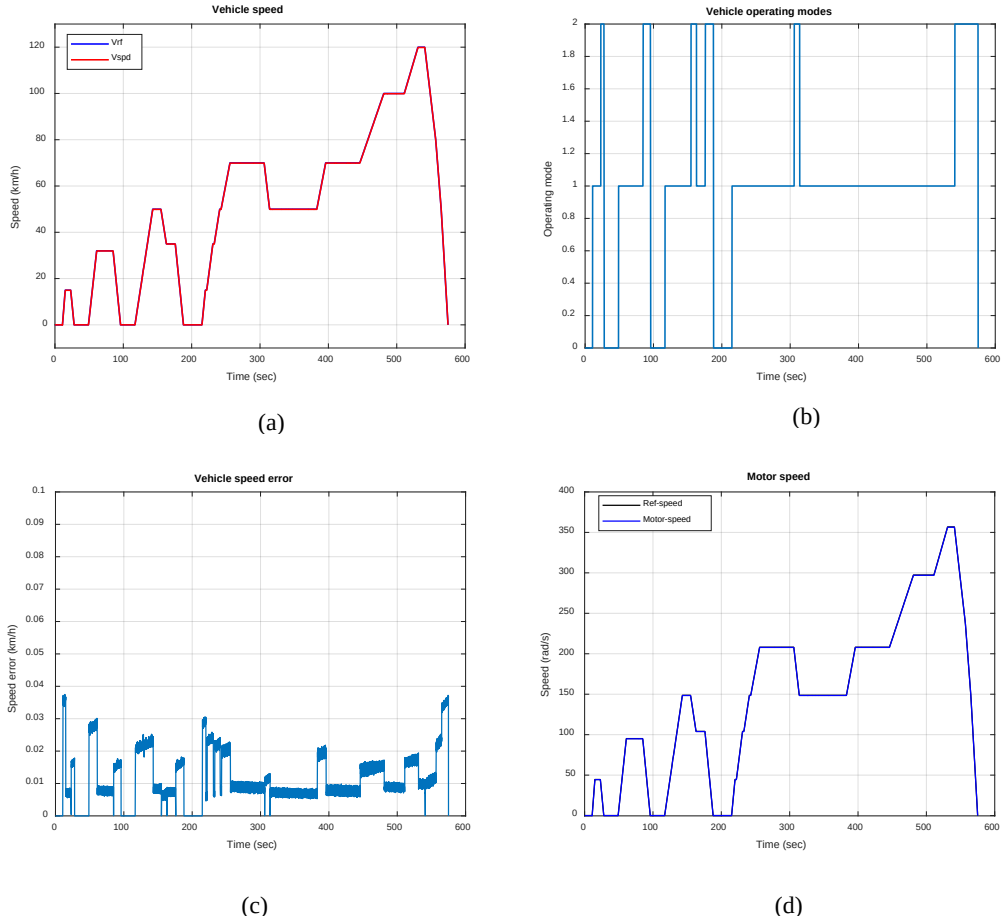

Figure 4.47. NEDC driving cycle: a) Vehicle speed response. b) Vehicle operating modes. c) Vehicle speed error. d) Motor speed. EV based PMSM-DTC-SMC.

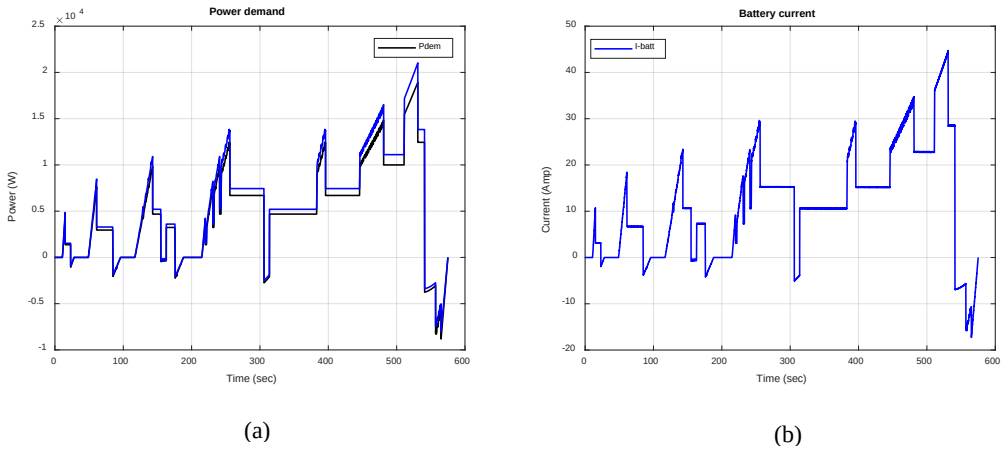

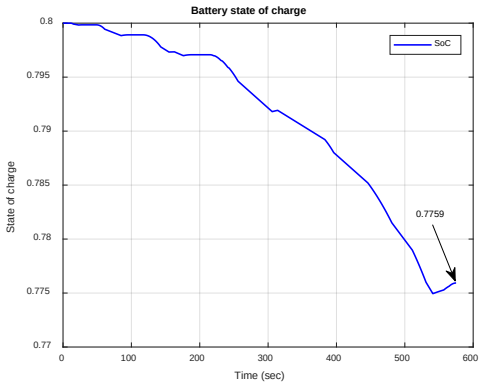

(c)

Figure 4.48. NEDC driving cycle: a) Power demand & Power split. b) Battery current. c) State of charge of Battery. EV based PMSM- DTC-SMC.

4.1.2.4. Simulation Based HESS (DTC for PI, FLC and SMC)

Similar to the case of EV driven by IM-DTC based HESS, in this part, EV-PMSM-DTC is simulated using HESS to provide all demand energy during simulation of the NEDC drive cycle. The EV simulated for PI, FLC, and SMC controller and then achieved results presented in the following figures.

In the case of the PI controller, the EV tracked the desired reference speed with an average error equal to 0.1097 (km/h), as shown in Figure 4.49, also, the SoC end value of the battery pack reduced to 0.7718, on the other hand; the SoC end value of the SC was equal to 0.7808 at the end time of NEDC drive cycle as seen in Figure 4.50.

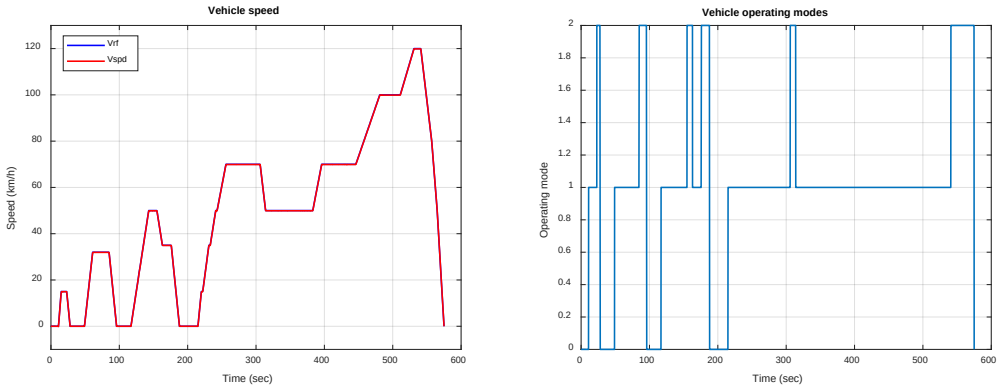

(a) (b)

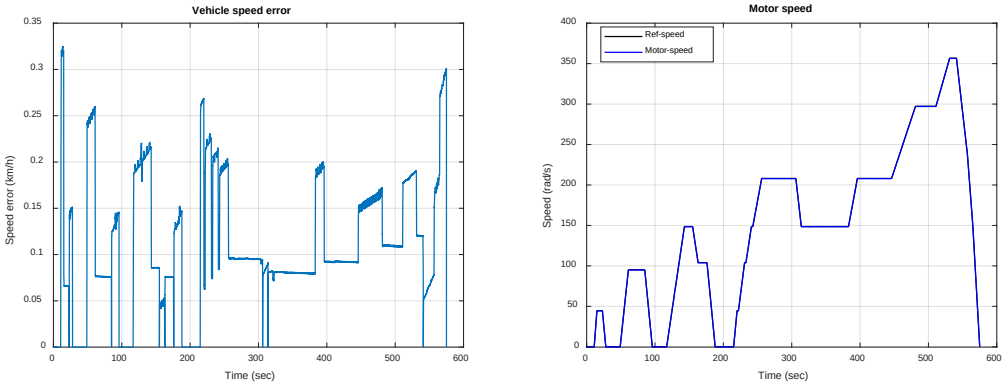

(c) (d)

Figure 4.49. NEDC driving cycle: a) Vehicle speed response. b) Vehicle operating modes. c) Vehicle speed error. d) Motor speed. EV based PMSM- DTC-PI.

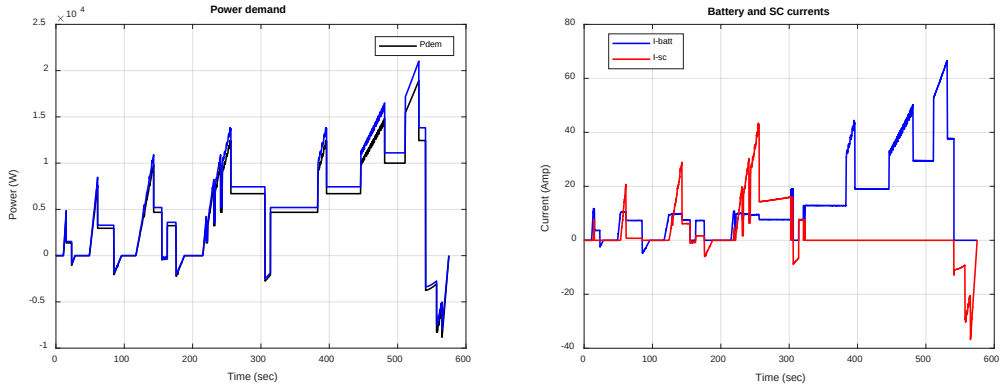

(a) (b)

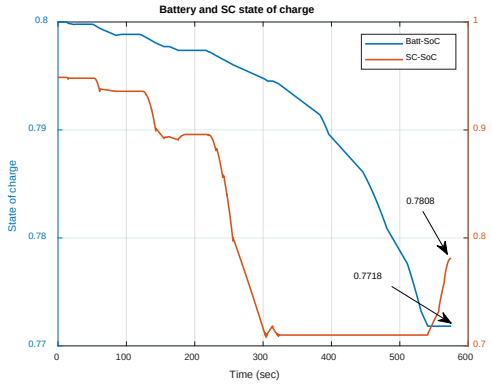

(c)

Figure 4.50. NEDC driving cycle: a) Power demand & Power split. b) Battery & SC currents. c) State of charge of Battery & SC. EV based PMSM- DTC-PI.

FLC controller in Figure 4.51 and Figure 4.52 achieved better performance in speed tracking with an average speed error equal to 0.0551 (km/h), also the SoC end value of both battery pack and SC were 0.7756 and 0.7673 respectively.

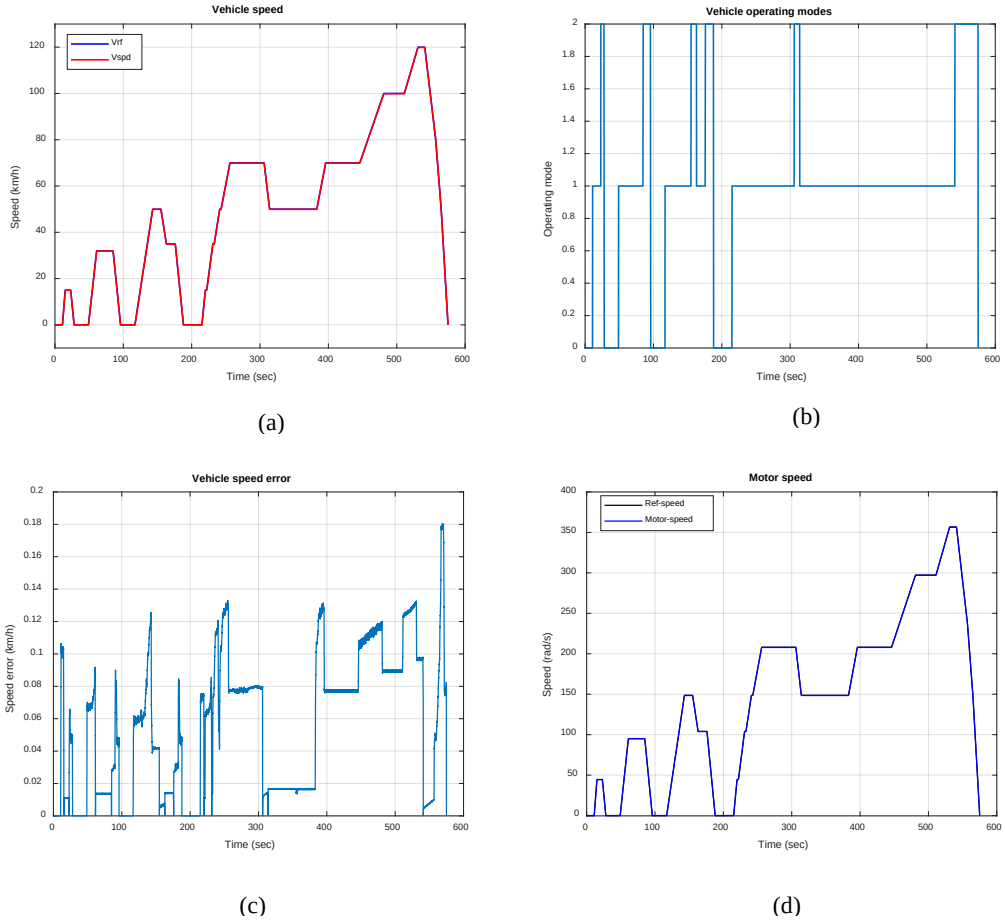

Figure 4.51. NEDC driving cycle: a) Vehicle speed response. b) Vehicle operating modes. c) Vehicle speed error. d) Motor speed. EV based PMSM- DTC-FLC.

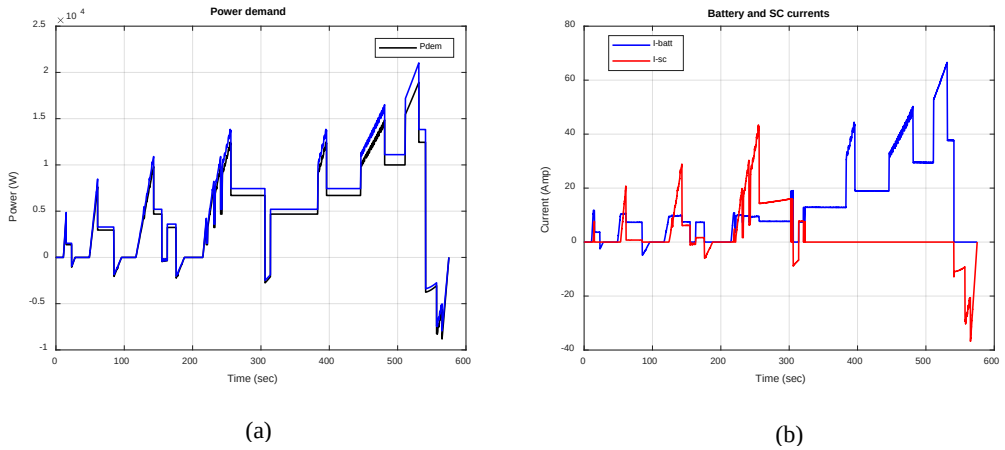

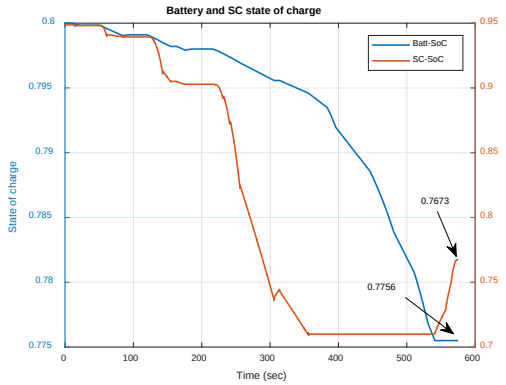

(c)

Figure 4.52. NEDC driving cycle: a) Power demand & Power split. b) Battery & SC currents. c) State of charge of Battery & SC. EV based PMSM- DTC-FLC.

Lastly, in the case of the SMC controller as presented in Figure 4.53 and Figure 4.54; the performance was as expected with a much lower average speed error at 0.0094 (km/h) if compared to the case of PI and FLC controllers. Furthermore, the end value of the SoC was 0.7809 for the battery pack and 0.7607 for SC.

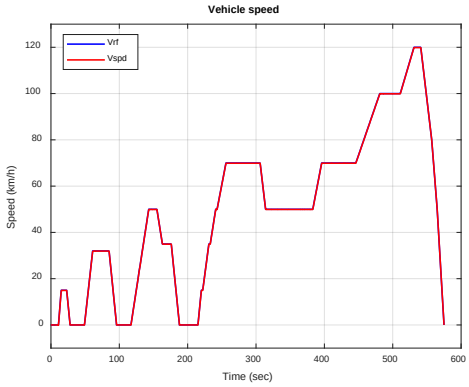

(a)

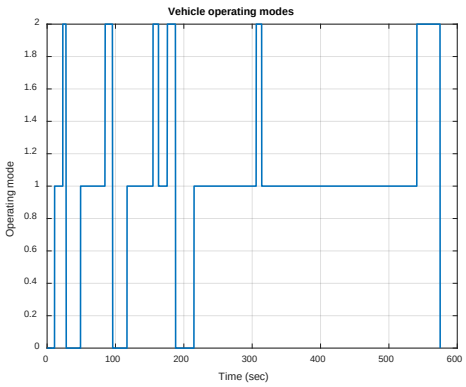

(b)

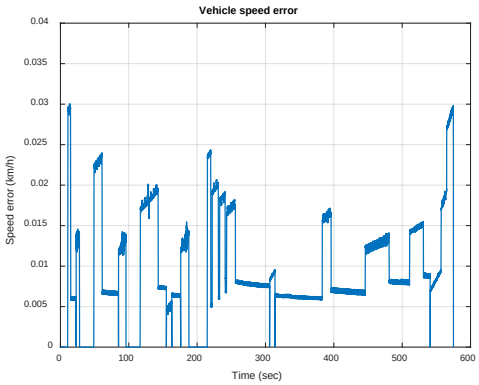

(c)

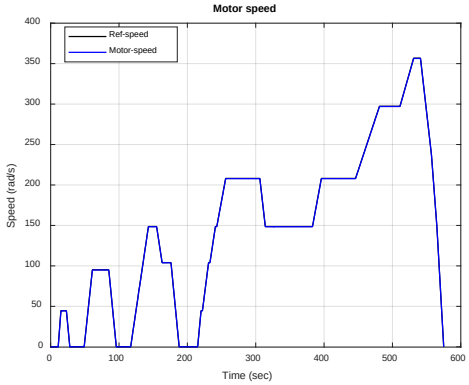

(d)

Figure 4.53. NEDC driving cycle: a) Vehicle speed response. b) Vehicle operating modes. c) Vehicle speed error. d) Motor speed. EV based PMSM- DTC-SMC.

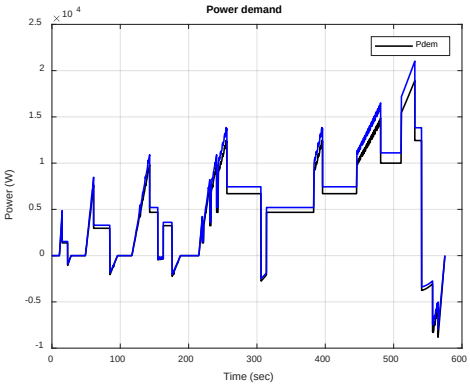

(a)

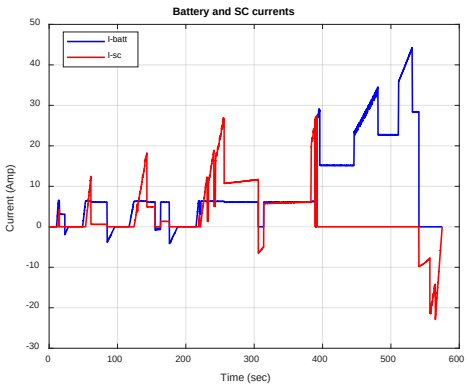

(b)

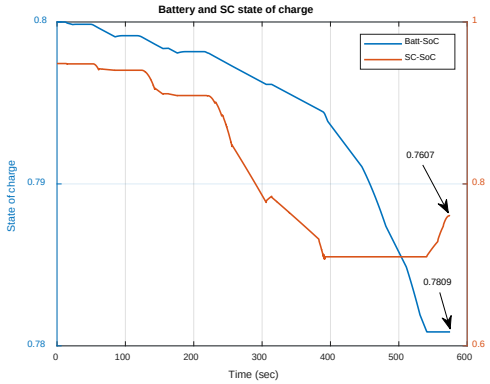

(c)

Figure 4.54. NEDC driving cycle: a) Power demand & Power split. b) Battery & SC currents. c) State of charge of Battery & SC. EV based PMSM- DTC-SMC.

4.1.2.5. Results Comparison

Similar to the comparison of EV driven by IM; Figure 4.55 to Figure 4.60 illustrate comparison plots of the state of charge and the change in energy of the battery pack in both HESS and battery-only cases for all simulated situations. The end values of all plotted variables are written on each corresponding figure. Furthermore; Table 4.2 presents a detailed comparison for all possible simulated situations for the EV-PMSM.

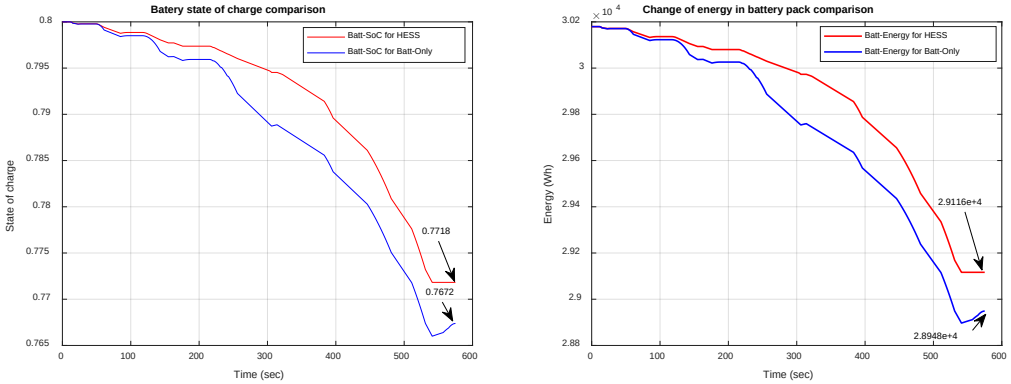

(a) (b)

Figure 4.55. NEDC driving cycle: a) Battery state of charge comparison. b) Change of energy in battery pack comparison. EV Based PMSM-IFOC-PI.

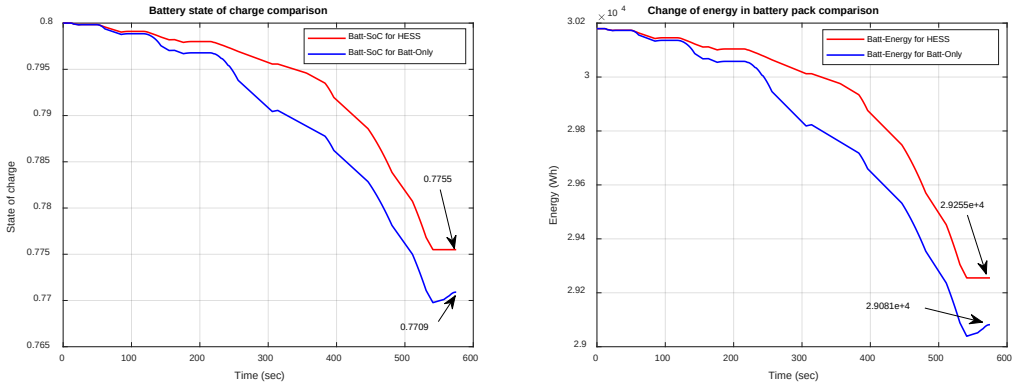

(a) (b)

Figure 4.56. NEDC driving cycle: a) Battery state of charge comparison. b) Change of energy in battery pack comparison. EV Based PMSM-IFOC-FLC.

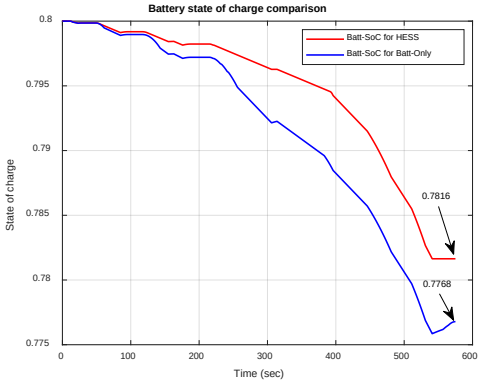

(a)

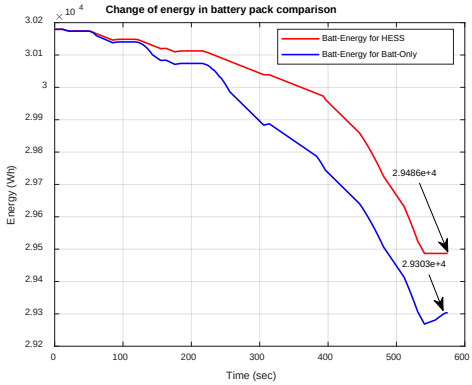

(b)

Figure 4.57. NEDC driving cycle: a) Battery state of charge comparison. b) Change of energy in battery pack comparison. EV Based PMSM-IFOC-SMC.

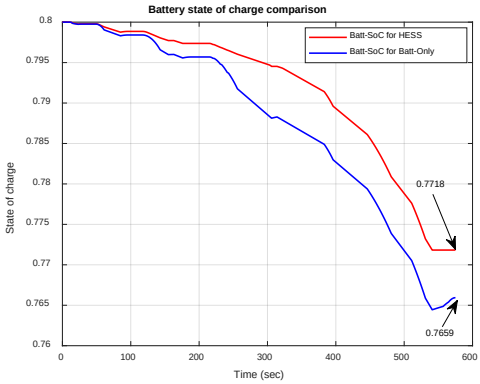

(a)

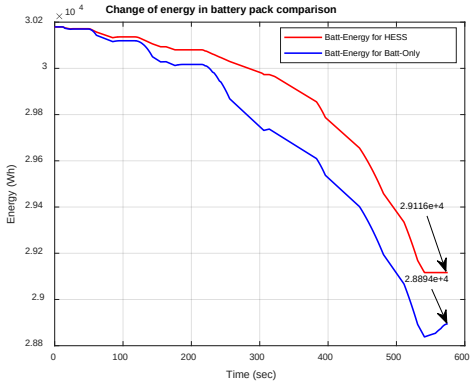

(b)

Figure 4.58. NEDC driving cycle: a) Battery state of charge comparison. b) Change of energy in battery pack comparison. EV Based PMSM-DTC-PI.

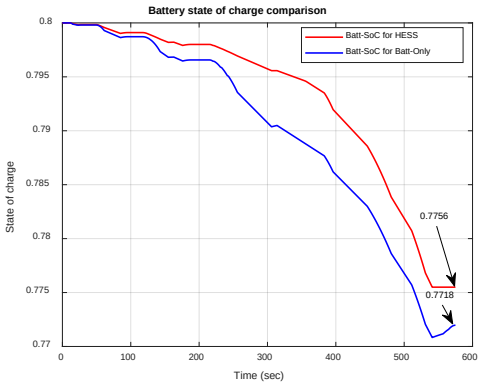

(a)

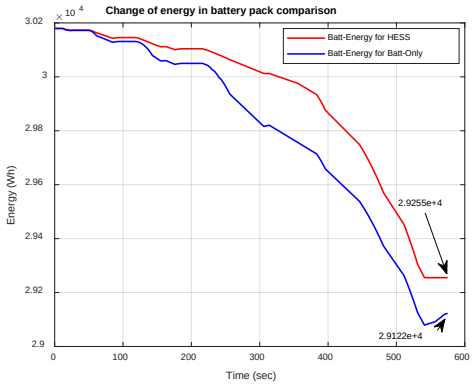

(b)

Figure 4.59. NEDC driving cycle: a) Battery state of charge comparison. b) Change of energy in battery pack comparison. EV Based PMSM-DTC-FLC.

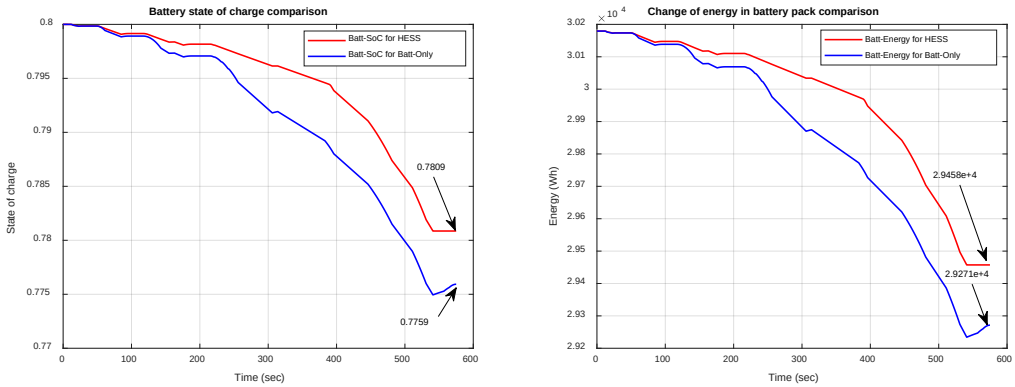

(a) (b)

Figure 4.60. NEDC driving cycle: a) Battery state of charge comparison. b) Change of energy in battery pack comparison. EV Based PMSM-DTC-SMC.

Similar to the case of EV driven by IM, Table 4.2 illustrates a numerical comparison of the SoC and the remained energy of the battery pack at the end of the simulation time of the NEDC drive cycle. This data obtained in both HESS and battery-only cases for IFOC and DTC control strategies and also for PI, FLC, and SMC controllers. Also, the percentage of the energy reduction in the battery pack is calculated in Table 4.2 for this comparison.

Table 4.2. EV based PMSM numerical comparison.

	Controller Type	**Energy Storage Configuration**	**SoC end value**	**Energy end value**	**Energy Reduction %**
EV-PMSM-IFOC	PI	Batt-only	0.7672	2.8948e+4	4.07%
		Batt/SC	0.7718	2.9116e+4	3.522%
	FLC	Batt-only	0.7709	2.9081e+4	3.63%
		Batt/SC	0.7755	2.9255e+4	3.06%
	SMC	Batt-only	0.7768	2.9303e+4	2.902%
		Batt/SC	0.7816	2.9486e+4	2.29%
EV-PMSM-DTC	PI	Batt-only	0.7659	2.8894e+4	4.257%
		Batt/SC	0.7718	2.9116e+4	3.522%
	FLC	Batt-only	0.7718	2.9122e+4	3.502%
		Batt/SC	0.7756	2.9255e+4	3.06%
	SMC	Batt-only	0.7759	2.9271e+4	3.008%
		Batt/SC	0.7809	2.9458e+4	2.389%

In the case of EV-PMSM-IFOC, it can be seen from Figure 4.55 to Figure 4.57 that more energy consumed in case of using the PI controller if compared to FLC and SMC cases, however, SMC shows better performance if compared to PI and FLC, where it reached the end of the simulation time with 2.902% reduction of the start value of the energy in the battery pack, while it was 4.07% and 3.63% for PI and FLC respectively. Moreover, the effectiveness of utilizing the HESS is noticed as it reduces the reduction in the energy of the battery pack from 4.07% to 3.522% in the case of PI controller, and from 3.63% to 3.06% in the case of the FLC controller, and from 2.902% to 2.29% for the SMC controller.

Similarly, for the case of EV-PMSM-DTC, the superior performance of the SMC is demonstrated if compared to the results obtained when utilizing PI and FLC controllers. Also, the improved energy consumption of the battery pack is achieved while applying hybridization of the energy storage system. However, this achievement led to improve the EV range and battery life.

In detail, in the case of battery only configuration SoC decreased to 0.7659 and 0.7718 in the case of PI and FLC controller respectively, while remained at 0.7759 for SMC controller, also for HESS configuration the simulation time ended with 0.7718 for PI and 0.7756 for FLC whereas in case of SMC ended with 0.7809. Moreover, consumed energy is improved from 4.257% to 3.522% for PI controller, and from 3.502% to 3.06% in the case of FLC controller while for SMC was saved from 3.008% to 2.389%.

In summary, the proposed SMC proved better performance over the PI and FLC controllers' performances. However, the SMC achieved the desired speed with fast speed tracking and lower speed error. And also, the energy consumption from the battery pack is improved in the case of SMC for the driving scenario that enhanced the vehicle performance, vehicle operating range, and battery lifetime.

Furthermore, the HESS configuration and its developed EMS demonstrate a reduction in the energy usage of the battery pack that also led to improve energy consumption and enhance vehicle energy efficiency. Additionally, the performance of the SMC-based DTC strategy showed better behavior with less energy consumed if compared to the IFOC control strategy results for both IM and PMSM.

4.2. PARALLEL HEV SIMULATION RESULTS

To reduce repetitive figures and simulation situations, only the configuration of using IM-IFOC based SMC will be considered in simulating Parallel HEV. However, validation and investigation of the developed simulation platform are performed in this section for the Parallel HEV under Max-SoC EMS and FRB EMS, and also these two configurations will be performed for both HESS and Battery only configuration. Three different drive cycles are selected to compare the behavior of the vehicle under these different configurations. NEDC, FTP75, and Highway drive cycles will be utilized. NEDC drive cycle will be performed for a total time of 575 sec with a maximum speed of 120 (km/h) and average speed of 50 (km/h) as shown in Figure 4.61a, and the total simulation time of the FTP75 drive cycle is 1874 sec at an average speed of 34 (km/h) and a maximum speed of 91 (km/h) as sown in Figure 4.64a. Also, the Highway drive cycle will be simulated for 760 sec at an average speed of 79 (km/h) and a maximum speed of 97 (km/h) as presented in Figure 4.67a.

4.2.1. Parallel HEV Based IM with Max-SoC EMS

Max-SoC-EMS is based on using Engine as a primary mover for the vehicle, accordingly; it is used in most of the simulation period where the engine is operated between its minimum and maximum limits and can meet demand power, otherwise; if the vehicle speed is in the low-speed region the engine is turned off and only electric motor propelling in used. Furthermore; if power demand is greater than engine maximum power the vehicle will work in hybrid traction mode, and the power demand will be shared between both power sources. In deceleration, the engine will be turned off and the only motor will be utilized as a generation to recover kinetic energy.

4.2.1.1. Simulation Based Battery-Only for SMC controller

In this subsection, the SMC controller is utilized as a vehicle speed controller due to its superior behavior proved previously against PI and FLC controllers. Figure 4.61 to Figure 4.63 illustrate obtained results of the Parallel HEV-based SMC for the NEDC drive cycle. Figure 4.61a and Figure 4.61c show that the vehicle tracked the desired

speed with good performance and very low-speed error. Also, Figure 4.61b illustrates the vehicle operating modes for the NEDC scenario. For the Parallel HEV, there will be five different operation modes which have been explained earlier. As well Figure 4.61d shows the motor and engine speed that is corresponded to the vehicle's actual speed. Moreover, Figure 4.62a illustrates the power demand split between the engine and traction motor during the drive cycle performed by the EMS. Furthermore, Figure 4.62b and 4.62c present the battery pack current and SoC respectively, where the SoC end value was at 0.7988. And finally, the engine consumed fuel and efficiency are plotted in Figure 4.63a and Figure 4.63b.

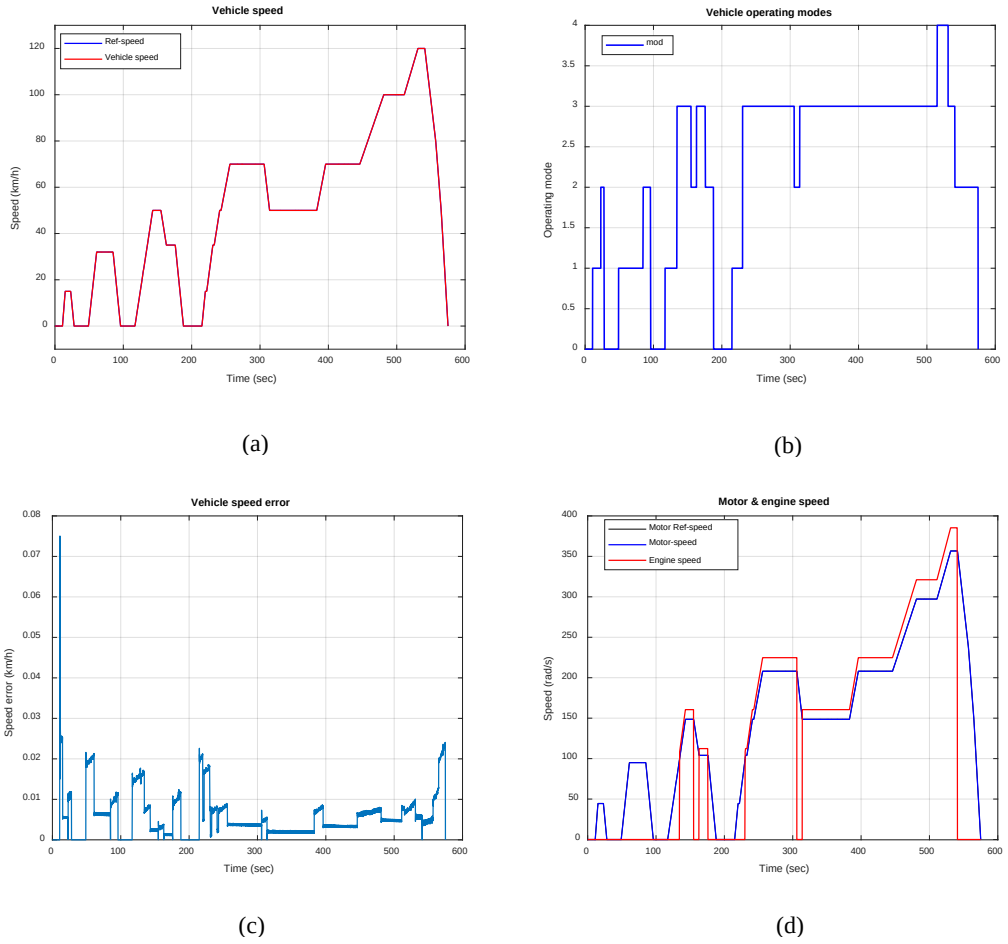

Figure 4.61. NEDC driving cycle: a) Vehicle speed. b) Operating modes. c) Vehicle speed error. d) Engine and IM speeds. HEV based IM-SMC-Max-SoC-EMS.

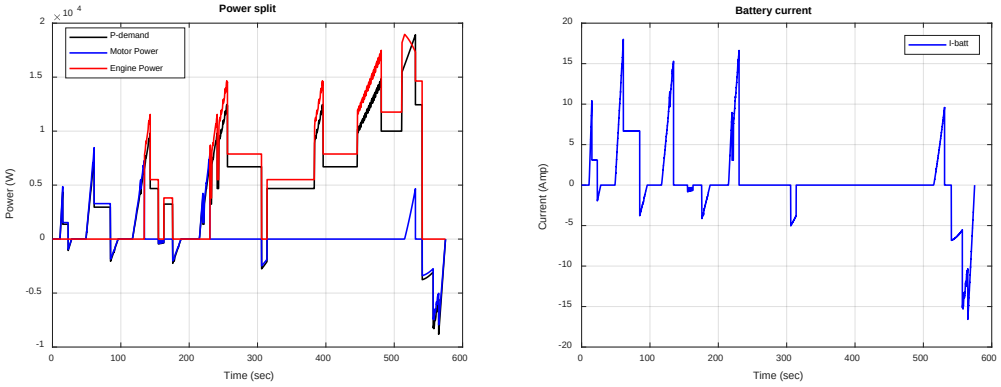

(a) (b)

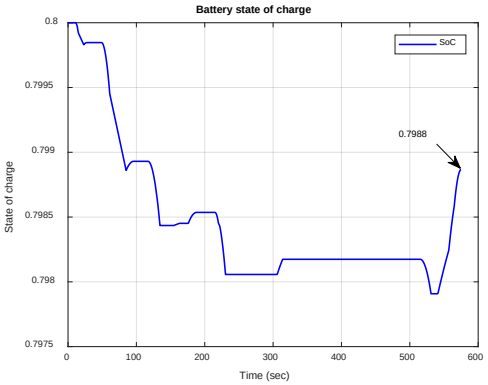

(c)

Figure 4.62. NEDC driving cycle: a) Power demand & Power split. b) Battery current. c) State of charge of Battery. HEV based IM-SMC-Max-SoC-EMS.

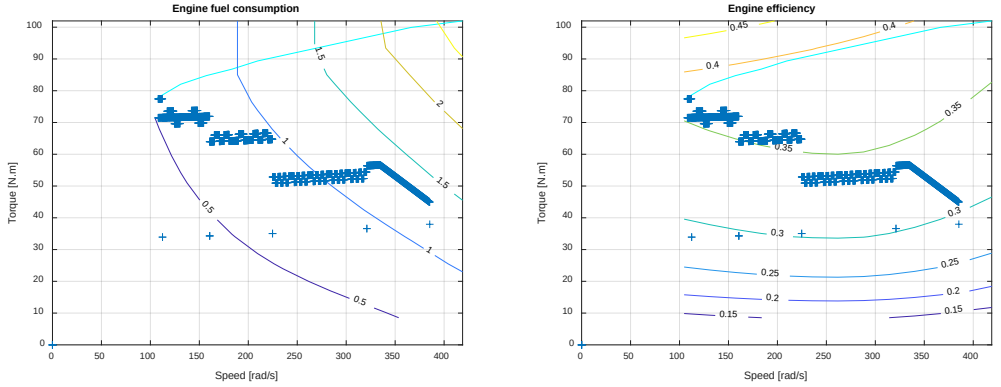

(a) (b)

Figure 4.63. NEDC driving cycle: a) Engine fuel consumption. b) Engine efficiency. HEV Based IM-SMC-Max-SoC-EMS.

Similar to the NEDC obtained results, for the FTP75 drive cycle; Figures 4.64a and 4.64c show very good performance in terms of speed tracking and speed error. Also Figure 4.64b presents the operating modes of the vehicle, however; the operating mode of the vehicle is changing frequently during the FTP75 drive cycle because of the frequent change in the desired driving speed. And the engine and motor speed are plotted in Figure 4.64d. power demand split between engine and electric traction motor is shown in Figure 4.65a, and the battery pack current and its related SoC is illustrated in Figure 4.65b and 4.65c. the SoC of the battery pack is decreased to 0.7926 at end of the total time of the FTP75 drive cycle. Furthermore, the fuel consumed and efficiency of the engine is presented in Figure 4.66.

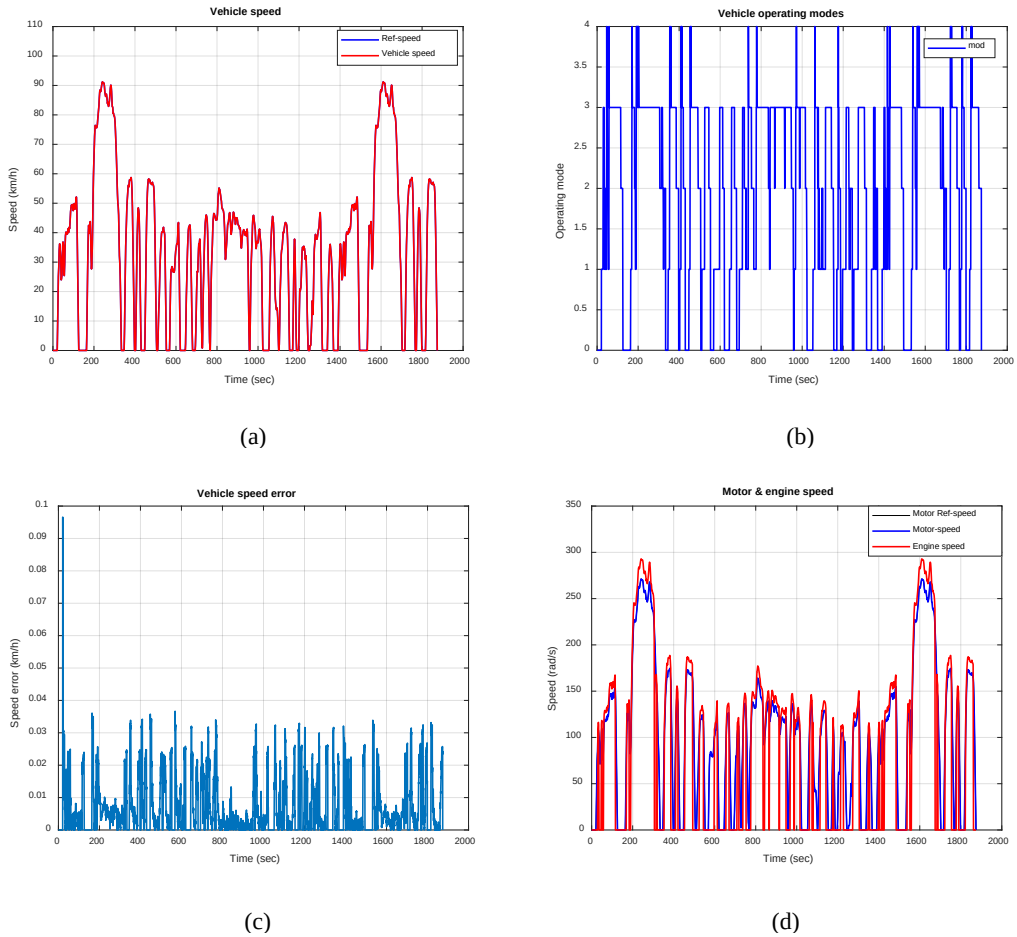

Figure 4.64. FTP75 driving cycle: a) Vehicle speed. b) Operating modes. c) Vehicle speed error. d) Engine and IM speeds. HEV based IM-SMC-Max-SoC-EMS.

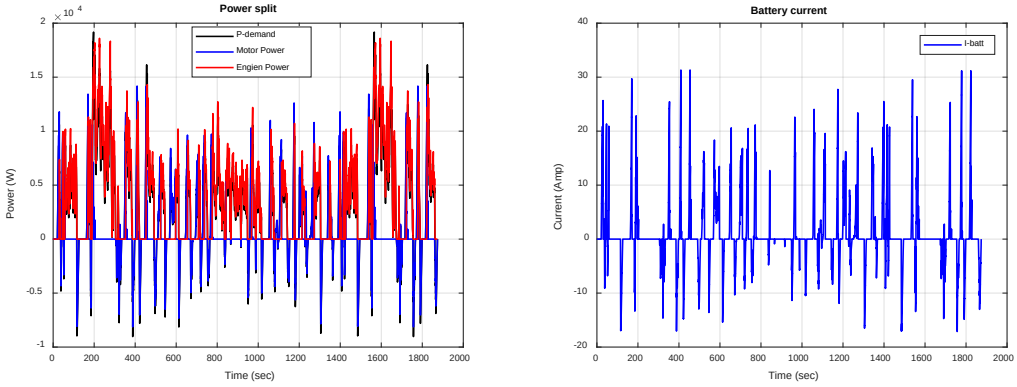

(a) (b)

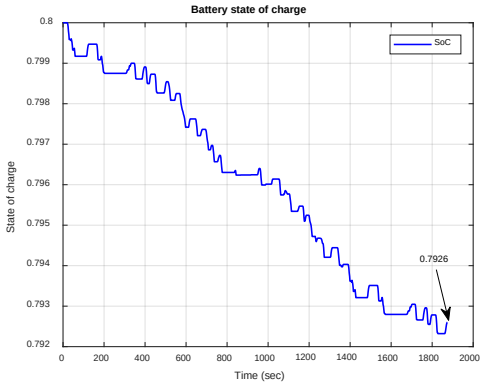

(c)

Figure 4.65. FTP75 driving cycle: a) Power demand & Power split. b) Battery current. c) State of charge of Battery. HEV based IM-SMC-Max-SoC-EMS.

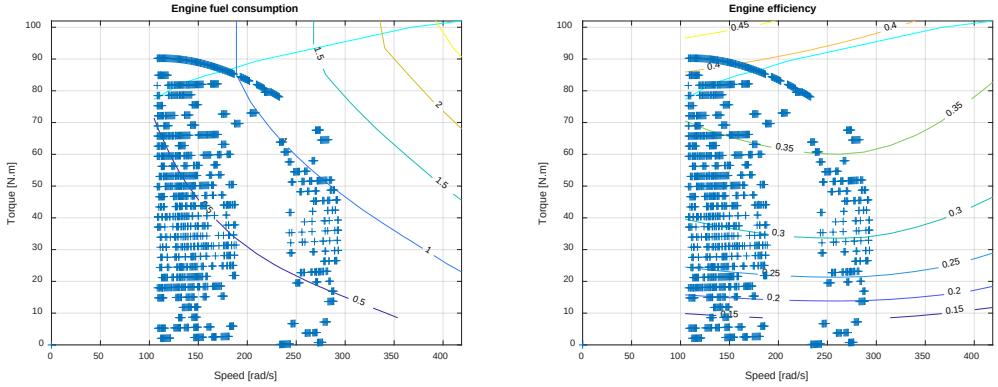

(a) (b)

Figure 4.66. FTP75 driving cycle: a) Engine fuel consumption. b) Engine efficiency. HEV Based IM-SMC-Max-SoC-EMS.

The third drive scenario performed is the Highway drive cycle. However, due to the high average speed of this drive cycle which is 79 km/h, it can be considered high way driving scenario. Thus, for most of the drive time, the vehicle will be operated in Engine only mode or hybrid mode as illustrated in Figure 4.76b. Also, from figure 4.76a and Figure 4.76c; it can be seen that the vehicle with SMC is performing well in terms of speed tracking for this configuration with very low-speed error. Moreover, Figure 4.76d illustrates the engine and motor speed plot.

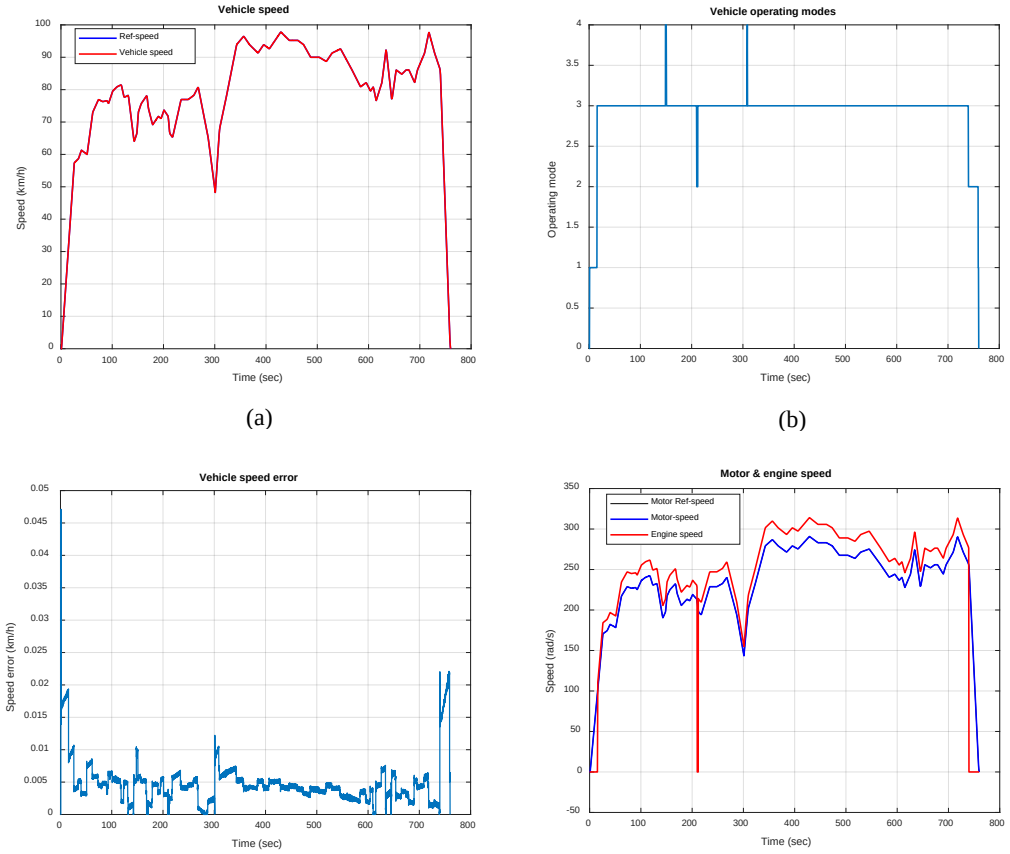

Figure 4.67. Highway driving cycle: a) Vehicle speed. b) Operating modes. c) Vehicle speed error. d) Engine and IM speeds. HEV based IM-SMC-Max-SoC-EMS.

Figure 4.86a displays the power demand split between both engine and electric motor for the Max-SoC EMS applied in this section, furthermore; from Figure 4.86b and Figure 4.86c, it can be noticed that the battery pack is utilized only for a short period during the simulation. This is due to the nature of the Max-SoC EMS explained previously, that the engine is considered as a primary mover in the vehicle. Also, in

this configuration, the end value of the SoC of the battery pack remained nearly to the start value as written in Figure 4.86c below.

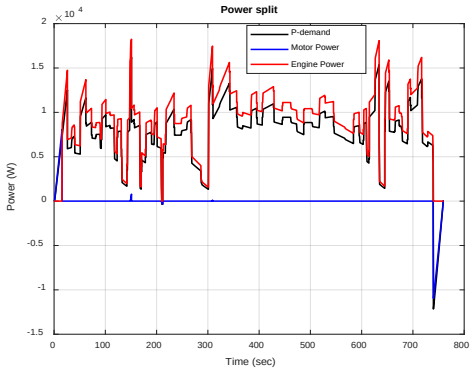

(a)

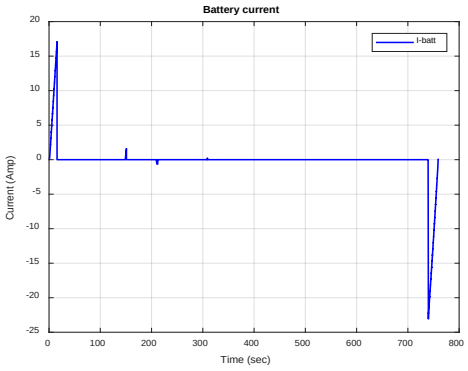

(b)

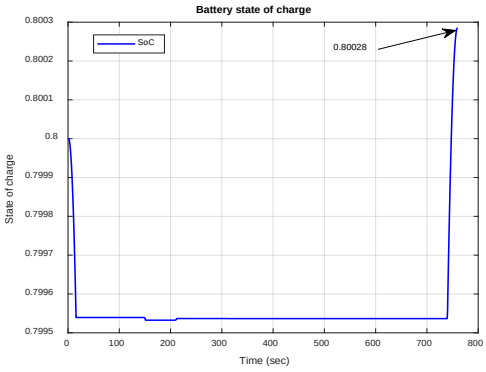

(c)

Figure 4.68. Highway driving cycle: a) Power demand & Power split. b) Battery current. c) State of charge of Battery. HEV based IM-SMC-Max-SoC-EMS.

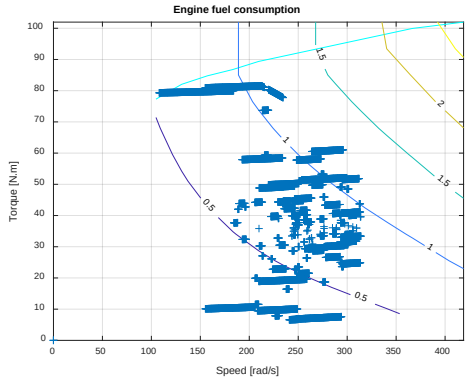

(a)

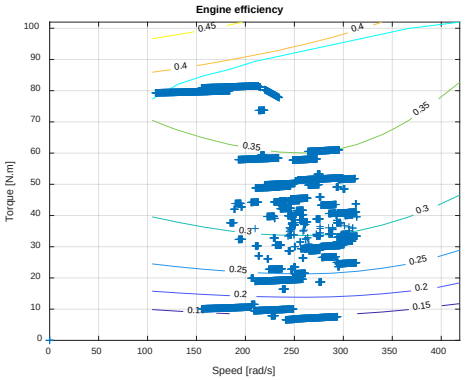

(b)

Figure 4.69. Highway driving cycle: a) Engine fuel consumption. b) Engine efficiency. HEV Based IM-SMC-Max-SoC-EMS.

Operating points of the engine through the simulation time of the Highway driving cycle are plotted on the fuel consumption and efficiency maps of the engine in Figure 4.69a and Figure 4.69b respectively.

4.2.1.2. Simulation Based HESS for SMC controller

The Parallel HEV based on Max-SoC EMS is simulated here based on utilizing HESS for further comparison and validation of the HESS EMS applied in this work. Similarly, this configuration is simulated for the three selected drive cycles, NEDC, FTP75, and Highway drive cycles.

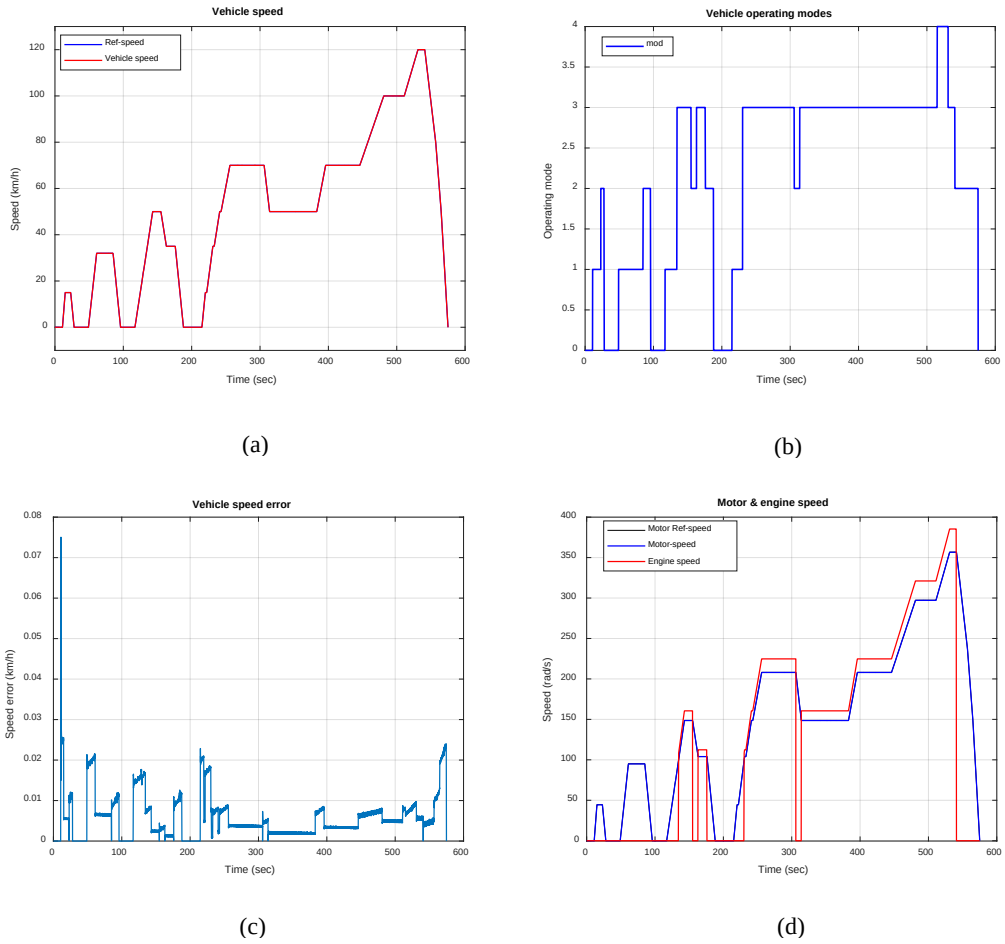

Figure 4.70. NEDC driving cycle: a) Vehicle speed response. b) Vehicle operating modes. c) Vehicle speed error. d) Motor speed. HEV Based IM-SMC-Max-SoC-EMS.

However, Figure 4.70 shows very good performance in terms of speed tracking and vehicle speed error, also figure 4.71a illustrates the power demand split between both traction movers. The effect of using HESS can be seen in Figure 4.71b and Figure 4.71c, where the electric motor current is split between the battery pack and the SC that led to end the simulation with 0.7995 of the SoC instead of 0.7988 in case of using battery only.

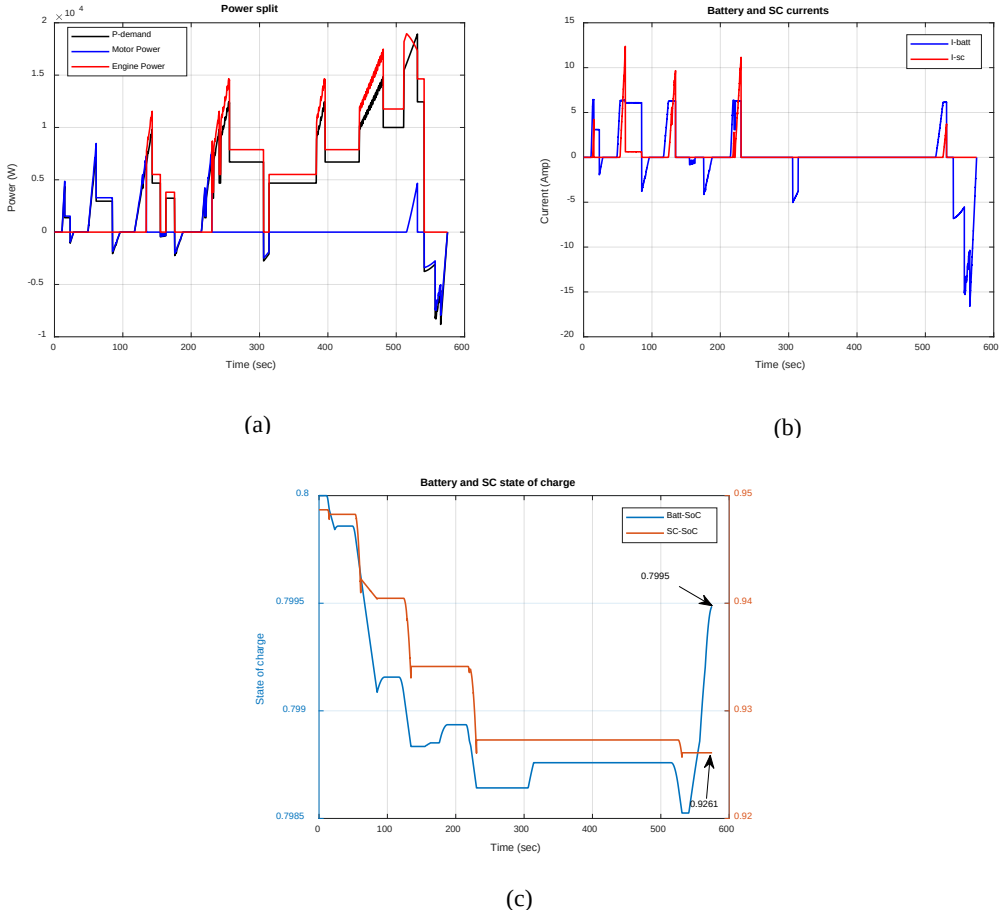

(a) (b)

(c)

Figure 4.71. NEDC driving cycle: a) Power demand & Power split. b) Batt/SC currents. c) State of charge of Battery & SC. HEV Based IM-FLC-Max-SoC-EMS.

Figure 4.72a and Figure 4.72b illustrate the operating points of the engine on the fuel consumption map and the efficiency map respectively.

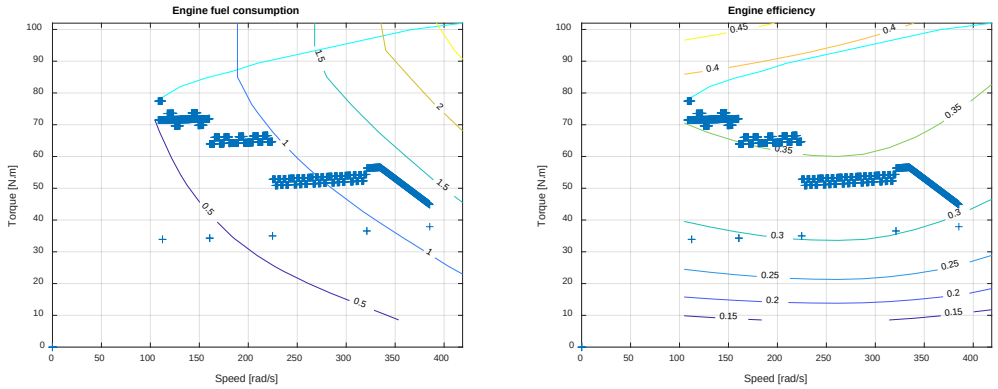

(a) (b)

Figure 4.72. NEDC driving cycle: a) Engine fuel consumption. b) Engine efficiency. HEV Based IM-SMC-Max-SoC-EMS.

Likewise, for the FTP75 drive cycle, the performance was as expected as shown in Figure 4.73 in terms of speed tracking and Figure 4.74 for power demand split and current split between both battery pack and SC. The HESS EMS splits the electric traction motor current between both energy storage as illustrated in Figure 4.74b, and the related change in the SoC for both storage is shown in Figure 4.74c that led to the end value of the SoC of the battery pack at 0.7949 and for the SC at 0.8796.

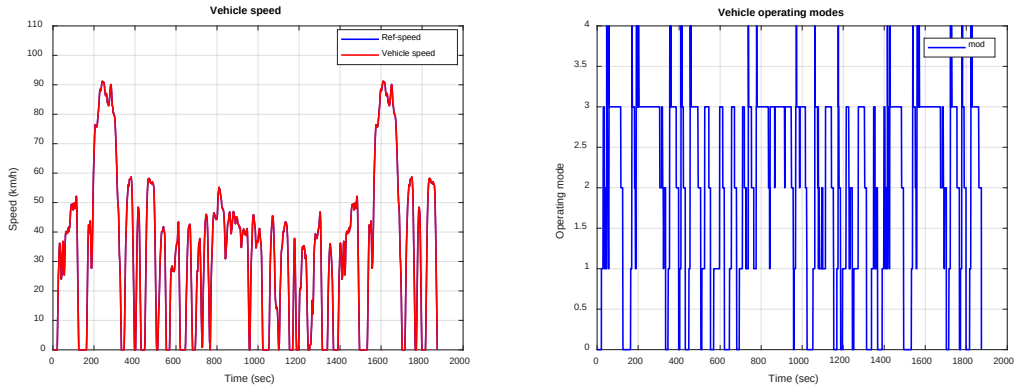

(a) (b)

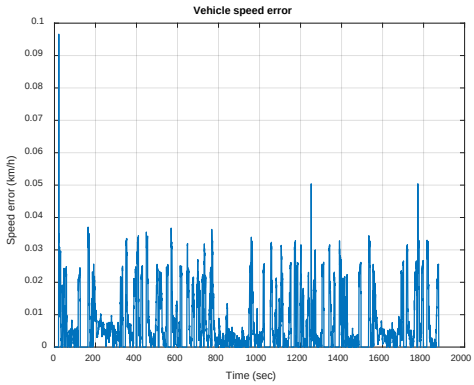

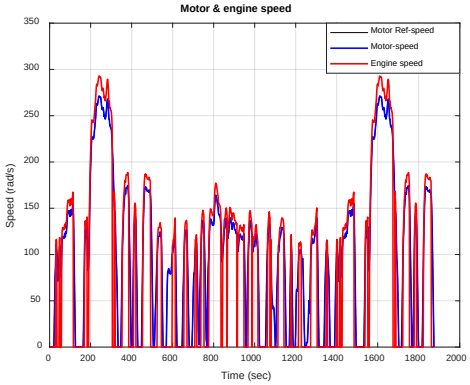

(c) (d)

Figure 4.73. FTP75 driving cycle: a) Vehicle speed. b) Operating modes. c) Vehicle speed error. d) Engine and IM speeds. HEV based IM-SMC-Max-SoC-EMS.

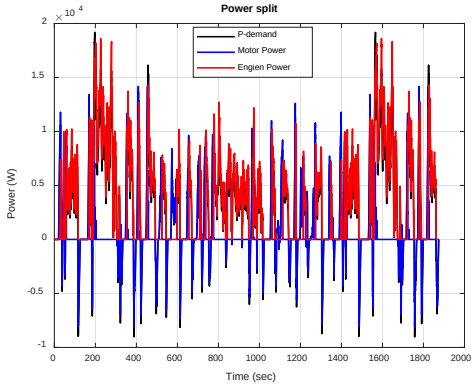

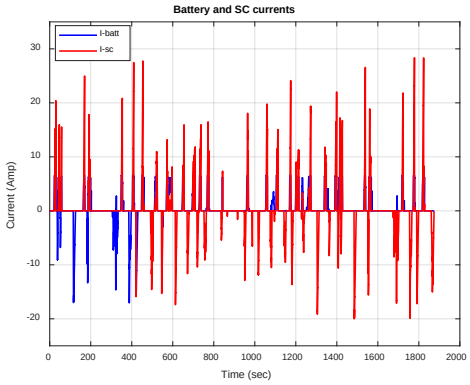

(a) (b)

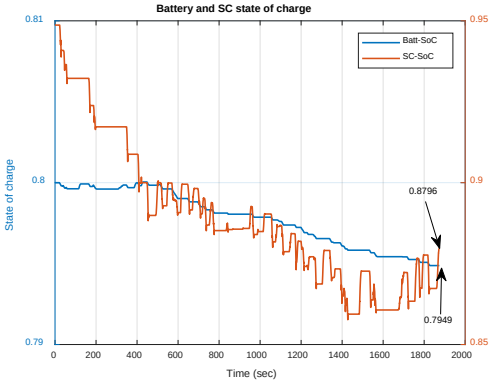

(c)

Figure 4.74. FTP75 driving cycle: a) Power demand & Power split. b) Batt/SC currents. c) State of charge of Battery & SC. HEV Based IM-FLC-Max-SoC-EMS.

And similarly, in Figure 4.75 the engine operating points are plotted on the engine maps of fuel consumption and efficiency.

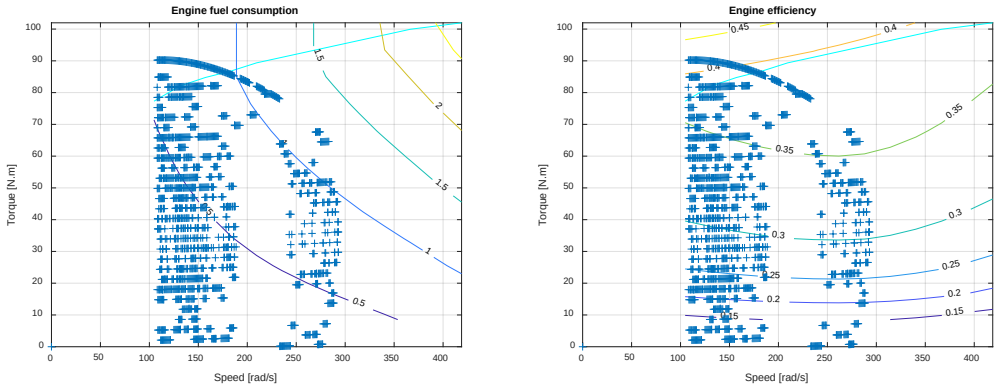

(a) (b)

Figure 4.75. FTP75 driving cycle: a) Engine fuel consumption. b) Engine efficiency. HEV Based IM-SMC-Max-SoC-EMS.

Figure 4.76 to Figure 4.78 show similar results to the case of battery only for the Highway drive cycle, and it reveals a small improvement in the battery pack SoC if compared to the previous configuration as seen in the plot of SoC in Figure 4.77c.

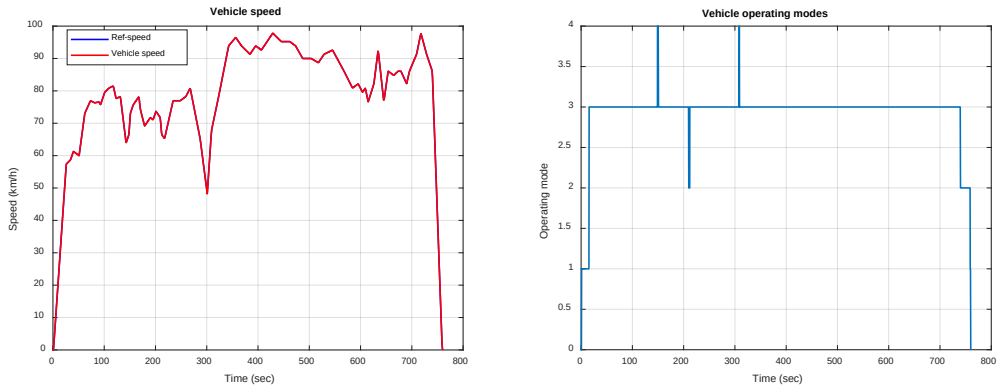

(a) (b)

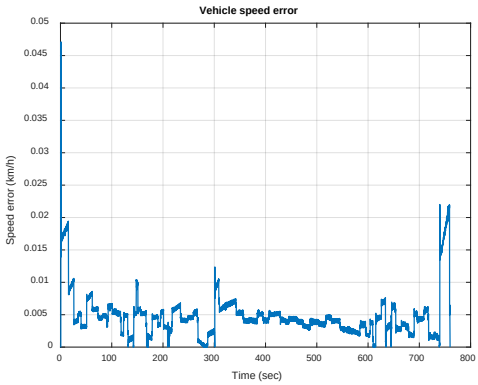

(c)

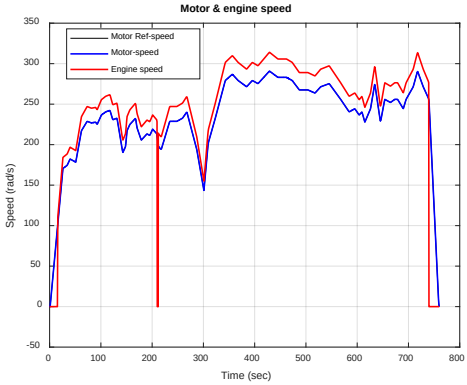

(d)

Figure 4.76. Highway driving cycle: a) Vehicle speed. b) Operating modes. c) Vehicle speed error. d) Engine and IM speeds. HEV based IM-SMC-Max-SoC-EMS.

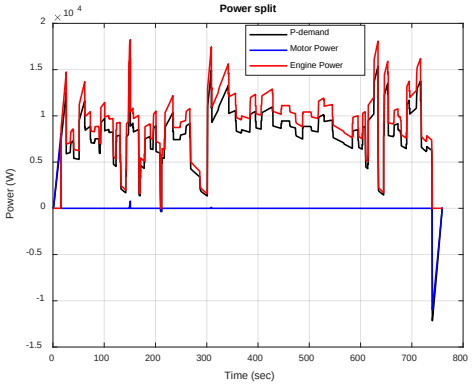

(a)

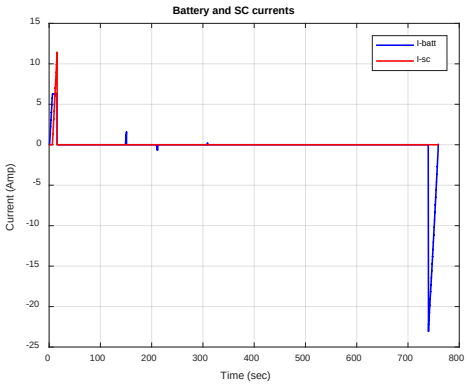

(b)

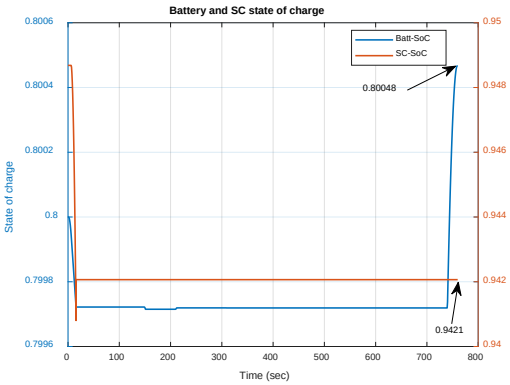

(c)

Figure 4.77. Highway driving cycle: a) Power demand & Power split. b) Batt/SC currents. c) State of charge of Battery & SC. HEV Based IM-FLC-Max-SoC-EMS.

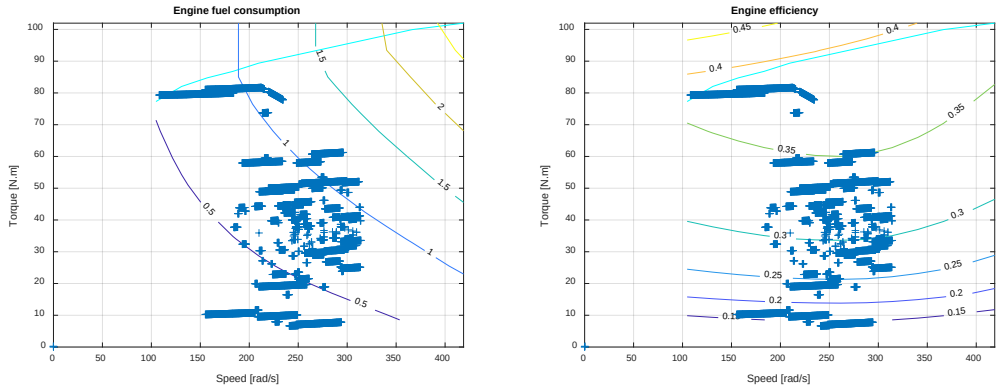

(a) (b)

Figure 4.78. Highway driving cycle: a) Engine fuel consumption. b) Engine efficiency. HEV Based IM-SMC-Max-SoC-EMS.

4.2.1.3. **Results comparison**

To compare and validate the HESS EMS effect of all drive cycles utilized for the case of Parallel HEV based on the Max-SoC EMS; the data of SoC and Energy consumed in the battery pack is plotted below. And then detailed data are arranged in Table 4.3 for further comparison. Figure 4.79a and Figure 4.79b illustrate that the SoC of the battery pack is improved from 0.7988 in battery only case to 0.7995 in the HESS case, and simultaneously the battery pack remained energy is improved from 3.0136e+4Wh to 3.0160e+4Wh.

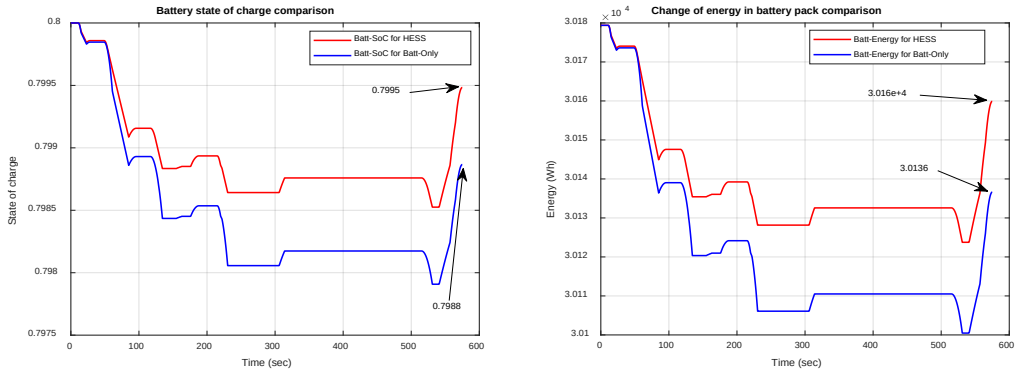

(a) (b)

Figure 4.79. NEDC driving cycle: a) Battery state of charge of Battery comparison. b) Change of energy in battery pack comparison. HEV Based IM-SMC-Max-SoC-EMS.

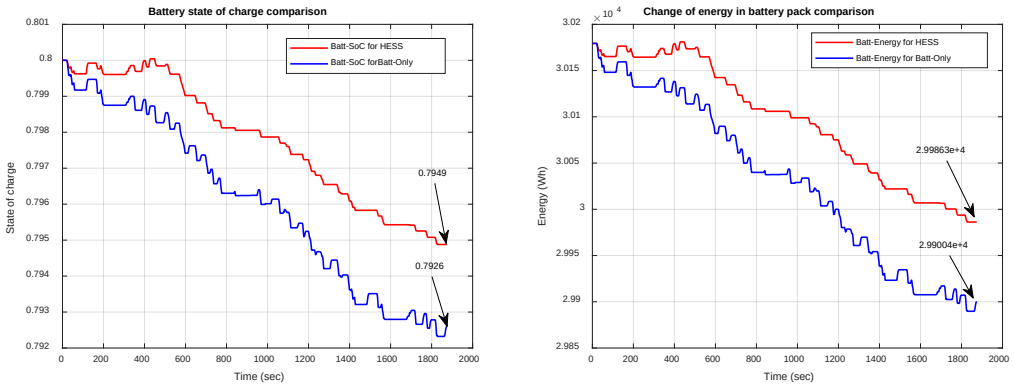

(a) (b)

Figure 4.80. FTP75 driving cycle: a) Battery state of charge of Battery comparison. b) Change of energy in battery pack comparison. HEV Based IM-SMC-Max-SoC-EMS.

Also, for the FTP75 drive cycle in Figure 4.80, the SoC is improved from 0.7926 to 0.7949, and the remained energy enhanced from 2.99004+4Wh to 2.99863e+4Wh when utilizing HESS. Correspondingly, in Figure 4.81 for the Highway drive cycle, the remained energy in the battery pack is increased by a small margin from 3.0190e+4Wh to 3.0197e+4Wh.

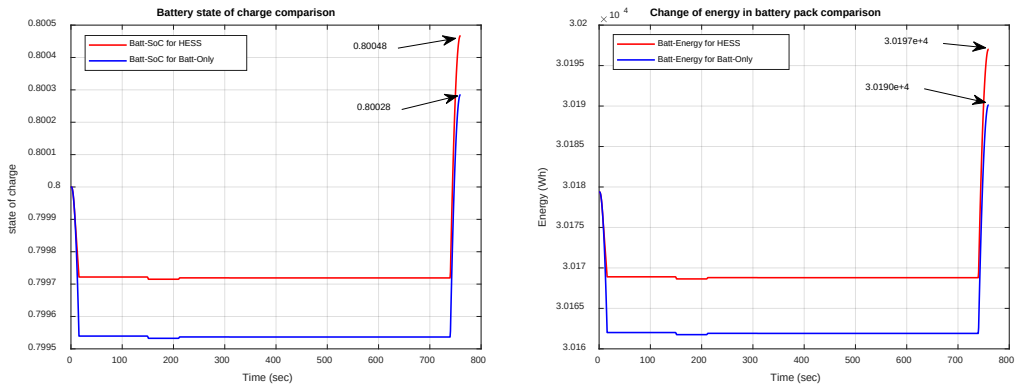

(a) (b)

Figure 4.81. Highway driving cycle: a) Battery state of charge of Battery comparison. b) Change of energy in battery pack comparison. HEV Based IM-SMC-Max-SoC-EMS.

Table 4.3 demonstrates numerical data of the battery pack state of charge and the remained energy at the end of each drive cycle. Also, the reduction percentage in the energy of the battery pack is determined in the last column.

The energy usage from the battery pack is improved from 0.139% to 0.056% For the NEDC drive cycle, while the FTP75 drive cycle is enhanced from 0.919% to 0.636%. On the other hand, in the case of the Highway drive cycle; the battery pack was recharged by 0.0629% over the starting value for the HESS case, while it was recharged by 0.039% in the case of battery only configuration.

Table 4.3. HEV based IM-SMC-Max-SoC-EMS numerical comparison.

Vehicle configuration	**Drive Cycle**	**Energy Storage Configuration**	**SoC end value**	**Energy end value**	**Energy reduction in Battery pack (%)**
HEV-IM-IFOC-SMC-Max-SoC-EMS	NEDC	Batt-only	0.7988	3.0136e+4	0.139%
		Batt/SC	0.7995	3.0160e+4	0.056%
	FTP75	Batt-only	0.7926	2.99004e+4	0.919%
		Batt/SC	0.7949	2.9986e+4	0.636%
	Highway	Batt-only	0.80028	3.0190e+4	+0.039%
		Batt/SC	0.80048	3.0197e+4	+0.0629%

4.2.2. Parallel HEV Based IM with FRB- EMS

The power split in FRB-EMS that explained previously in chapter 2 is mainly based on sharing the power demand between both engine and electric motor while the reference speed is greater than the engine minimum speed, but if the reference speed is less than minimum engine speed, only motor propelling is performed. And during deceleration, the vehicle will be in regenerative braking mode and the engine will be turned off.

In the following sections, the Parallel HEV-based FRB-EMS is simulated firstly for battery-only configuration and then for HESS configuration.

4.2.2.1. Simulation Based Battery-Only for SMC controller

For the NEDC drive cycle, speed tracking and vehicle speed error performances are illustrated in Figure 4.82a and Figure 4.82c, also operating modes under FRB-EMS is

illustrated in Figure 4.82bm where the vehicle is propelled in hybrid mode except when the reference speed is less than engine minimum speed the EV propelling mode is activated. Moreover, the power demand split between engine and motor is plotted in Figure 4.83a, furthermore; Figure 4.83b shows the current of the battery pack while its relative change in the SoC presented in Figure 4.83c with an end value equal to 0.7870. And then fuel consumption and efficiency maps with the engine operating points are plotted in Figure 4.84a and Figure 4.84b respectively.

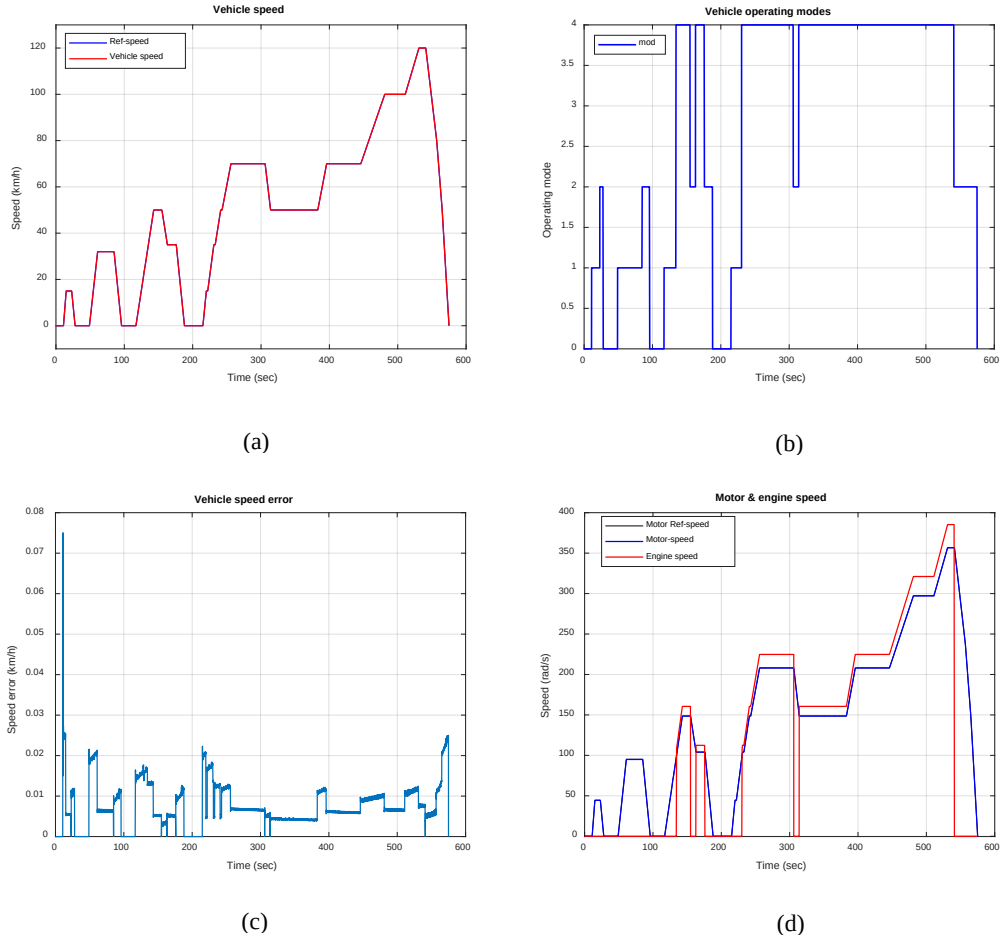

(a) (b)

(c) (d)

Figure 4.82. NEDC driving cycle: a) Vehicle speed response. b) Vehicle operating modes. c) Vehicle speed error. d) Motor speed. HEV Based IM-SMC and FRB-EMS.

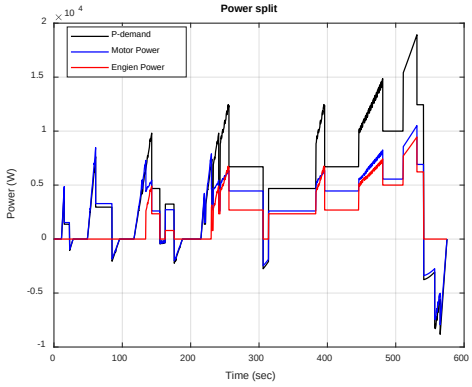

(a)

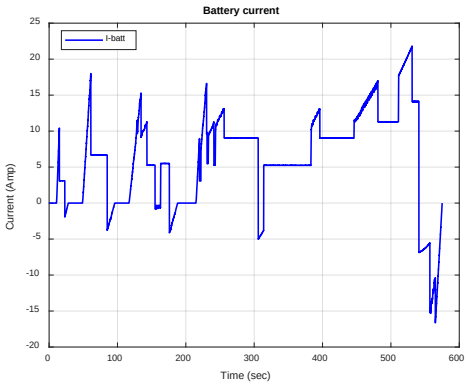

(b)

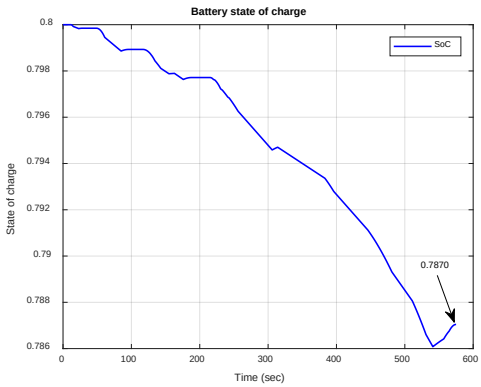

(c)

Figure 4.83. NEDC driving cycle: a) Power demand & Power split. b) Battery current. c) State of charge of Battery. HEV Based IM-SMC and FRB-EMS.

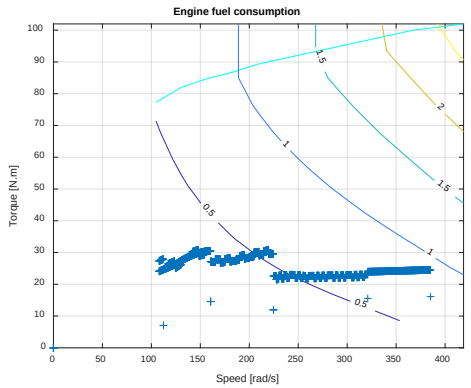

(a)

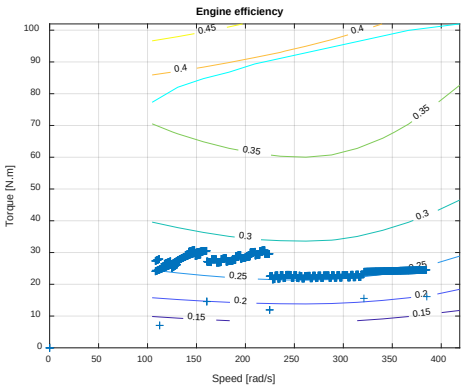

(b)

Figure 4.84. NEDC driving cycle: a) Engine fuel consumption. b) Engine efficiency. HEV Based IM-SMC and FRB-EMS.

The obtained results for the FTP75 drive cycle illustrated in Figure 4.85 to Figure 4.87. the performance was good as expected in terms of speed tracking for the SMC controller, and also for the power demand split as shown in Figure 4.86a.

Moreover, the SoC of the battery pack decreased to 0.7681 at the end of simulation time as shown in Figure 4.86c, and the corresponding battery pack current is plotted in Figure 4.86b. Furthermore, the engine operating points of the engine are plotted on the fuel consumption map and efficiency map in Figure 4.87a and figure 4.87b respectively.

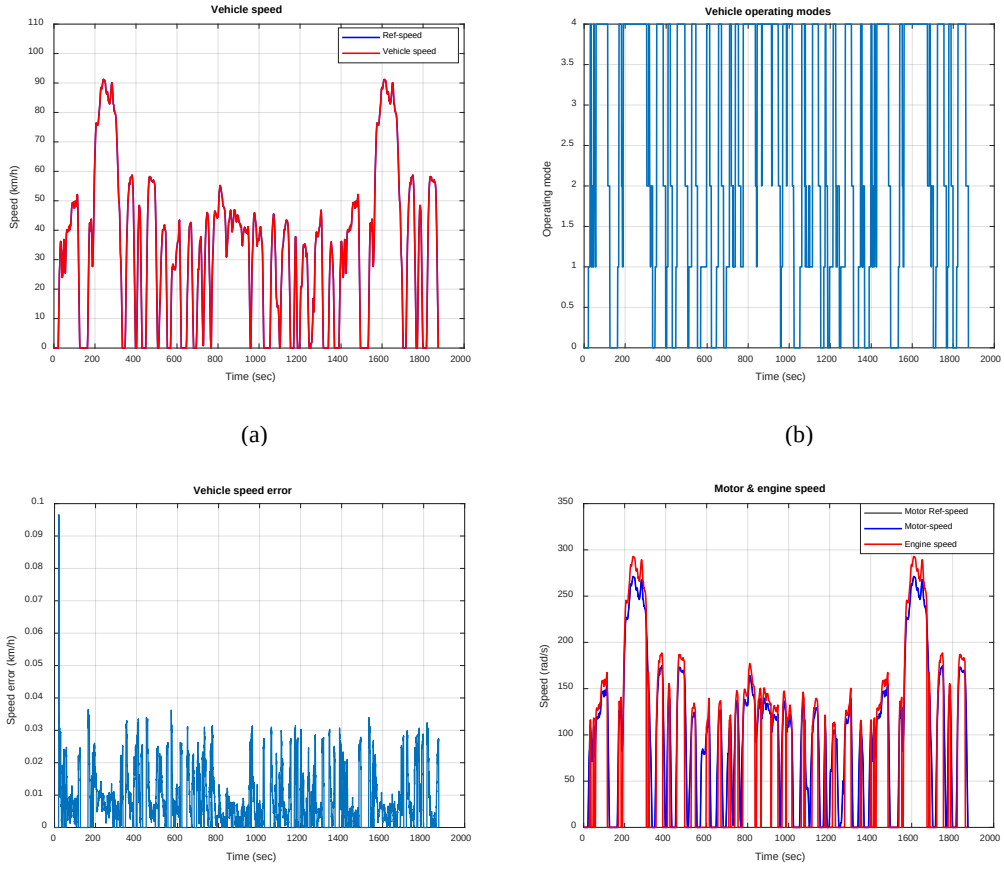

(a) (b)

(c) (d)

Figure 4.85. FTP75 driving cycle: a) Vehicle speed. b) Operating modes. c) Vehicle speed error. d) Engine and IM speeds. HEV Based IM-SMC and FRB-EMS.

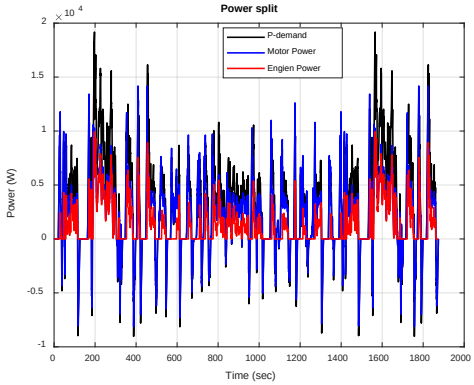

(a)

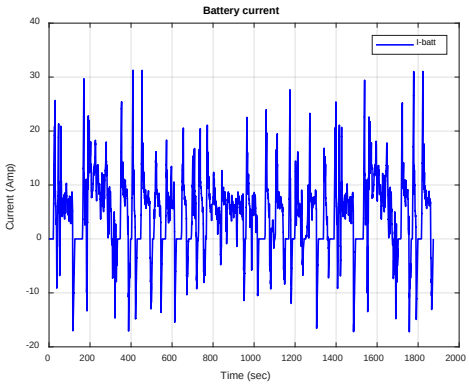

(b)

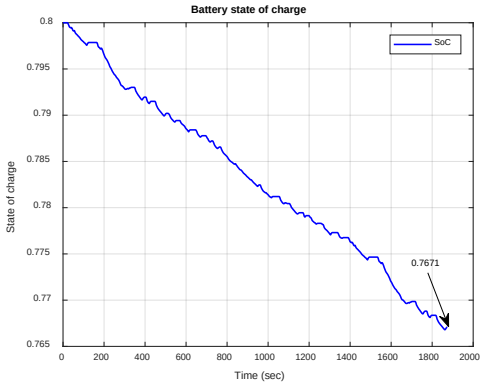

(c)

Figure 4.86. FTP75 driving cycle: a) Power demand & Power split. b) Battery current. c) State of charge of Battery. HEV Based IM-SMC and FRB-EMS.

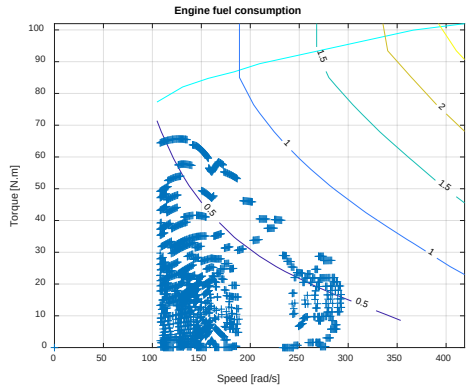

(a)

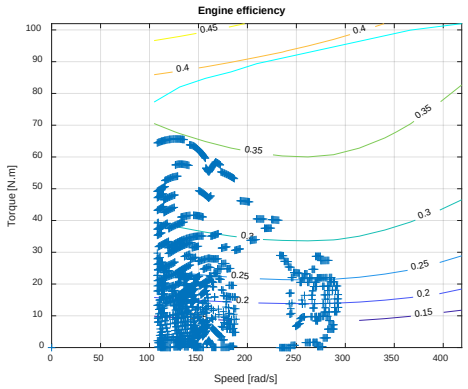

(b)

Figure 4.87. FTP75 driving cycle: a) Engine fuel consumption. b) Engine efficiency. HEV Based IM-SMC and FRB-EMS.

The vehicle is operated in hybrid mode for most of the duration time of the Highway drive cycle as seen from Figure 4.88b. Also, the vehicle showed good performance in terms of speed tracking and speed error, moreover; the power demand split is plotted in Figure 4.89a, while the battery pack current and its corresponding changing in the SoC is illustrated in Figure 4.89b and Figure 4.89c. The SoC decreased to 0.7748 at the end of simulation time. And then engine operating points are plotted in Figure 4.90a and Figure 4.90b for both fuel consumption map and efficiency map.

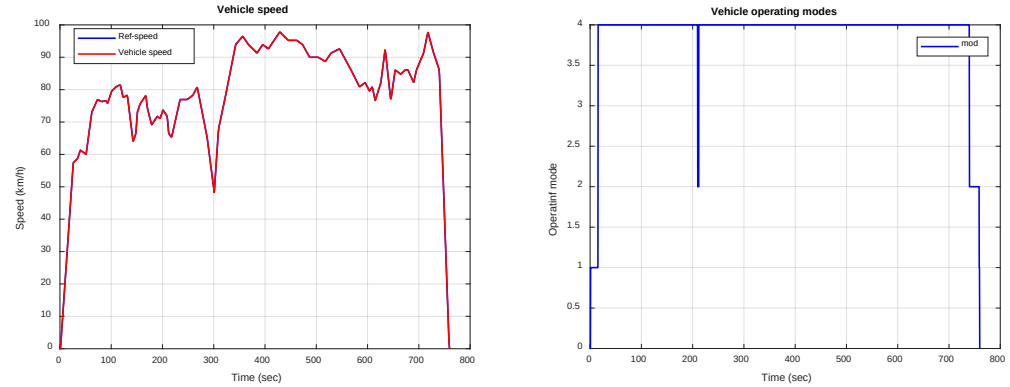

(a)

(b)

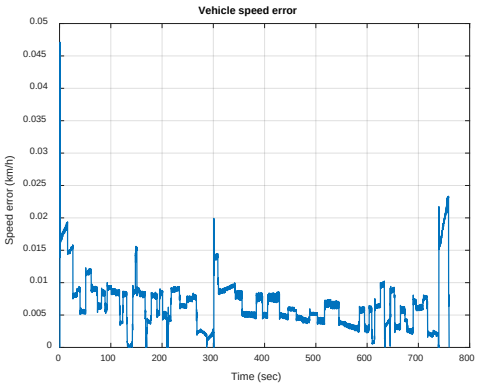

(c)

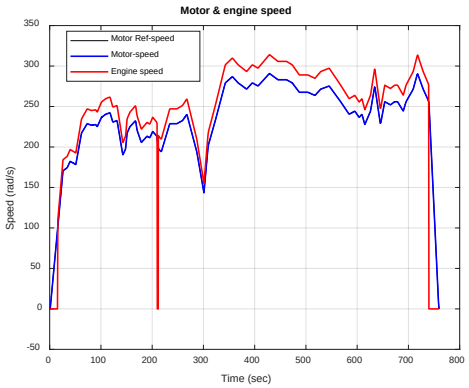

(d)

Figure 4.88. Highway driving cycle: a) Vehicle speed response. b) Vehicle operating modes. c) Vehicle speed error. d) Motor speed. HEV Based IM-SMC and FRB-EMS.

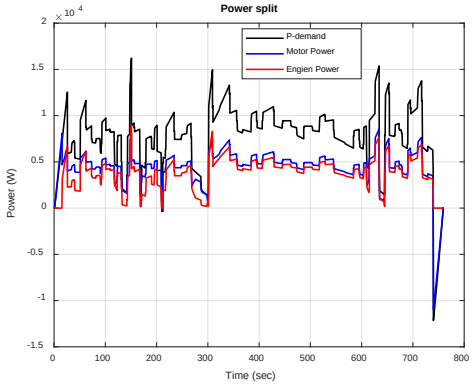

(a)

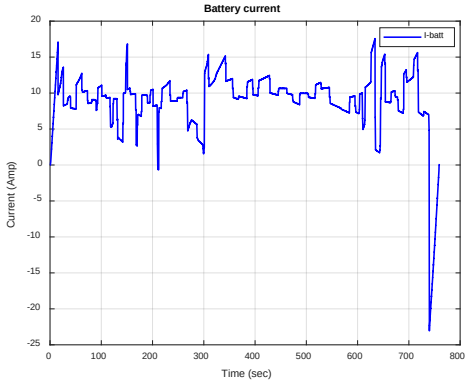

(b)

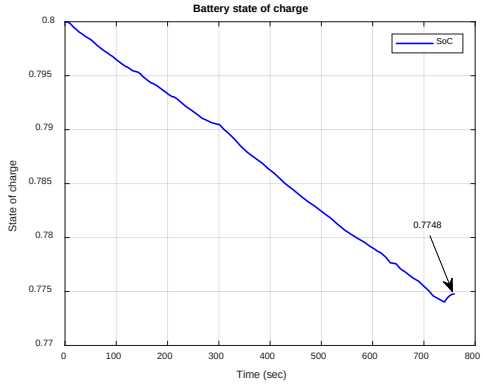

(c)

Figure 4.89. Highway driving cycle: a) Power demand & Power split. b) Battery current. c) State of charge of Battery. HEV Based IM-SMC and FRB-EMS.

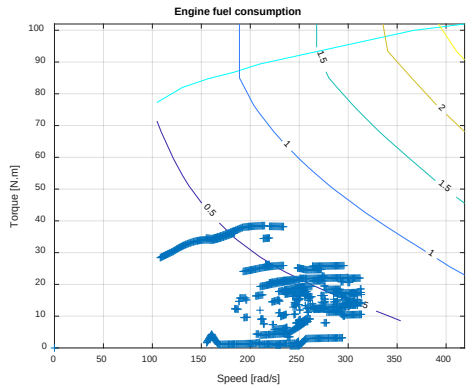

(a)

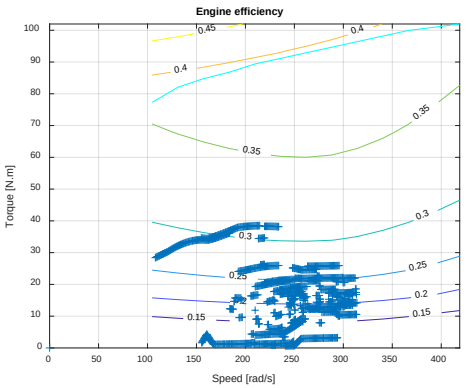

(b)

Figure 4.90. Highway driving cycle: a) Engine fuel consumption. b) Engine efficiency. HEV Based IM-SMC and FRB-EMS.

4.2.2.2. Simulation Based HESS for SMC controller

In general, the parallel HEV performance achieved good performance in the case of using HESS for all drive scenarios. However, the current split between the battery pack and the SC for the NEDC drive cycle is illustrated in Figure 4.92b, and its relevant changes in the SoC for the battery pack and the SC is shown in Figure 4.92c. However, the end value of the SoC of the battery pack decreased to 0.7913 and for the SC at 0.7842.

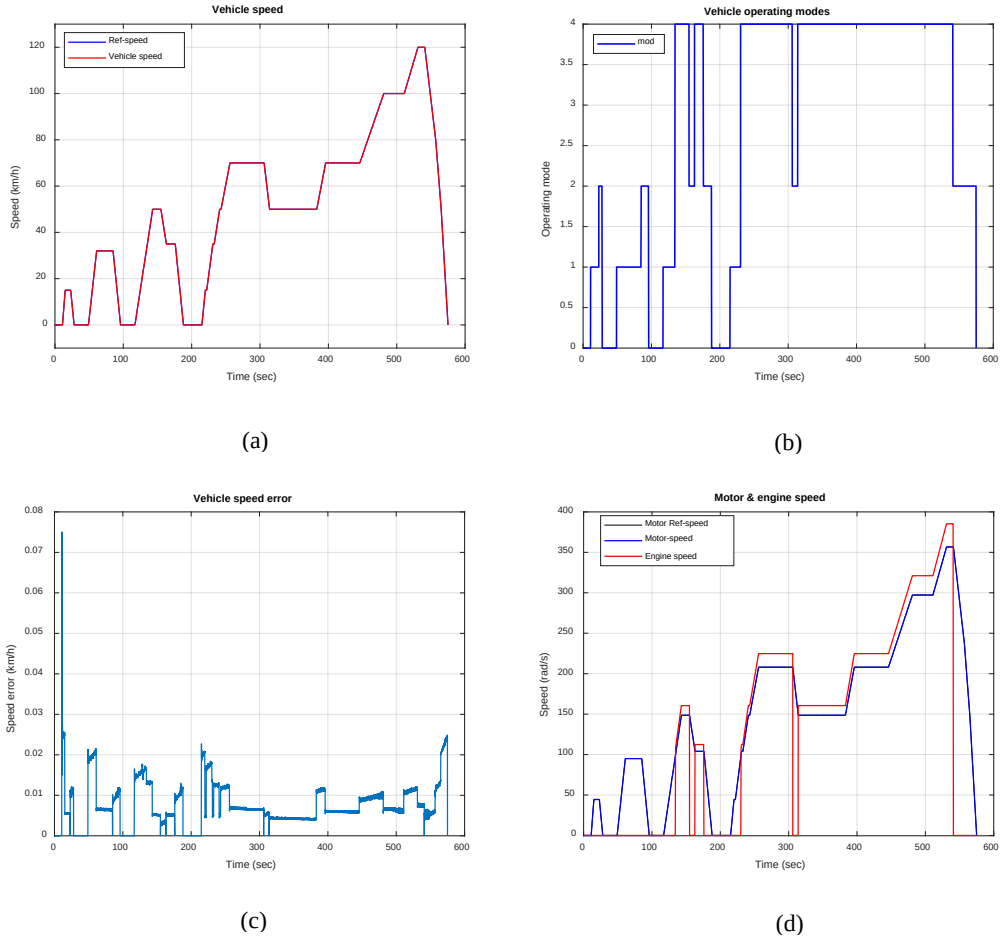

Figure 4.91. NEDC driving cycle: a) Vehicle speed response. b) Vehicle operating modes. c) Vehicle speed error. d) Motor speed. HEV Based IM-SMC and FRB-EMS.

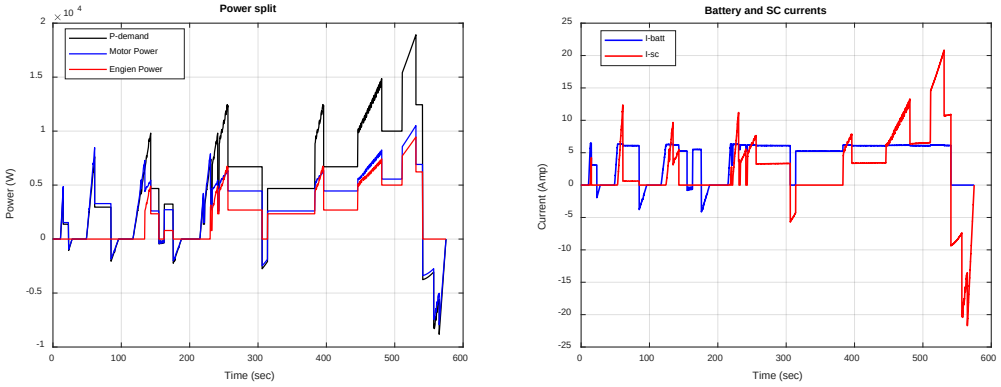

(a) (b)

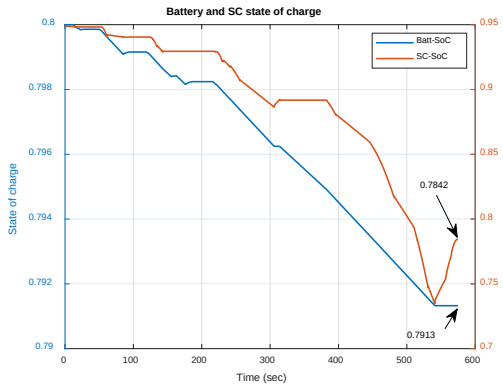

(c)

Figure 4.92. NEDC driving cycle: a) Power demand & Power split. b) Batt/SC currents. c) State of charge of Battery & SC. HEV Based IM-SMC and FRB-EMS.

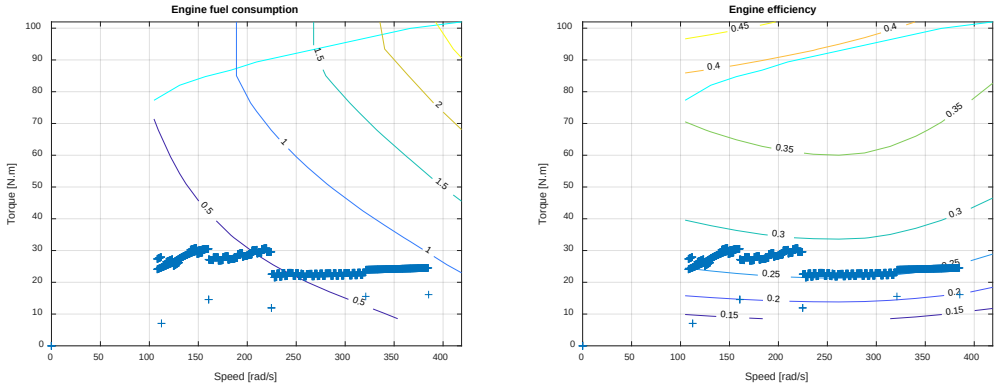

(a) (b)

Figure 4.93. NEDC driving cycle: a) Engine fuel consumption. b) Engine efficiency. HEV Based IM-SMC and FRB-EMS.

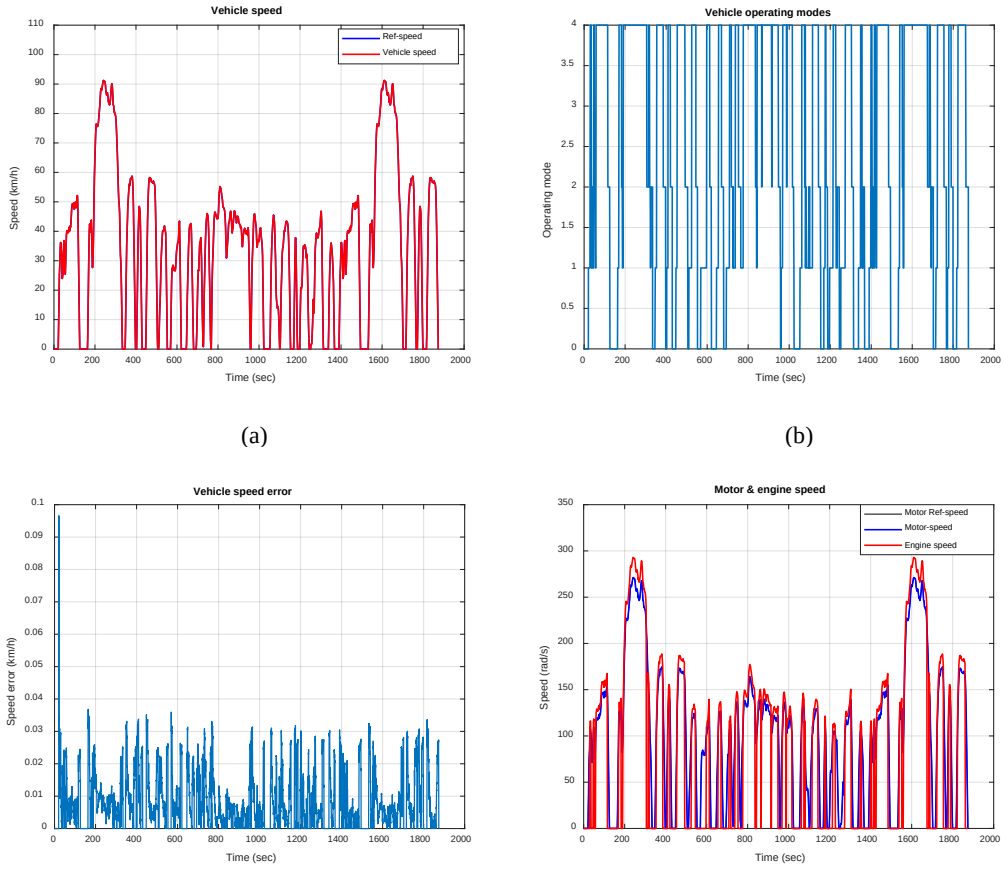

Figure 4.94. FTP75 driving cycle: a) Vehicle speed. b) Operating modes. c) Vehicle speed error. d) Engine and IM speeds. HEV Based IM-SMC and FRB-EMS.

On the other hand, the SoC of the battery pack decreased to 0.7731 and SC to 0.7251 for the FTP75 drive cycle. Its simulation results are illustrated from Figure 4.94 to Figure 4.96. all these obtained results reveal good and expected performance.

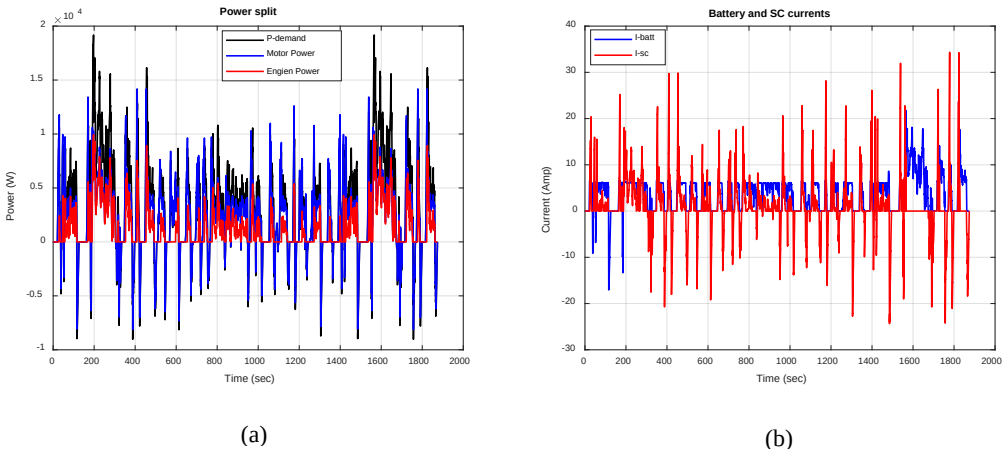

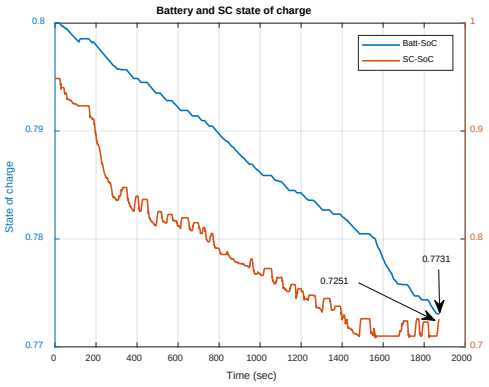

(c)

Figure 4.95. FTP75 driving cycle: a) Power demand & Power split. b) Battery current. c) State of charge of Battery. HEV Based IM-SMC and FRB-EMS.

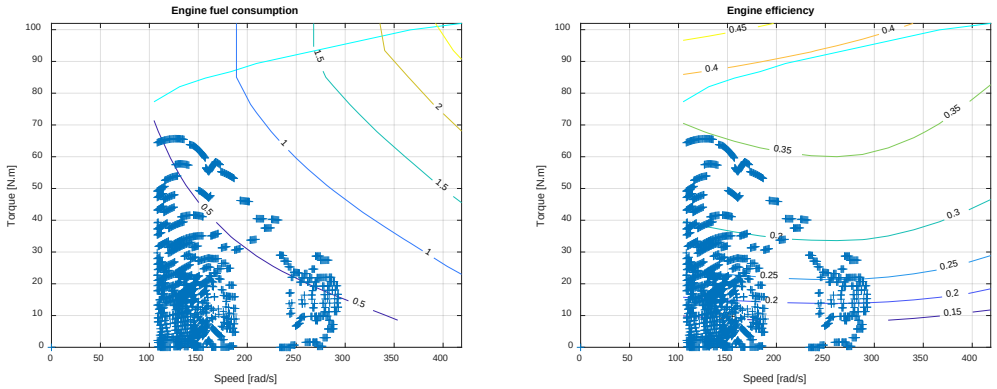

(a) (b)

Figure 4.96. FTP75 driving cycle: a) Engine fuel consumption. b) Engine efficiency. HEV Based IM-SMC and FRB-EMS.

Furthermore, the Highway drive scenario is performed and the obtained results are illustrated from Figure 4.97 to Figure 4.99.

The performances can be seen well from the graphs below, where the energy consumption from the battery pack reduces the SoC to 0.7798 and for the SC reduced to 0.7494. Also, the electric current split between both energy storage sources is demonstrated in Figure 4.98b. Furthermore, engine operating points during this scenario are plotted on the fuel consumption and efficiency maps in Figure 4.99.

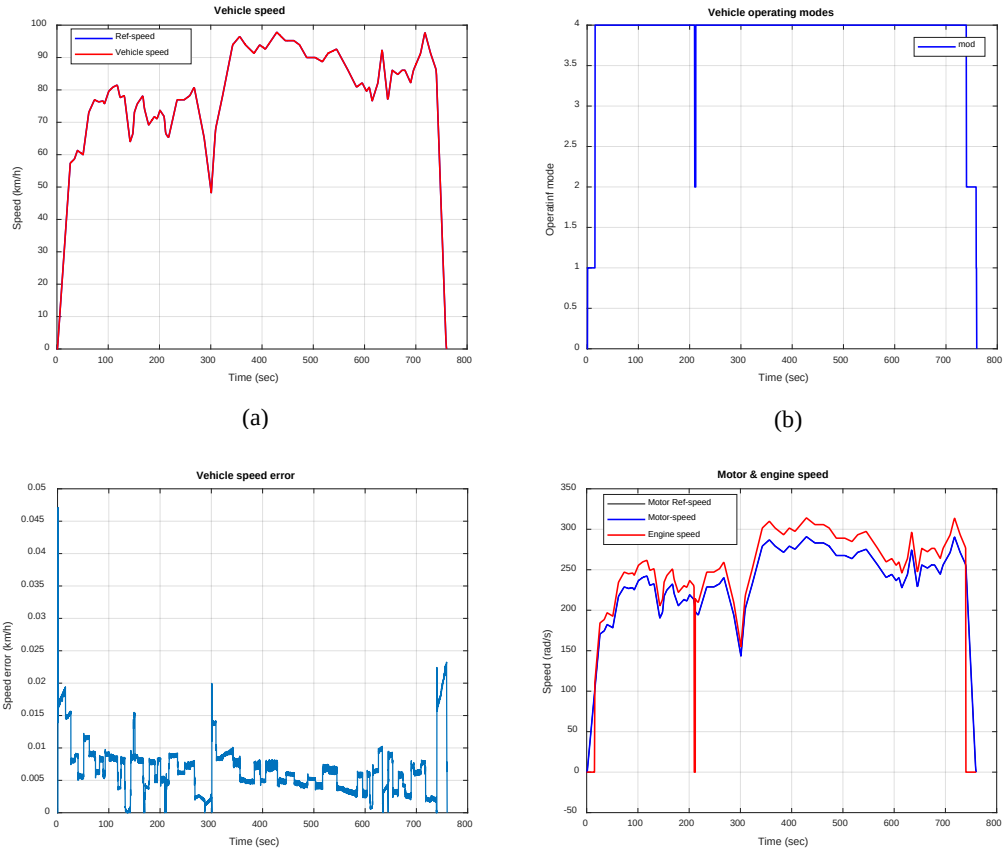

Figure 4.97. Highway driving cycle: a) Vehicle speed response. b) Vehicle operating modes. c) Vehicle speed error. d) Motor speed. HEV Based IM-SMC and FRB-EMS.

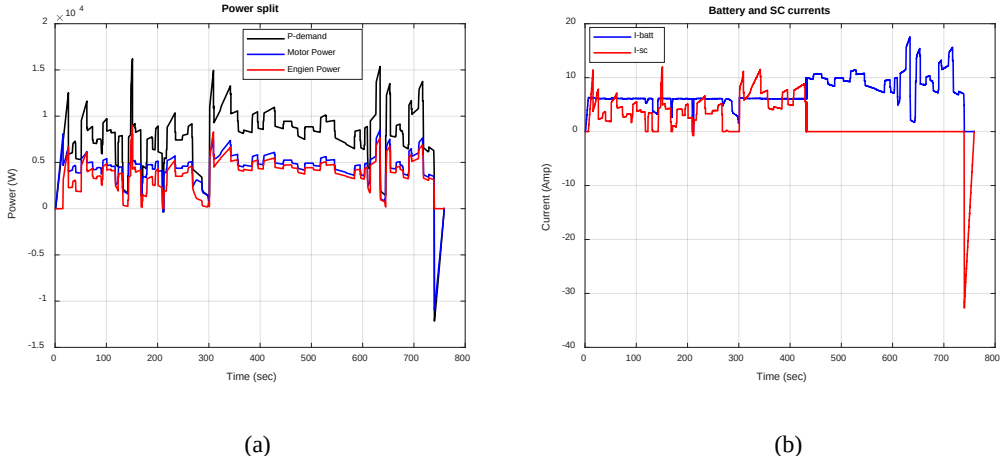

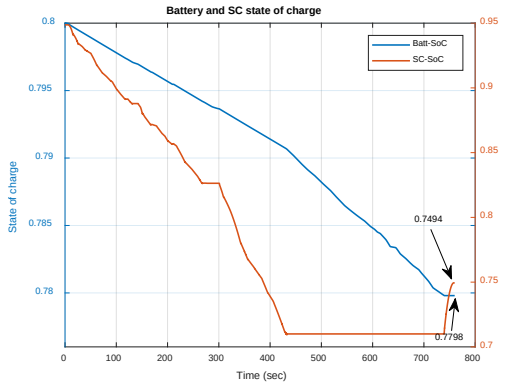

(c)

Figure 4.98. Highway driving cycle: a) Power demand & Power split. b) Batt/SC currents. c) State of charge of Battery & SC. HEV Based IM-SMC and FRB-EMS.

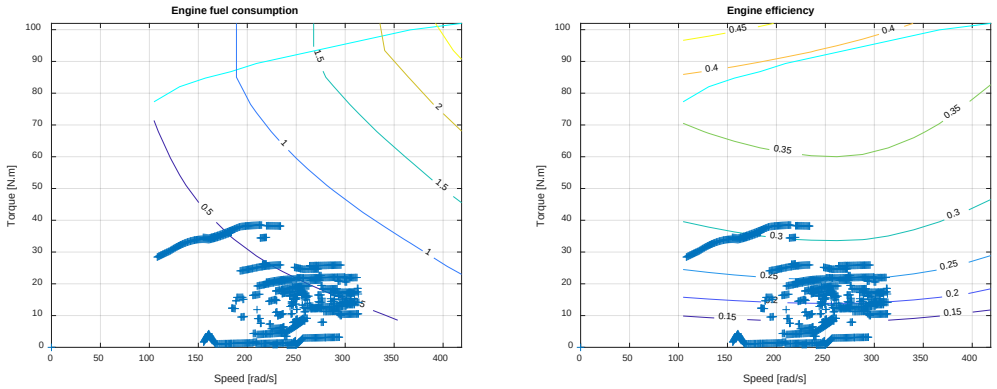

(a) (b)

Figure 4.99. Highway driving cycle: a) Engine fuel consumption. b) Engine efficiency. HEV Based IM-SMC and FRB-EMS.

4.2.2.3. **Results comparison**

In the same arrangement, the comparison graphs to validate the effect of the HESS EMS in this section are illustrated from Figure 4.100 to Figure 4.102. Figure 4.100 shows that the SoC of the battery pack is enhanced from 0.7870 to 0.7913 for the NEDC scenario, and the remained energy in the battery pack increased from 2.969e+4Wh to 2.9895e+4Wh, moreover; for the FTP75 drive cycle, the remained energy improved from 2.8937e+4Wh to 2.9164e+4Wh and the SoC from 0.7671 to 0.7731 as seen from Figure 4.101.

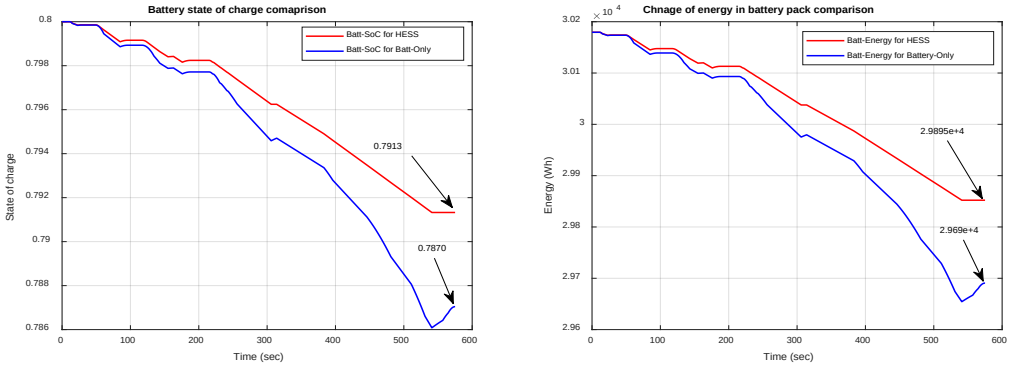

(a) (b)

Figure 4.100. NEDC driving cycle: a) Battery state of charge of Battery comparison. b) Change of energy in battery pack comparison. HEV Based IM-SMC- FRB-EMS.

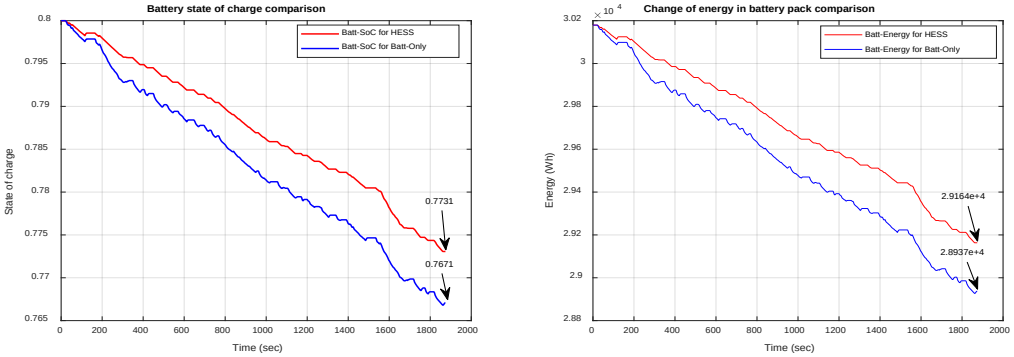

(a) (b)

Figure 4.101. FTP75 driving cycle: a) Battery state of charge of Battery comparison. b) Change of energy in battery pack comparison. HEV Based IM-SMC- FRB-EMS.

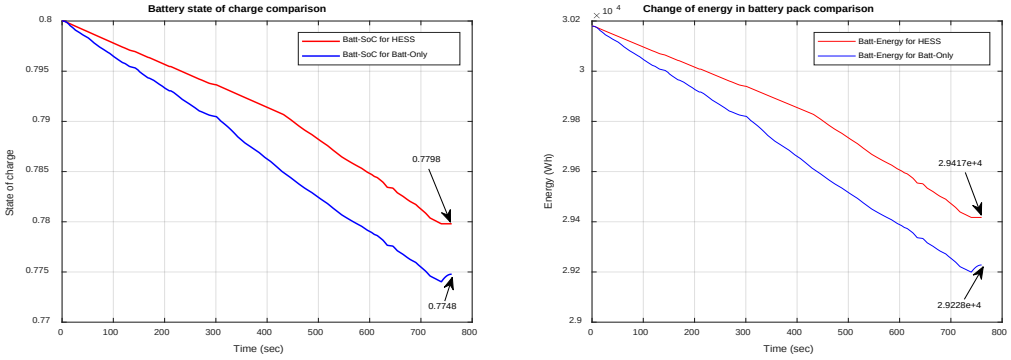

(a) (b)

Figure 4.102. Highway driving cycle: a) Battery state of charge of Battery comparison. b) Change of energy in battery pack comparison. HEV Based IM-SMC-FRB-EMS.

Additionally, a good improvement was achieved for the Highway drive cycle as shown in Figure 4.102a and Figure 4.102b, however; the SoC remained value is increased from 0.7748 to 0.7798, and in the same way the battery pack remained energy is improved from 2.9228e+4Wh to 2.9417e+4Wh.

In addition, Table 4.4 shows that the battery energy consumption reduced from 1.617% to 0.937% in the case of HESS for the NEDC drive cycle, and for the FTP75 drive cycle, the reduction percentage improved from 4.112% to 3.36%. Also, for the Highway drive cycle, the improvement in the energy consumption was from 3.147% to 2.52% as presented in the comparison table below.

Table 4.4. HEV based IM-SMC-FRB-EMS numerical comparison.

Vehicle configuration	**Drive Cycle**	**Energy Storage Configuration**	**SoC end value**	**Energy end value**	**Energy reduction in Battery pack (%)**
HEV-IM-IFOC-SMC-FRB-EMS	NEDC	Batt-only	0.7870	2.9690e+4	1.617%
		Batt/SC	0.7913	2.9895e+4	0.937%
	FTP75	Batt-only	0.7671	2.8937e+4	4.112%
		Batt/SC	0.7731	2.9164e+4	3.36%
	Highway	Batt-only	0.7748	2.9228e+4	3.147%
		Batt/SC	0.7798	2.9417e+4	2.52%

In summary, the simulation results of the Parallel HEV and the data illustrated in Table 4.3 and Table 4.4 demonstrate that the vehicle has consumed less energy from the battery pack in the case of the Max-SoC EMS for all drive scenarios if compared to the FRB EMS results. However, this improvement increases the vehicle's range and the battery pack lifetime that enhanced the vehicle's energy efficiency. Furthermore, the engine operating points illustrated on the engine fuel map and the engine efficiency map show that the engine runs more efficiently under the Max-SoC EMS for all scenarios. Additionally, utilizing the HESS configuration has indicated more improvement in energy consumption in the battery pack, as illustrated in the comparison tables.

PART 5

SUMMARY

A simulation platform for the EV and Parallel HEV is developed and validated. The development of this platform started by modeling all vehicle components from scratch. This work has improved the background knowledge of the vehicle subsystems. Further achieved task is implementing the IFOC and the DTC control strategies to control the IM and PMSM using PI, FLC, and the proposed SMC controllers. However, the vehicle performance using the proposed SMC as a speed controller revealed superior performance such as fast speed-tracking, less speed error, and steady-state error as compared to the PI and the FLC controllers' performance. Moreover, the results demonstrate good performance in both IFOC and DTC, with more advantage in the case of DTC. Moreover, the EV based the proposed SMC simulation results proved an improvement in the energy consumption during simulation time in both cases of IM and PMSM. And I have published a paper based this contribution utilizing EV driven by IM [85]. Also, the hybridization of the ESS by the battery-SC combination is implemented. The designed HESS met the energy demand of the vehicle during the simulation period for all possible configurations of the EV. The developed HESS EMS controlled the power split between the battery and the SC to meet the power demand during driving cycle time. An improvement in the energy consumption in the battery pack is achieved utilizing the HESS configuration, as illustrated in the comparison tables for IM and PMSM cases.

The Parallel HEV model is achieved by the combination of the EV with the ICE. And the obtained results illustrate the good performance of both Max-SoC and FRB energy management strategies to control the power split between the engine and the electric traction motor. Obtained results and the comparison tables demonstrate that the Parallel HEV based on the Max-SoC EMS achieved better performance. However, low energy consumption in the battery pack with a more efficient operating point of the ICE is achieved in the case of Max-SoC EMS during different driving scenarios.

Further improvement in the consumed energy is achieved for the Parallel HEV by implementing the HESS configuration. The advantage of utilizing HESS is proved for the Parallel HEV as well.

The final task in modeling this platform was designing the GUI. The GUI gives the developed software package the advantage of simulating different configurations with different control strategies without interacting with the main code. However, changing the vehicle parameters or the vehicle configuration can be performed directly via the GUI.

To conclude, a simulation platform for the EV and the Parallel HEV is developed and its performance validated under different vehicle configurations. The vehicle performance under the proposed SMC is improved in terms of speed tracking and energy consumption for EV and Parallel HEV. Furthermore, implementing the HESS configuration and its power-split EMS improved the energy consumption and enhanced the vehicle range and the battery pack lifetime.

Some additional future work to improve this platform is mentioned in the following points:

- Including other EVs and HEVs configurations for further investigation.
- Including other energy sources such as FC and PV.
- Implementing and investigation of another storage component such as Flywheel.
- Implementing modern and advanced energy management strategies such as Model Predictive Control energy management strategy.

REFERENCES

1. Bose, B.K., "Global energy scenario and impact of power electronics in 21st century", ***IEEE Transactions on Industrial Electronics***, 60(7): p. 2638-2651, (2012).

2. López, I., et al., "Next generation electric drives for HEV/EV propulsion systems: Technology, trends and challenges", ***Renewable and Sustainable Energy Reviews***, 114: p. 109336, (2019).

3. Vidyanandan, K., "Overview of electric and hybrid vehicles", ***Energy Scan***, 3: p. 7-14, (2018).

4. Nandurkar, V. and V. Virulkar., "Modelling and Simulation of Electric and Hybrid Electric Vehicles", ***in 2020 IEEE First International Conference on Smart Technologies for Power, Energy and Control (STPEC)***, (2020).

5. Ehsani, M., et al., "State of the Art and Trends in Electric and Hybrid Electric Vehicles", ***Proceedings of the IEEE***, (2021).

6. He, X. and J.W. Hodgson., "Modeling and simulation for hybrid electric vehicles-Part I: Modeling", ***IEEE Transactions on Intelligent Transportation Systems***, 3(4): p. 235-243, (2002).

7. Singh, K.V., H.O. Bansal, and D. Singh., "A comprehensive review on hybrid electric vehicles: architectures and components", ***Journal of Modern Transportation***, 27(2): p. 77-107, (2019).

8. Zhuang, W., et al., "A survey of powertrain configuration studies on hybrid electric vehicles", ***Applied Energy***, 262: p. 114553, (2020).

9. Un-Noor, F., et al., "A comprehensive study of key electric vehicle (EV) components, technologies, challenges, impacts, and future direction of development", ***Energies***, 10(8): p. 1217, (2017).

10. Enang, W. and C. Bannister., "Modelling and control of hybrid electric vehicles (A comprehensive review) ", ***Renewable and Sustainable Energy Reviews***, 74: p. 1210-1239, (2017).

11. Krithika, V. and C. Subramani., "A comprehensive review on choice of hybrid vehicles and power converters, control strategies for hybrid electric vehicles", ***International journal of energy research***, 42(5): p. 1789-1812, (2018).

12. Rind, S.J., et al., “Configurations and control of traction motors for electric vehicles: A review”, ***Chinese Journal of Electrical Engineering***, 3(3): p. 1-17, (2017).

13. Rind, S.J., M. Jamil, and A. Amjad., “Electric motors and speed sensorless control for electric and hybrid electric vehicles: A review”, ***in 2018 53rd International Universities Power Engineering Conference (UPEC)***, (2018).

14. Dandan, S., D. Yugang, and Z. Chengning., “Sliding mode controller for permanent magnetic synchronous motors”, ***Energy Procedia***, 105: p. 2641-2646, (2017).

15. Bennassar, A., et al., “Real time high performance of sliding mode controlled induction motor drives”, ***Procedia computer science***, 132: p. 971-982, (2018).

16. Arisoy, A., et al., “High order sliding mode control of a space robot manipulator”, ***in Recent Advances in Space Technologies (RAST), 2011 5th International Conference***, (2011).

17. Abdelfatah, N., et al., “Two wheel speed robust sliding mode control for electric vehicle drive”, ***Serbian journal of electrical engineering***, 5(2): p. 199-216 ,(2008).

18. Ltifi, A., M. Ghariani, and R. Neji., “Performance comparison of PI, SMC and PI-Sliding Mode Controller for EV”, ***in 2014 15th International Conference on Sciences and Techniques of Automatic Control and Computer Engineering (STA)***, (2014).

19. Alagna, S., et al., “Sliding mode torque control of an induction motor for automotive application with sliding mode flux observer”, ***in 2016 IEEE International Conference on Renewable Energy Research and Applications (ICRERA)***, (2016).

20. Nasri, A., B. Gasbaoui, and B.M. Fayssal., “Sliding mode control for four wheels electric vehicle drive”, ***Procedia Technology***, 22: p. 518-526, (2016).

21. Nasri, A., et al., “Fuzzy-sliding mode speed control for two wheels electric vehicle drive”, ***Journal of Electrical Engineering and Technology***, 4(4): p. 499-509, (2009).

22. Boumediène, A. and L. Abdellah., “A novel sliding mode fuzzy control based on SVM for electric vehicles propulsion system”, ***ECTI Transactions on Electrical Engineering, Electronics, and Communications***, 10(2): p. 153-163, (2014).

23. Ghezouani, A., B. Gasbaoui, and J. Ghouili., “Modeling and Sliding Mode DTC of an EV with Four In-Wheel Induction Motors Drive”, ***in 2018 International Conference on Electrical Sciences and Technologies in Maghreb (CISTEM)***, (2018).

24. Kumar, V., K. Rana, and P. Mishra., “Robust speed control of hybrid electric vehicle using fractional order fuzzy PD and PI controllers in cascade control loop”, ***Journal of the Franklin Institute***, 353(8): p. 1713-1741, (2016).

25. Sathishkumar, H. and S. Parthasarathy., “A novel fuzzy logic controller for vector controlled induction motor drive”, ***Energy Procedia***, 138: p. 686-691, (2017).

26. Öztürk, T. and M. Aktaş., “Research on Control Strategy and Energy Consumption for Electric Vehicles”, ***IFAC Proceedings Volumes***, 46(7): p. 444-449, (2013).

27. Talib, M., et al., “An improved simplified rules Fuzzy Logic Speed Controller method applied for induction motor drive”, ***ISA transactions***, 105: p. 230-239, (2020).

28. Gor, C.P., V.A. Shah, and M.P. Gor., “Electric vehicle drive selection related issues”, ***in 2016 International Conference on Signal Processing, Communication, Power and Embedded System (SCOPES)***, (2016).

29. Li, S., “A review of electric motor drives for applications in electric and hybrid vehicles”, ***Researchgate***, March, (2017).

30. Saha, S., et al., “Comparative Analysis between Direct Torque Control and v/f Control for Electric Vehicles”, ***in 2020 11th International Conference on Computing, Communication and Networking Technologies (ICCCNT)***, (2020).

31. Chrenko, D., et al., “Novel classification of control strategies for hybrid electric vehicles”, ***in 2015 IEEE vehicle power and propulsion conference (VPPC)***, (2015).

32. Banvait, H., S. Anwar, and Y. Chen., “A rule-based energy management strategy for plug-in hybrid electric vehicle (PHEV) ”, ***in 2009 American control conference***, (2009).

33. Zhu, C. and B. Yang., “Energy management in parallel hybrid vehicle using fuzzy control”, ***in 2012 IEEE International Conference on Information Science and Technology***, (2012).

34. Ming, L., et al., “Energy management strategy of a plug-in parallel hybrid electric vehicle using fuzzy control”, ***Energy Procedia***, 105: p. 2660-2665 (2017).

35. Horn, M., et al., “Supercapacitors: A new source of power for electric cars? ”, ***Economic Analysis and Policy***, 61: p. 93-103, (2019).

36. Kouchachvili, L., W. Yaïci, and E. Entchev., “Hybrid battery/supercapacitor energy storage system for the electric vehicles”, ***Journal of Power Sources***, 374: p. 237-248, (2018).

37. Song, Z., et al., “Sliding-mode and Lyapunov function-based control for battery/supercapacitor hybrid energy storage system used in electric vehicles”, ***Energy***, 122: p. 601-612, (2017).

38. Carter, R., A. Cruden, and P.J. Hall., “Optimizing for efficiency or battery life in a battery/supercapacitor electric vehicle”, ***IEEE Transactions on Vehicular Technology***, 61(4): p. 1526-1533, (2012).

39. Mohammadi, F., G.-A. Nazri, and M. Saif., “Modeling, Simulation, and analysis of hybrid electric vehicle using MATLAB/simulink”, ***in 2019 International Conference on Power Generation Systems and Renewable Energy Technologies (PGSRET)***, (2019).

40. Halvaii, A.E. and M. Ehsani., “Computer aided design tool for electric, hybrid electric and plug-in hybrid electric vehicles”, ***in 2011 IEEE Vehicle Power and Propulsion Conference***, (2011).

41. Eskandari Halvaii, A., “Computer Aided Design Tool for Electric, Hybrid Electric and Plug-in Hybrid Electric Vehicles”, ***Texas A&M University***. p. 107, (2012).

42. Valle, J.M.G., J.C.C. García, and E.R., “Cadaval. Electric vehicle monitoring system by using MATLAB/App Designer”, ***in 2017 International Young Engineers Forum (YEF-ECE)***, (2017).

43. Kalevo, M., “Building a Graphical User Interface with MATLAB”, Bachelor's thesis, ***Metropolia University of Applied Sciences***, (2019).

44. Aliasand, A.E. and F. Josh., “Selection of motor foran electric vehicle: A review”, ***Materials Today: Proceedings***, 24: p. 1804-1815, (2020).

45. Yılmaz, M. and S. Özdemir., “Review of Motors used in Commercial Electric Vehicles”, ***in 5th International Mediterranean Science and Engineering Congress (IMSEC 2020)***, (2020).

46. Cai, W., et al., “Review and Development of Electric Motor Systems and Electric Powertrains for New Energy Vehicles”, ***Automotive Innovation***, 4(1): p. 3-22, (2021).

47. Liu, C., et al., “A critical review of advanced electric machines and control strategies for electric vehicles”, ***Proceedings of the IEEE***, (2020).

48. Poorfakhraei, A., M. Narimani, and A. Emadi., “A review of modulation and control techniques for multilevel inverters in traction applications”, ***IEEE Access***, 9: p. 24187-24204, (2021).

49. Situ, L., “Electric vehicle development: the past, present & future”, ***in 2009 3rd International Conference on Power Electronics Systems and Applications (PESA)***, (2009).

50. Zakaria, H., et al., “Recent advancements and developments for electric vehicle technology”, ***in 2019 International Conference of Computer Science and Renewable Energies (ICCSRE)***, 2019.

51. Sun, X., et al., “Technology development of electric vehicles: A review”, ***Energies***, 13(1): p. 90, (2020).

52. Ehsani, M., et al., “Modern electric, hybrid electric, and fuel cell vehicles”, ***CRC press***, (2018).

53. Larminie, J. and J. Lowry., “Electric vehicle technology explained”, ***John Wiley & Sons***, (2004).

54. Mi, C., M.A. Masrur, and D.W. Gao., “Hybrid electric vehicles: principles and applications with practical perspectives”, ***John Wiley & Sons***, (2011).

55. Liu, W., “Hybrid electric vehicle system modeling and control”, ***John Wiley & Sons***, (2017).

56. Ehsani, M., Y. Gao, and J.M. Miller., “Hybrid Electric Vehicles: Architecture and Motor Drives”, ***Proceedings of the IEEE***, 95(4): p. 719-728, (2007).

57. Zhu, Z.Q. and D. Howe., “Electrical Machines and Drives for Electric, Hybrid, and Fuel Cell Vehicles”, ***Proceedings of the IEEE***, 95(4): p. 746-765, (2007).

58. Sevinc, A., “Speed sensorless control of induction motors”, a PhD thesis, ***University of Bristol***, Bristol, England, (2001).

59. Shetty, P. and S. Dawnee., “Modeling and simulation of the complete electric power train of a hybrid electric vehicle”, ***in 2014 Annual International Conference on Emerging Research Areas: Magnetics, Machines and Drives (AICERA/iCMMD)***, (2014).

60. Vas, P., “Vector control of AC machines”, ***Oxford University Press***, USA, Vol. 22, (1990).

61. Boldea, I. and S.A. Nasar., “Vector control of AC drives”, ***CRC press***, (1992).

62. Proca, A.B., “Induction motor control for hybrid electric vehicle applications”, ***The Ohio State University***, (2001).

63. Abu-Rub, H., A. Iqbal, and J. Guzinski., “High performance control of AC drives with MATLAB/Simulink models”, ***John Wiley & Sons***, (2012).

64. Donikian, V., “Model predictive control of advanced hybrid powertrain systems”, ***UC Irvine***, (2016).

65. Khaligh, A. and Z. Li., “Battery, Ultracapacitor, Fuel Cell, and Hybrid Energy Storage Systems for Electric, Hybrid Electric, Fuel Cell, and Plug-In Hybrid

Electric Vehicles: State of the Art", ***IEEE Transactions on Vehicular Technology***, 59(6): p. 2806-2814, (2010).

66. Danilov, D., A. Lyedovskikh, and P. Notten., "Voltage and temperature dynamic simulations for advanced battery management systems", ***in Vehicle Power and Propulsion Conference (VPPC)***, (2011).

67. Juda, Z., "Advanced batteries and supercapacitors for electric vehicle propulsion systems with kinetic energy recovery", ***Journal of KONES***, 18: p. 165-171, (2011).

68. Gao, Y. and M. Ehsani., "Design and Control Methodology of Plug-in Hybrid Electric Vehicles", ***IEEE Transactions on Industrial Electronics***, 57(2): p. 633-640, (2010).

69. Liu, X.L., et al., "SOC calculation method based on extended Kalman filter of power battery for electric vehicle", ***in 2017 12th International Conference on Intelligent Systems and Knowledge Engineering (ISKE)***, (2017).

70. Liu, Y., et al., "Dynamic SOC estimation method of energy storage battery against load power change", ***in 2017 IEEE Conference on Energy Internet and Energy System Integration (EI2)***, (2017).

71. Yaïci, W., et al., "Dynamic Simulation of Battery/Supercapacitor Hybrid Energy Storage System for the Electric Vehicles", ***in 2019 8th International Conference on Renewable Energy Research and Applications (ICRERA)***, (2019).

72. Bououchma, Z., J. Sabor, and H. Aitbouh., "New electrical model of supercapacitors for electric hybrid vehicle applications", ***Materials Today: Proceedings***, 13: p. 688-697, (2019).

73. Hidalgo-Reyes, J., et al., "Classical and fractional-order modeling of equivalent electrical circuits for supercapacitors and batteries, energy management strategies for hybrid systems and methods for the state of charge estimation: A state of the art review", ***Microelectronics Journal***, 85: p. 109-128, (2019).

74. El Fadil, H., et al., "Nonlinear modeling and observer for supercapacitors in electric vehicle applications, ***IFAC-PapersOnLine***, 50(1): p. 1898-1903, (2017).

75. Helseth, L.E., "Modelling supercapacitors using a dynamic equivalent circuit with a distribution of relaxation times", ***Journal of Energy Storage***, 25: p. 100912, (2019).

76. Sharma, P. and V. Kumar., "Investigation of the behaviour of supercapacitors using theoretical models", ***Physica B: Condensed Matter***, p. 413212, (2021).

77. Cao, J. and A. Emadi., "A new battery/ultracapacitor hybrid energy storage system for electric, hybrid, and plug-in hybrid electric vehicles", ***IEEE Transactions on power electronics***, 27(1): p. 122-132, (2011).

78. Ju, F., et al., “Review of structures and control of battery-supercapacitor hybrid energy storage system for electric vehicles”, ***in 2014 IEEE International Conference on Automation Science and Engineering (CASE)***, (2014).

79. Song, Z., et al., “Energy management strategies comparison for electric vehicles with hybrid energy storage system”, ***Applied Energy***, 134: p. 321-331, (2014).

80. Geetha, A. and C. Subramani., “A comprehensive review on energy management strategies of hybrid energy storage system for electric vehicles”, ***International Journal of Energy Research***, 41(13): p. 1817-1834, (2017).

81. Song, Z., et al., “The battery-supercapacitor hybrid energy storage system in electric vehicle applications: A case study”, ***Energy***, 154: p. 433-441, (2018).

82. Wirasingha, S.G. and A. Emadi., “Classification and review of control strategies for plug-in hybrid electric vehicles”, ***IEEE Transactions on vehicular technology***, 60(1): p. 111-122, (2010).

83. Alegre, S., J.V. Míguez, and J. Carpio., “Modelling of electric and parallel-hybrid electric vehicle using Matlab/Simulink environment and planning of charging stations through a geographic information system and genetic algorithms”, ***Renewable and Sustainable Energy Reviews***, 74: p. 1020-1027, (2017).

84. Liu, W., “Introduction to hybrid vehicle system modeling and control”, ***John Wiley & Sons***, (2013).

85. Aktas, M., et al., “Direct torque control versus indirect field-oriented control of induction motors for electric vehicle applications”, ***Engineering Science and Technology, an International Journal***, 23(5): p. 1134-1143, (2020).

86. Lan, D., H. Li, and S. Yu., “Sorless Model Predictive Current Control by Using HF Pulsating Injection Method for PMSM Drive System”, ***in IOP Conference Series: Materials Science and Engineering***, ***IOP Publishing***, (2019).

APPENDIX A.

Table Appendix A.1 to Table Appendix A.3 illustrate the parameters of the vehicle, IM and PMSM used in this thesis respectively.

Table Appendix A.1. Vehicle parameters [26].

Parameter Name	Value
Vehicle mass (m)	700 kg
Front area (A)	1.8 m2
Aerodynamic drag coefficient (Cd)	0.19
Rolling resistance coefficient (μrr)	0.048
Air density (ρ)	0.23 kg/m3
Wheel radius (r)	0.27 m
Gravitational acceleration constant (g)	9.81 m/s2

Table Appendix A.2. IM parameters [26].

Parameter Name	Value
Power rating (P)	15 kW
Number of poles	4
Stator resistance (Rs)	0.2147 Ω
Rotor resistance (Rr)	0.2205 Ω
Stator inductance (Ls)	0.065181 H
Rotor inductance (Lr)	0.065181 H
Mutual inductance (M)	0.0641 H
Moment of inertia (Jm)	0.102 Kg.m2
Friction torque coefficient (Bf)	0.009541 N.ms

Table Appendix A.3. PMSM parameters [86].

Parameter Name	Value
Power rating (P)	18 kW
Number of poles	4
Stator resistance (Rs)	0.06 Ω
D axis inductance (Ld)	0.31 mH
Q axis inductance (Lq)	1.04 mH
Flux permanent magnet (phi_m)	0.1005 Wb
Moment of inertia (Jm)	0.11 Kg.m2
Friction torque coefficient (Bf)	0.002 N.ms

APPENDIX B.

Figure Appendix B.1 illustrate the execution sequence of the designed GUI to simulate the EV and Parallel HEV behavior.

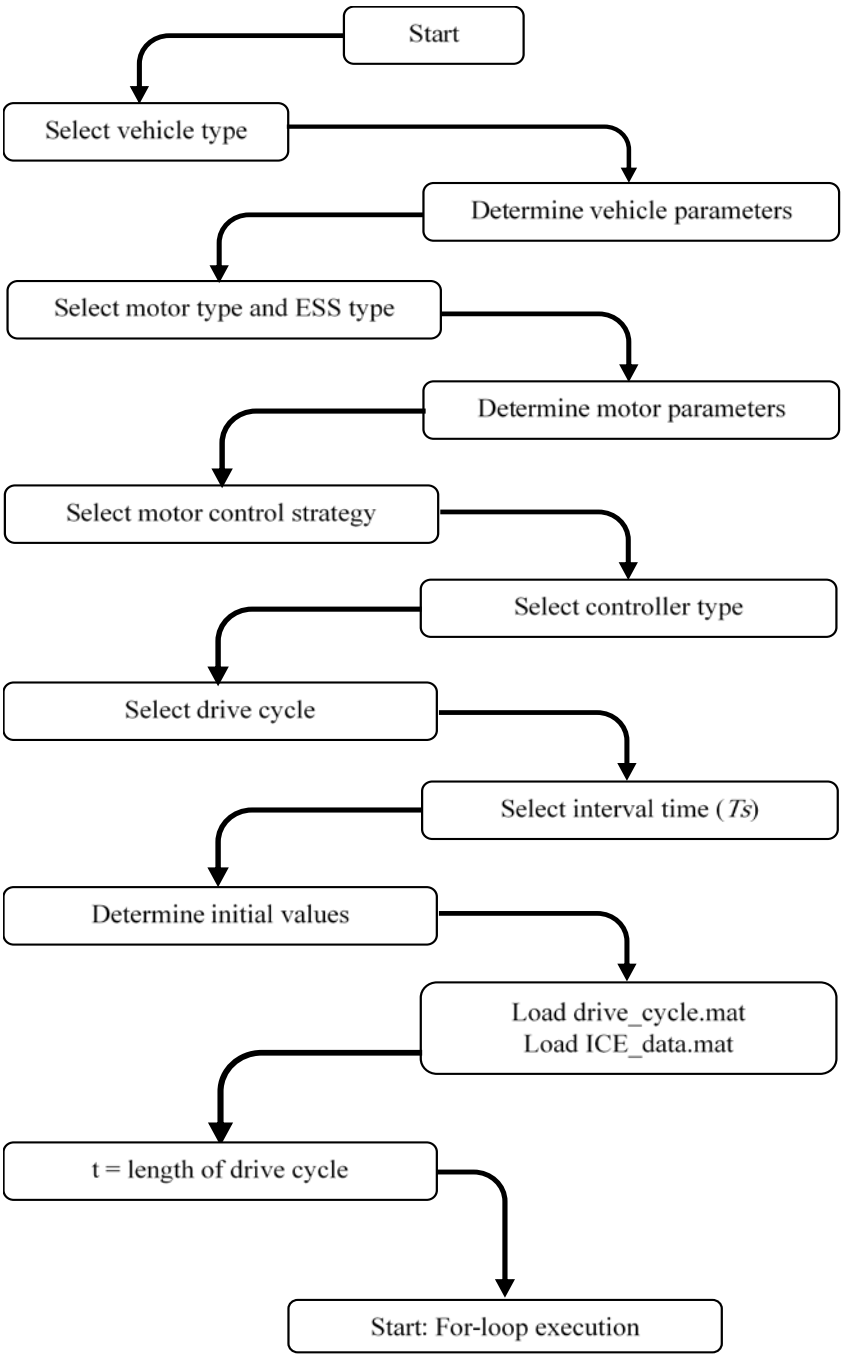

Figure Appendix B.1. GUI executing sequence.

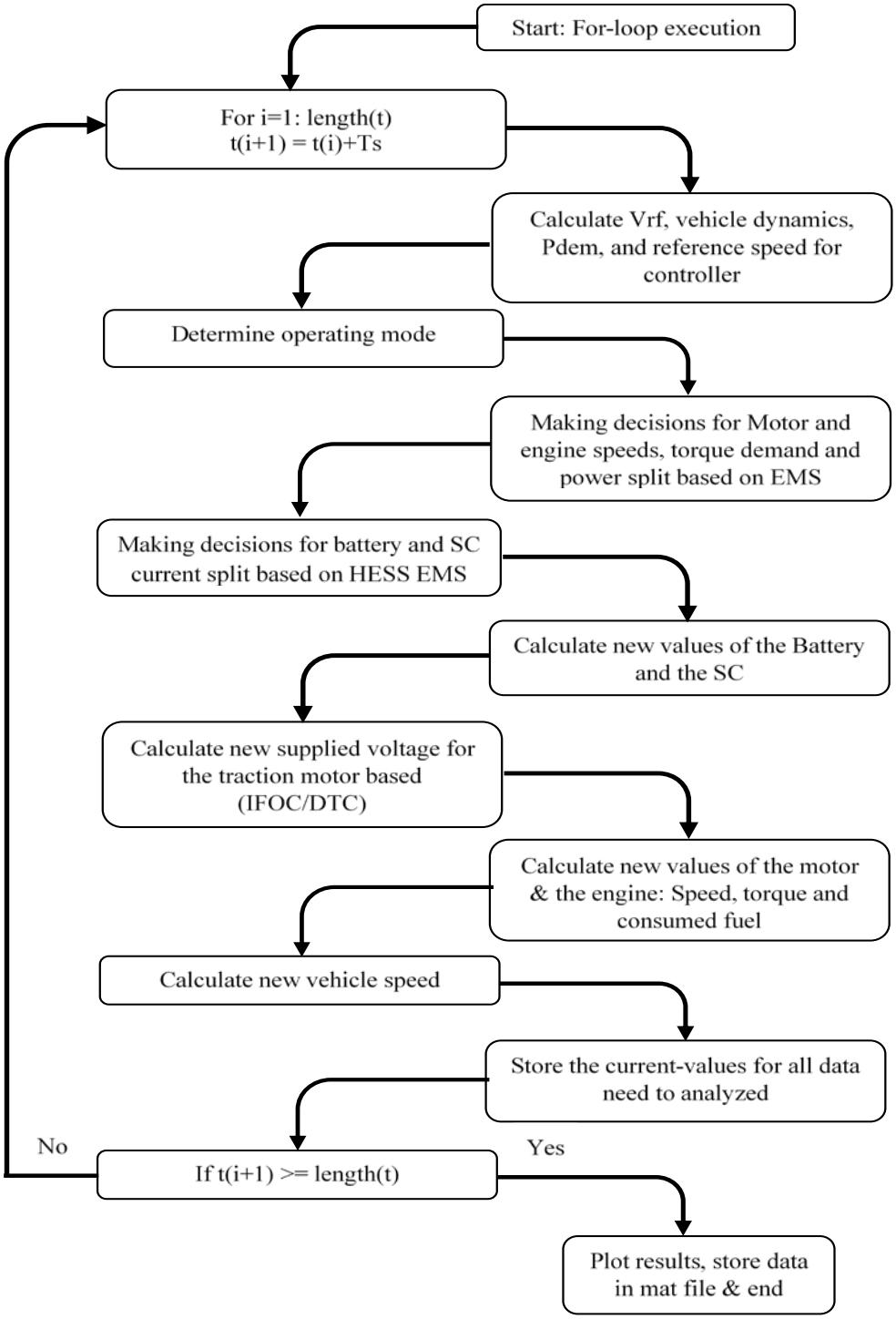

Figure Appendix B.1. (Continuing).